SAGARMATHA

Snow and Glacier aspects of Water Resources Management in the Himalayas

Final Technical Report: Volume 2

An assessment of the impacts of deglaciation on the water resources of the Himalaya

by

Gwyn Rees[1] and David N Collins[2]

[1]Centre for Ecology and Hydrology, Wallingford, UK

[2]Alpine Glacier Project, University of Salford, UK

June 2004

SAGARMATHA

Snow and Glacier aspects of Water Resources Management in the Himalayas

DFID KAR Project No. R7980

Final Technical Report: Volume 2

An assessment of the impacts of deglaciation on the water resources of the Himalaya

by

Gwyn Rees[1] and David N Collins[2]

[1]Centre for Ecology and Hydrology, Wallingford, UK

[2]Alpine Glacier Project, University of Salford, UK

June 2004

Centre for Ecology and Hydrology
Crowmarsh Gifford
Wallingford
Oxfordshire, OX10 8BB

Tel: +44 (0)1491 838800
Fax: +44 (0)1491 692424

Contents

Executive Summary

Deglaciation is considered to be a world-wide problem, but there is particular concern at the alarming rate of retreat of Himalayan glaciers. Glaciers in the Himalayas have generally been retreating since AD 1850, and recent publications confirm that, for many, the rate of retreat is accelerating. This has led to speculation by some experts that Himalayan glaciers will disappear within the next 40 years, as a result of global warming, and that flow of Himalayan rivers will eventually diminish, resulting in widespread water shortages. In March 2001, the United Kingdom's Department for International Development (DFID) commissioned a project called SAGARMATHA (Snow and Glacier Aspects of water Resources Management in The Himalaya), to assess the impact of deglaciation on the seasonal and long-term water resources in snow and glacier fed rivers of the Himalayan region. This technical report provides a brief outline of the model developed within the project and presents an analysis of the results from running the model with a variety of climate change scenarios.

To determine the impact of deglaciation on the water resources of the entire Himalayan region requires a regional hydrological model that can represent how glaciers and river flows respond to changes in climate. The model developed within the SAGARMATHA project provides estimates of seasonal and annual runoff for grid cells at a 20km by 20km resolution for the Indus, Ganges and Brahmaputra river basins, and consists of three key components: a rainfall-runoff model; a snow-pack model for representing the build-up of snow and its subsequent melting; and an innovative glacier-melt model for estimating the runoff contribution from glaciers. The glacier-melt model conceptualises all glaciers contributing runoff to any individual 20 km x 20 km cell in the study area as a single "generic glacier", having an idealised shape and depth profile.

The regional hydrological model was applied in each of the three basins of the study area, using climatological data, downscaled to the 20km x 20 km grid resolution, from the 0.5° x 0.5° standard period (1961-90) baseline climatology of the Climate Research Unit (CRU) of the University of East Anglia. First, the model ran with the baseline climatology for a 30-year period to give estimates of seasonal and annual runoff for each cell in each basin of the study area. It was then applied with 4 incremental scenarios of increasing temperature, 2 incremental scenarios of increasing

temperature with increasing precipitation, 2 incremental scenarios of increasing temperature but decreasing precipitation and one climate-model based scenario, based on output from the HadRM2 regional climate model (RCM). Apart from the "RCM" scenario, all model-runs were for a period of 100 years, with the outputs presented as decadal averages of annual and seasonal runoff. For the RCM scenario, the model ran for a period of 70 years, to represent the period 1991 to 2060.

The model output represents how runoff varies decade by decade from a nominal start date of 1991. To assess the impact of deglaciation on the water resources of the Himalayas, the 20 km x 20 km output grids were "translated" into 1 km grids of river flows. Comparisons were then made between baseline flows and those from the various scenarios to analyse how the surface water resource availability of rivers may be affected by climate change. To understand the regional variation of impacts, attention was focused on 21 locations in the four "focus-areas": six sites in the Upper Indus basin were studied, along with 7 sites in the Brahmaputra basin and 8 sites in two parts of the Ganges river basin.

According to the model results, for many areas, the catastrophic water shortages forecast by some experts are unlikely to happen for many decades, if at all. Rather, some areas may benefit from increased water availability for the foreseeable future. While the threat, that all of the region's glaciers will soon disappear, would seem ill-founded, the project identified certain areas of the region, such as in the Upper Indus, where deglaciation may, indeed, cause a significant reduction of river flows within the next few decades.. This would have serious consequences for water availability and use throughout the basin.

The results also show distinct differences in the potential impacts of deglaciation both regionally, in an east-west direction along the Himalayan arc, and within catchments. In the Upper Indus, the study sites show initial increases of between +14% and +90% in mean flows (compared to the baseline) over the first few decades of the 100-year incremental scenario runs, which are generally followed by flows decreasing to between -30% and -90% of baseline by decade 10. This contrasts with the apparent behaviour in the Kaligandaki basin in the east of the region, where decadal mean flows increase for all scenarios, with the most extreme temperature scenario attaining a peak mean flow of between +30% and +90% of baseline some 5 decades, or more, into the 100-year model run. For the Ganges, the response of the river, near the headwaters in Uttarkashi is significantly different from what is seen

downstream at Allahbad. At Uttarkashi, flows peak at between +20% and +33% of baseline within the first two decades and then recede to around -50% of baseline by decade 6; further downstream the deglaciation impacts are barely noticeable. In the headwaters of the Brahmaputra, there is a general decrease in decadal mean flows for all temperature scenarios; glaciers are few in this area and flows recede as the permanent snow cover reduces with increasing temperatures.

Highly glaciated catchments and those (catchments) where melt-water contributes significantly to the runoff appear to be most vulnerable to deglaciation. Results from the different focal-areas further indicate the very important role precipitation has in protecting glaciers from melting and rapid mass loss: a thick covering of snow resulting from a strong monsoon would insulate the glacier and delay melt, whereas, a weak monsoon would expose a glacier to melting earlier and for longer. In glaciated catchments where precipitation is relatively high, the impacts of deglaciation diminish rapidly downstream, as the runoff contribution from rainfall over the non-glaciated part of the catchment quickly swamps the melt-water contribution. Where precipitation is low, the melt-water contribution to runoff remains proportionately high for a significant distance downstream. It can be concluded, therefore, that catchments in the eastern Himalaya, which benefit from high precipitation of the summer monsoon every year, are less susceptible to the impacts of deglaciaton than those in the west, where the monsoon is very much weaker.

Whilst some alarmist claims can be discounted with confidence, the timing and magnitude of the modeled impacts derived should not be taken too literally: they show results of various hypothetical scenarios applied to a conceptual model, and, as such, only provide an indication of what might happen, if such conditions prevail. Much work remains, through the continuation of monitoring and further research, to ensure the future impacts of deglaciation and climate change on water resources are better understood.

This is the second volume of four that comprise the Final Technical Report for the SAGRMATHA project. Volume 1, provides an overview of the project; Volume 3 presents details of the livelihoods impacts assessment; the fourth volume, “Background Papers”, includes the various interim progress reports and technical documents that were produced during the course of the project.

Acknowledgements

The authors of this report thank the following for the help and support provided during the development of the regional model described in this report:

- Ms. Heather Musgrave, Dr. Alan Gustard, Dr. Vicky Bell, Dr. Chris Huntingford, Mr. Nick Reynard, Dr. Christel Prudhomme, and Dr. Andy Young, at the Centre for Ecology and Hydrology, Wallingford, UK;
- Mr. Nick Pelham, of the Alpine Glacier Project at the University of Salford, UK;
- Dr. Arun Bhakta Shrestha and Mr. Adarsha Pokhrel, at the Department of Hydrology and Meteorology, Kathmandu, Nepal;
- Ms. Mandira Shrestha and Mr. Pradeep K. Mool, at the International Centre for Integrated Mountain Development (ICIMOD), Kathmandu;
- Dr. Rajesh Kumar and Prof. Syed Hasnain, at Jawaharlal Nehru University, New Delhi, India;
- Dr. David Archer and Dr. Rob Lamb, at Jeremy Benn Associates Ltd., UK;
- Dr. Richard Jones, at the Hadley Centre for Climate Prediction and Research, UK.

The following organisations are also acknowledged for the data used in the project:

- The Climate Research Unit at the University of East Anglia, Norwich, UK, for the baseline climatology data;
- The Land Processes Distributed Active Archive Center (LP DAAC), located at the U.S. Geological Survey's EROS Data Center (http://LPDAAC.usgs.gov), for the HYDRO1k Elevation Derivative Database and Eurasia Land Cover Characteristics Database;
- The Land and Water Development Division of the Food and Agriculture Organization of the United Nations, Rome, for the Digital Soil Map of the World;
- The Hadley Centre for Climate Prediction and Research, for the HadRM2 regional climate model data;
- Environmental Systems Research Institute, Inc. (ESRI), USA, for the Digital Chart of the World; and the
- World Meteorological Organization's Global Runoff Data Centre, Koblenz, Germany, for data from selected gauging stations in study area.

This project was funded by the United Kingdom's Department for International Development (DFID) Knowledge and Research Programme. The authors are grateful for the support provided by DFID and its officers: Mr. Martin Walshe, Mr. Ian Curtis, Mr. Peter O'Neil and Mr. James Dalton.

The project has been undertaken as an activity of the Snow and Glacier Group of the Hindu Kush – Himalayan FRIEND[1] project, and, as such, is a contribution to the 6th International Hydrological Programme (IHP-VI) of UNESCO.

[1] FRIEND: Flow Regimes from International Experimental and Network Data

1 Introduction

There is compelling evidence that deglaciation is a widespread problem, with serious consequences for water resources around the world. More than half of humanity relies on the fresh water that accumulates in mountains. Growing populations, intensifying agriculture, increasing urbanization and industrialization have led to a fourfold increase in global freshwater abstractions since 1940. To avoid a water crisis over coming decades, effective management of mountain water resources is essential to staisfy these growing demands. Nowhere is this need greater than in the Indian subcontinent, where the snow and glaciers of the Hindu Kush and Himalayas provide up to 90% of the lowland dry-season flows of the Indus, Ganges and Brahmaputra rivers and their vast irrigation networks.

While deglaciation is considered to be a world-wide problem, there is particular concern at the alarming rate of retreat of Himalayan glaciers. Some have predicted that glaciers in the region will vanish within 40 years as a result of global warming and that flow of Himalayan rivers will eventually diminish, resulting in widespread water shortages. Glacier retreat is likely to lead to a temporary increase followed by a reduction in river flows but the quantities, timing and consequences are unknown.

In March 2001, a three-year project was commissioned, under the United Kingdom's Department for International Development (DFID) Knowledge and Research (KAR) programme, to assess the impact of deglaciation on the seasonal and long-term water resources in snow and glacier fed rivers of the Himalayan region. The project, called SAGARMATHA (Snow and Glacier Aspects of water Resources Management in The Himalaya), was led by the Centre for Ecology and Hydrology of Wallingford and involved organizations from India[2], Nepal[3,4,5] and the UK[6]. The development of a regional hydrological model, incorporating an innovative snow- and glacier-melt component, was a major part of the project. The model provides

[2] Jawaharlal Nehru Univeristy (JNU), New Delhi, India

[3] His Majesty's Government of Nepal Department of Hydrology and Meteorology (DHM)

[4] International Centre for Integrated Mountain Development (ICIMOD), Kathmandu, Nepal

[5] Tribhuvan University. Kathmandu, Nepal

[6] School of Environment and Life Sciences, The University of Salford, United Kingdom

predictions of the effects of deglaciation on future water resource availability in the Indus, Ganges and Brahmaputra river basins.

This report provides an outline of the model and presents an analysis of the results from running the model with a variety of climate change scenarios, and is the second volume of four that comprise the Final Technical Report for the SAGRMATHA project. Volume 1, provides an overview of the project; Volume 3 presents details of the livelihoods impacts assessment; the fourth volume, "Background Papers", includes the various interim progress reports and technical documents that were produced during the course of the project.

2 Evidence of deglaciation

2.1 Deglaciation: a worldwide phenomenon

Mountain Glaciers are considered to be particularly sensitive indicators of climate change and glacier observations have been used for climate system monitoring for many years (Haeberli, 1990; Wood 1990). The formal world-wide monitoring of glaciers began with the establishment of the International Glacier Commission in 1894 and regular reports on glacier variations around the world have been published ever since. Today, glacier observations are collated by the World Glacier Monitoring Service (WGMS) in Zurich. The Service is responsible for publishing standardised glacier fluctuation data in the *Fluctuation of Glaciers* series at intervals of 5 years (IAHS(ICSI)-UNEP-UNESCO, 1988, 1993*a*) and in the *Glacier Mass Balance Bulletin* every two years (IAHS(ICSI)-UNEP-UNESCO, 1991, 1993*b*). According to Haeberli and Hoelzle (2001) of the WGMS, the measurements taken over the last century "clearly reveal a general shrinkage of mountain glaciers on a global scale". They observed that the trend was most pronounced during the first half of the 20th century and that glaciers had started to grow again after about 1950. However, they claim that, since the 1980s mountain glacier retreat has been accelerating again, at a "rate beyond the range of pre-industrial variability."

Based upon a number of scientific investigations (e.g. Kuhn (1993), Oerlemans (1994), Oerlemans and Fortuin (1992) and Meier (1993)) the IPCC (1996) forecasts that up to a quarter of global mountain glacier mass could disappear by 2050 and up to half could be lost by 2100. A recent comparison by the United States' Geological Survey of images from the ASTER (Advance Spaceborne Thermal Emission and Reflection Radiometer) instrument on NASA's TERRA satellite with historical glacier data, revealed a significant shrinkage of mountain glaciers in the Andes, the Himalayas, the Alps and the Pyrenees over the past decade (Wessels *et al.*, 2001). These observations are consistent with the published results from many other glacier studies around the world which have also recorded rapid glacier retreat in recent years, including Duyrgerov and Meier (1997), who considered the mass balance changes of over 200 mountain glaciers globally and concluded that the

reduction in global glacier area amounted to between 6000 to 8000 km^2 over the 30 year period from 1961 to 1990.

2.2 Deglaciation in the Himalayas

Glaciers in the Himalayas have generally been retreating since AD 1850 (Mayewski and Jeschke, 1979) and recent publications confirm that, for many, the rate of retreat is accelerating. Several scientific papers report accelerated retreat over the last twenty years in Nepal and Bhutan (Fujita *et al.*,1997 & 2001; Kadota *et al.*, 1997 & 2000; Ageta *et al.*, 2001). In India, over a similar period, one of largest glaciers in the Himalayas, the Gangotri glacier that feeds the river Ganges, has retreated approximately 850 metres, compared to the 2 km it has retreated in the last 200 years (Naithani *et al.*, 2001).

Composite photographs prepared by a participant of the SAGARMATHA project, shows the extent of deglaciation of a single glacier in Central Nepal between 1985 and 2003 (see Figure 2.1 (a) & (b)), with the inverted triangle serving as a common reference point in both. Notice in Figure 2.1(b) how the lower, debris covered, part of the glacier has detached from its upper part and has, thus, become a mass of "dead ice", which is degrading rapidly, with rapid surface lowering, terminus retreat and ponding in front (*pers. comm.*, A B Shresta, 2003).

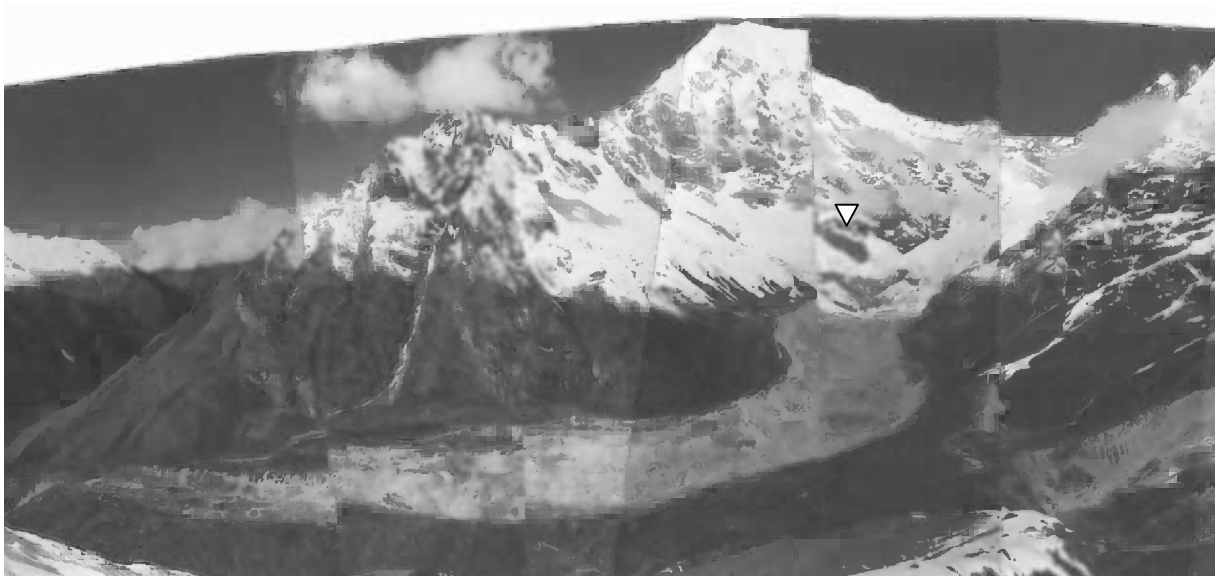

Figure 2.1 (a) *The Lirung Glacier in 1985*

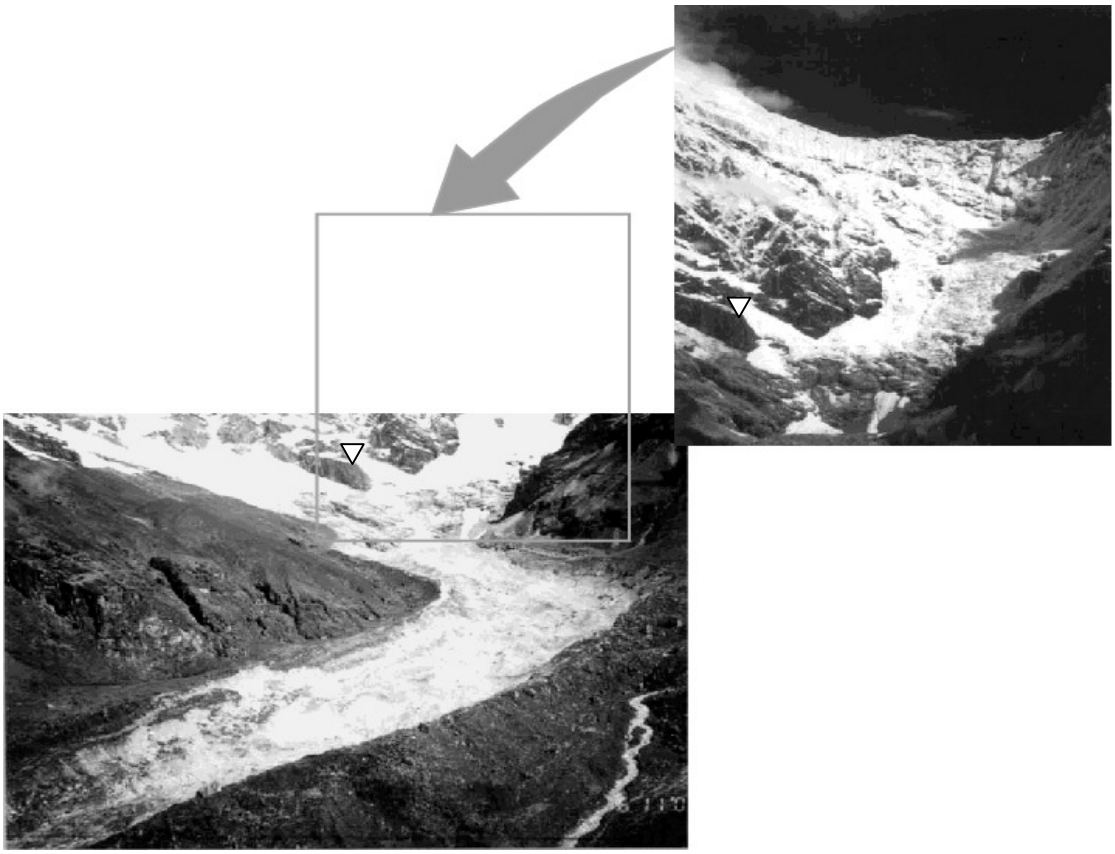

Figure 2.1(b) *The Lirung Glacier in 2003 (Photos courtesy of A.B. Shrestha, DHM)*

Similar behaviour has been observed throughout the region, and this has led to speculation by some experts that Himalayan glaciers will disappear within the next 40 years (Down to Earth, 1999). In 1999, a report by the Working Group on Himalayan Glaciology (WGHG) of the International Commission for Snow and Ice (ICSI) stated "glaciers in the Himalayas are receding faster than in any other part of the world and, if the present rate continues, the likelihood of them disappearing by the year 2035 is very high."

2.3 A changing climate?

Analysis of long-term hydrometeorological data helps to explain the apparent rapid retreat of the region's glaciers. Calculating the average annual temperature of the 119 temperature gauges in Nepal located at elevations on between 72 m and 4100 m above sea level, reveals an upward trend in values from 1961 to 1996 at a rate of almost 7°C per 100 years (or 0.07°C/year), as can be seen in Figure 2.2.

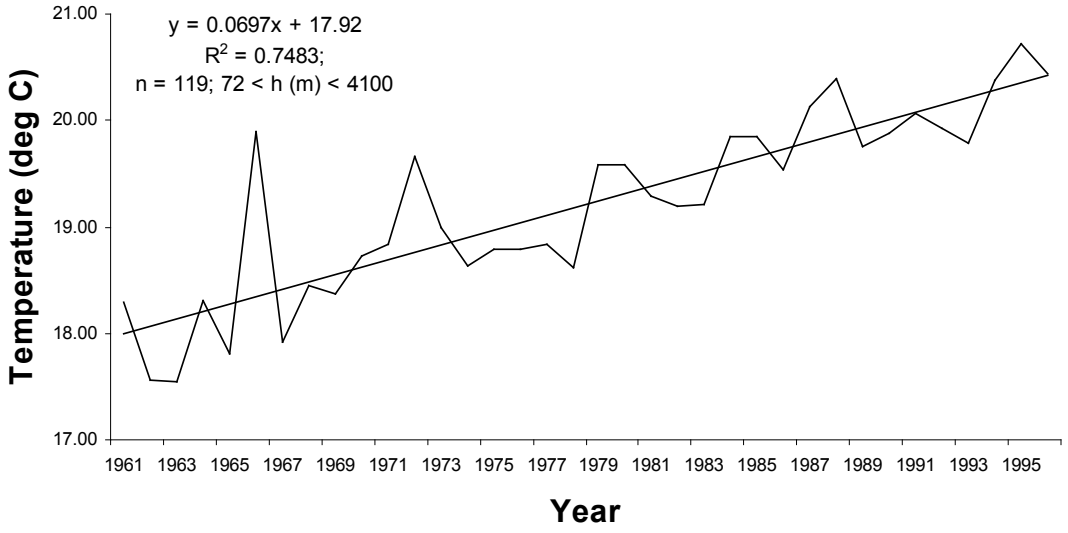

Figure 2.2 *Average annual temperature for Nepal, 1961-96 (all stations).*

While this observation in itself is more than double the +0.03 °C/yr average global warming predicted by the IPCC (IPCC, 2001a&b), an inspection of average annual temperature values for the 15 highest temperature gauges in Nepal, at elevations above 1800 m, show an even higher average annual increase of over 0.1 °C/yr over the twenty-year period for 1976 to 1996.

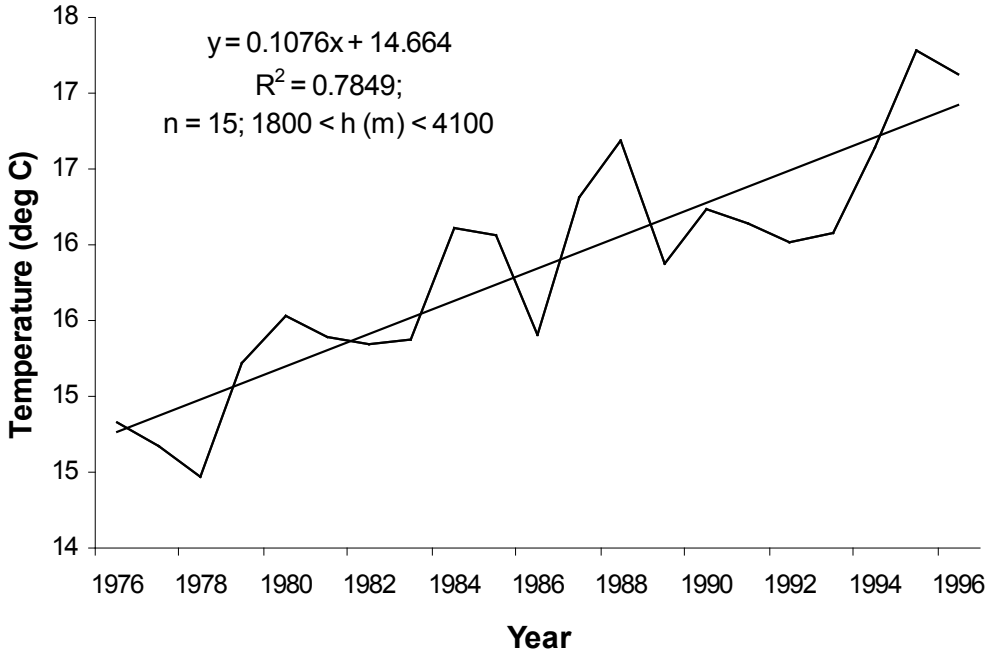

Figure 2.3 *Average annual temperature for Nepal, 1961-96 (15 stations > 1800m)*

These observations are consistent with those published by Shrestha *et al.* (1999), who reported warming trends from 0.06 to 0.12 °C/yr in annual maximum temperature data after 1977 for the Middle Mountains and Himalayan regions of Nepal.

An analysis of 78 long-term precipitation records from Nepal failed, however, to detect any significant trend (Shrestha et al., 2000), which would suggest that the apparent deglaciation in Nepal is occurring because of the increase in temperature rather than any change in the precipitation regime.

3 Modelling the impact of deglaciation

3.1 The need for a regional hydrological model

To determine the impact of deglaciation on the water resources of the entire Himalayan region requires a model that is capable of representing how glaciers and river flows respond to changes in climate. Inevitably, the impacts will vary, according to the relative importance of the monsoon and the contribution from snow and ice.

Several rainfall-runoff models havebeen applied successfully in the Himalayas. They include the HBV-ETH model (Bergström and Forsman, 1973), the HYCYMODEL from Japan (Fukushima, 1988), both of which have been applied to the Langtang Khola basin in eastern Nepal (Braun *et al.*, 1993, 1998; Fukushima *et al.,* 1991), the SLURP watershed model, which was used in the Satluj catchment in northern India (Jain *et al.,* 1998), the UBC watershed model, also applied to the Satluj (Singh and Quick, 1993), the HEC-1 model, applied to the Beas river basin in northern India (Verdhen and Prasad, 1993), and the Snowmelt-Runoff Model (SRM) (Martinec, 1975), which has been used in many Himalayan catchments including the Kabul river basin in Pakistan (Dey *et al.*, 1989) and the Beas and Parbati rivers in India (Kumar *et al.,* 1991, 1993). Although such models provide good predictions of river flows when calibrated for specific catchments, the parameter values that may be obtained for one model application may not necessarily be valid for another model in the same catchment or for the same model in a different catchment (Beven, 2001). For this project, a model was required that would estimate the river flows of many catchments across the entire Himalayan range; a model whose inputs are readily available throughout the region and whose parameter estimates are regionally applicable. Such a hydrological model, capable of being applied without calibration at the catchment scale, over a large geographic domain, is termed a "macro-scale model" (Arnell, 1999*a*).

3.2 The Regional Hydrological Model of the SAGARMATHA project

The regional hydrological model developed in the SAGARMATHA project is based on the macro-scale model described by Arnell (1999*b*), which provided grid estimates of average annual runoff, at a spatial resolution of 0.5° x 0.5° for the entire globe, using data from the Climate Research Unit (New *et al.*, 2000) as inputs to a modified

form of the CEH probability-distributed model (PDM) (Moore, 1985). The model was redefined in the project to provide estimates of seasonal and annual runoff for grid cells at a 20km by 20km resolution for the Indus, Ganges and Brahmaputra river basins (see Figure 3.1). The SAGARMATHA regional hydrological model consists of three key components: a rainfall-runoff model; a snow-pack model for representing the build-up of snow and its subsequent melting; and an innovative glacier-melt model for estimating the runoff contribution from many glaciers.

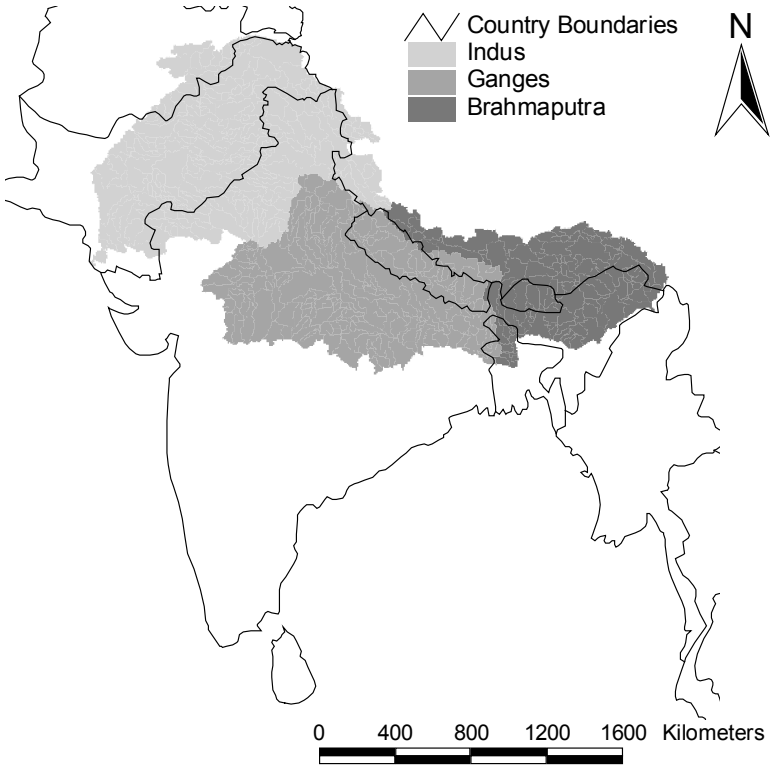

Figure 3.1 *Study area for the SAGARMATHA project*

3.2.1 The Probability-Distributed Model (PDM)

The PDM is a conceptual rainfall-runoff model, first developed at CEH in 1985 (Moore, 1985). The model described here is an adaptation of the original, and was developed to be applied across a large geographical domain, such that, its parameters could be defined *a-priori* according to the spatial distribution of vegetation and soil types. The model regards each grid cell as an individual catchment, with no routing of runoff between cells. It takes a conceptual water balance approach to rainfall-runoff

modelling, based on a soil moisture accounting procedure, and works at the daily time step.

Daily rainfall and potential evaporation (PE) data are required as inputs to the model. These were derived from the CRU 1961-90 standard period monthly climatological data. Monthly values of Penman-Monteith PE, calculated from the CRU data, were disaggregated to daily values by simply dividing the monthly average equally between the number of days in each month. The monthly rainfall was distributed evenly between the average number of rain days for the respective month, with the occurrence of rainfall (the rain days) arranged randomly every year of the model run.

The model also requires information on soil properties and vegetation within each cell. The soil data were obtained from the Food and Agriculture Digital Soil Map of the World and Derived Soil Properties (FAO, 1997) and the vegetation coverage from the USGS' Land Cover Characteristics Database, which contains 17 different land-types defined according to the IGBP land classification. The vegetation cover is required by the model to determine evaporation and soil moisture characteristics. The land cover data was also used to calculate the percentage cover of forest in each cell, while the soils information was used to calculate both the soil field capacity (the amount of water held in the soil against gravity) and soil saturation capacity (the amount of water held in the soil when all the pore spaces are full) (Vorosmarty *et al*.,1989). The PDM assumes a soil moisture store, with a capacity that varies across each cell, and a groundwater store. The parameters describe the size of these stores and the rate of removal of water from them. The soil moisture capacity (c) is assumed to be spatially variable across each cell and is represented by the following power distribution:

$$F(c) = 1 - \left[1 - \frac{c}{c_{\max}}\right]^{b} \qquad 0 \le c \le c_{\max} \qquad \ldots(3.1)$$

where the parameter, *b*, reflects the degree of spatial variability of the maximum storage capacity in the cell. A value of 0.0 would imply a constant capacity, with 1.0 representing a uniform variation. The c_{max} parameter is the maximum storage capacity within a cell. The amount of water that may be held in storage in the soil is represented by the integral of the above equation between 0.0 and c_{max}:

$$S_{\max} = \frac{c_{\max}}{(1+b)} \qquad \ldots(3.2)$$

The PDM works through a simple accounting procedure as follows:

$$S_t = S_{t-1} + P_t - AE_t - Q_t - D_t \qquad \ldots(3.3)$$

The soil moisture content (S_t) in the current period (day) is calculated as a function of the soil moisture content of the previous period (S_{t-1}), the rainfall (P_t) and the actual evaporation (AE_t). The soil moisture content is also reduced by direct runoff (Q_t) and the drainage of water from the soil into the groundwater store (D_t). The final runoff is determined as a function of Q_t and D_t, such that when the entire cell has reached capacity, direct runoff is:

$$Q_t = \left(P_t - AE_t - D_t\right) - (s_{\max} - S_t) \qquad \ldots(3.4)$$

It is assumed that all the water content in the soil above field capacity drains away in one day, so that the drainage term is:

$$D_t = S_t - FC \qquad \ldots(3.5)$$

where FC is the field capacity in millimetres. The AE_t is calculated as a function of the daily PE_t, which is an input to the model, and the field capacity. It is assumed that AE_t continues at the potential rate until field capacity is reached, thereafter it declines linearly to zero:

$$\frac{AE_t}{PE_t} = 1 \qquad \text{where} \quad S_t \geq FC \qquad \text{and} \qquad \ldots(3.6a)$$

$$\frac{AE_t}{PE_t} = \frac{S_t}{FC} \qquad \text{where} \quad S_t \leq FC \qquad \ldots(3.6b)$$

The model distinguishes between two vegetation types: grass and forest. The PE is assumed to be greater over forest than over grass, according to the ratio fPE (see Table 3.1). In addition to this distinction, the rainfall over the forest regions is assumed to be intercepted and subsequently evaporated. The daily interception model used was developed by Calder (1990):

$$I_d = \gamma\left(1 - e^{-\delta P}\right) \qquad \ldots(3.7)$$

where I_d is the daily interception, and γ and δ are parameters held constant across the entire study area.

The runoff is routed according to two parameters, S_{rout} and G_{rout}. The S_{rout} parameter determines the direct routing of runoff through two linear reservoirs and occurs once the entire catchment is saturated. The delayed runoff, or baseflow, is determined by the Q_{rout} parameter. The model, therefore, depends on 8 parameters as defined above and listed in Table 3.1 The s_{max} and FC parameters vary between cells, as defined by the spatial distribution of soils and vegetation data. The remaining 6 parameters are assigned values *a-priori,* based on previous applications of the PDM.

Table 3.1 *Parameters for the SAGARMATHA implementation of PDM*

Parameter	Value	Definition
b	0.25	Defines the variability in soil moisture content across each cell
S_{max}	Varies between cells	Total saturation capacity
FC	Varies between cells	Cell field capacity
S_{rout}	1	Direct runoff routing coefficient
G_{rout}	0.1	Delayed (baseflow) routing coefficient
Γ	0.75	Maximum daily interception loss
Δ	0.5	Parameter of the interception function
fPE	1.1	Ratio of forest to grass PE

3.2.2 The Snow-pack Module

The snow-pack module is applied only to cells where the mean monthly temperature of any month descends below +3 °C. Daily temperature and precipitation data, together with mean, minimum and maximum elevation of the cell are the key inputs.

As before, daily precipitation and temperature data were derived from the CRU 1961-90 baseline climatology. While daily precipitation was disaggregated evenly between rain-days (see Section 3.2.1), mean daily temperature values were calculated by linearly interpolating between the mean temperature of the previous and present month (for the first half of the month) and between the mean temperature of the present and next month (for the second half of the month). A degree of randomness was introduced to the interpolated values by adding, or subtracting, a

randomly generated value constrained to within ±1 °C of the original interpolated value.

Cells where snow is considered to occur are sub-divided into a number of equal height elevation bands (10, in the present application of the model). The distribution of cell area between bands (the cell hypsometry) is determined according to the Pareto distribution, such that *F(z)*, the proportion of the cell below the minimum elevation of any band, z, is expressed by:

$$F(z) = 1 - \left(1 - f(z)\right)^n \qquad \ldots(3.8a)$$

where

$$n = \frac{1}{f(z_{mean})} \qquad \text{and} \qquad f(z_{mean}) = \frac{z_{mean} - z_{\min}}{z_{\max} - z_{\min}} \qquad \ldots(3.8b)$$

and z_{mean}, z_{min} and z_{max} being the mean, minimum and maximum cell elevations respectively, which were obtained from overlaying the 20km x 20km onto the USGS' 1km x 1km HYDRO1k digital elevation data-set (USGS, 2001) in ArcGIS .

With the mean daily temperature for the cell, T_{mean}, assumed to apply at the cell's mean elevation, the daily temperature in each elevation band, T_{band}, is calculated by a temperature lapse rate model, as follows:

$$T_{band} = T_{mean} + \alpha\left(z_{mean} - z_{mid}\right) \qquad \ldots(3.9)$$

where z_{mid} is the mid-elevation of the band and α is the temperature lapse rate, taken as -5.5 °C/km. Precipitation is assumed to be uniformly distributed across all elevation bands in a cell.

Each elevation band is dealt with separately within the snow-pack module. For each band, precipitation is considered to fall as snow whenever the daily temperature of the band is less than a threshold temperature, T_{snow} . It is then assumed to melt as the temperature rises above a certain temperature, T_{melt} , at the constant rate of the degree-day-factor for snow, DDF_{snow} . The values used for these parameters are shown in Table 3.2.

Table 3.2 *Parameters for the snow-pack module*

Parameter	Value	Definition
T_{snow}	+2.0 °C	Temperature threshold to discriminate between rain and snow
T_{melt}	+1.0 °C	Temperature at which snow will begin to melt
DDF_{snow}	4 mm/°C/day	Degree-day-factor for snow, the volume of snow-melt in mm water equivalence per positive degree-day

The snow-pack module (Bell and Moore, 1999) conceptualizes the snow storage as a "dry" and "wet" store. New snow onto the snow-pack is added to the dry store. The wet store receives water directly as rainfall and as melt from the dry store, if the daily temperature is above T_{melt}. Water is released from the wet store at a rate proportional to the volume of melted snow. The melt-water then contributes to the PDM rainfall-runoff model that is applied to each elevation band. Where the dry-snow store in any elevation band is depleted, the rainfall contributes directly as input to the rainfall-runoff model in that band. The total daily runoff from the cell is thus calculated as sum of runoff from all bands, weighted by the area of each band:

$$Q = \sum_{i=1}^{n} Q_i \cdot \Omega_i \qquad \ldots(3.10)$$

where $\Omega_i = F(z_{i+1}) - F(z_i)$, the proportion of the cell area in elevation band *i*.

3.2.3 The Regional Glacier-melt Model

The vast majority of glacier–melt models previously developed have been applied and calibrated on single glaciers only. With an estimated 3000 glaciers in the Himalayas, it would be impossible to model each one individually. The regional glacier-melt model developed in this project is the first to attempt to represent the melt-water contribution from all glaciers in the region.

The model is based on the concept of a generic representation of glaciers postulated by Macdonald and Collins (2002). In this project, the concept is advanced further to conceptualise all glaciers contributing runoff to any individual 20 km x 20 km cell in the study area as a single "generic glacier". The generic glacier is ascribed an idealised shape and depth profile which are dependant on three key features of the contributing glaciers: minimum elevation, maximum elevation and area.

For this application, the spatial distribution and areal extent of Himalayan glaciers was obtained from the Environmental Systems Research Institute, Inc (ESRI) Digital Chart of the World (DCW), which was derived from 1:1,000,000 scale Operational Navigation Chart (ONC) vector base map (ESRI, 1993). All glaciers defined by the DCW were abstracted as polygons in ArcGIS and overlaid onto the HYDRO1k DEM to determine their minimum and maximum elevations and area. Every individual glacier was then associated to the respective 20km x 20km cell within which the minimum elevation occurred. If more than one glacier had its minimum in the same 20km x 20km cell, then the "generic glacier" of the cell was defined by the lowest minimum elevation, the highest maximum elevation and the total area of all contributing glaciers. The approach is illustrated with reference to Figure 3.1, where the generic glacier for the central 20 km x 20km cell is defined by glaciers A_1 and A_2, both of which have their minimum elevations in the same cell, but excludes glacier A_3, which has its minimum elevation in the adjacent cell. For *n* glaciers whose minimum elevations (or snouts) occur in a given cell, the generic glacier's defining features may be written as follows:

$$A = \sum_{i=1}^{n} A_i \qquad \text{and} \qquad \ldots(3.11a)$$

$$z\min = \min\{z\min_i, i = 1,2,..n\}, \quad z\max = \max\{z\max_i, i = 1,2,..n\} \qquad \ldots.(3.11b)$$

Each generic glacier was subdivided into 20 elevation bands of equal height between their respective *zmin* and *zmax*, and the area of each band was defined according to a pre-defined shape profile (Figure 3.3 & 3.4). The shape is considered to be "typical" of a Himalayan mountain glacier.

Attempts to characterise the depth of Himalayan glaciers have been few: Muller *et al.* (1997) estimated ice thickness in the Khumbu valley; Liu and Ding (1986) derived an equation for mean ice thickness, *H* (m), on the basis of a study in the Tianshan Mountains:

$$H = -11.32 + 53.21A^{0.3} \qquad \ldots(3.12)$$

where *A* (km^2) is the glacier area.

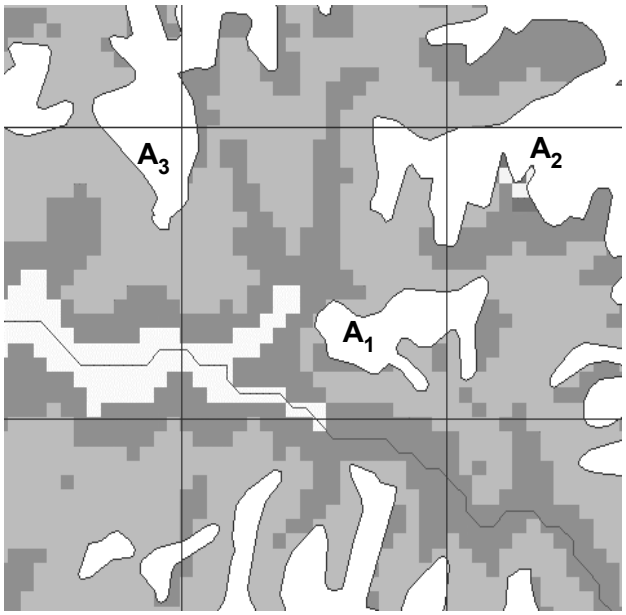

Figure 3.2 *Determining the areal extent of the generic glacier*

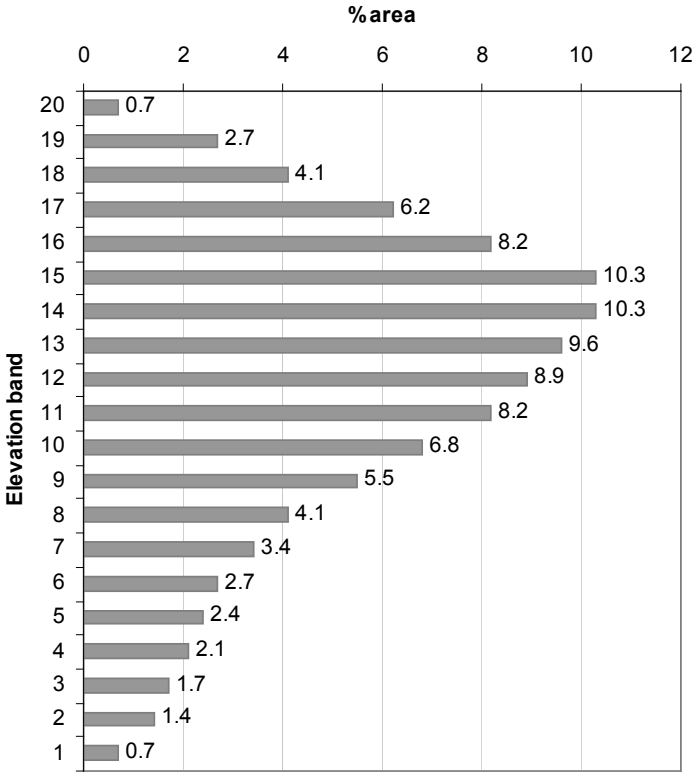

Figure 3.3 *Area distribution diagram for the generic glacier*

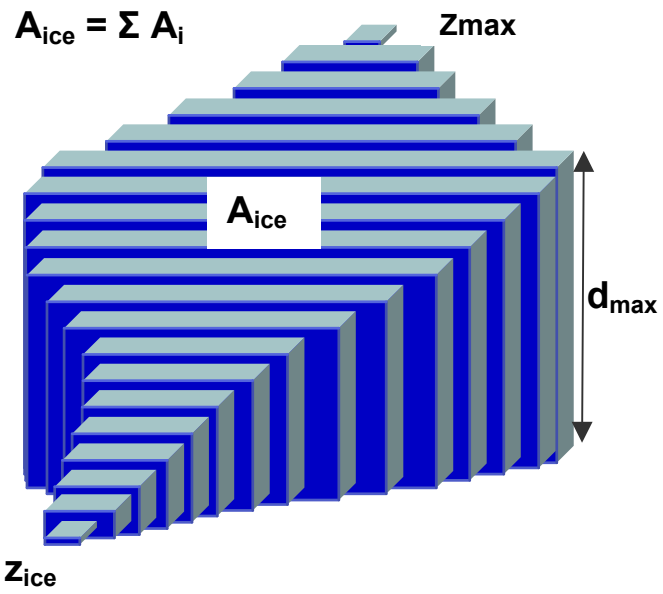

Figure 3.4 *A three-dimensional view of the generic glacier*

In the regional glacier-melt model, a triangular depth profile is assumed for the generic glacier, with the maximum depth occurring at three-quarters distance between *zmin* and *zmax* (i.e. at elevation band number 15) and a minimum depth of 10 m arbitrarily set at both extremes (elevation band numbers 1 and 20). The maximum depth is taken as *2H* (*H* being calculated according to *Equation 3.12* above, and where *A* is the total area of glaciers contributing to a cell, as in *Equation 3.11a*), but limited to a maximum depth of 240m (twice the maximum mean depth given by Muller *et al.* (1977)).

As with the Snow-pack Module, daily precipitation and temperature are used as inputs to the glacier-melt model. The mean daily temperature in each of the 20 elevation bands of the generic glacier is calculated from the 20 km cell's mean temperature, using the same temperature lapse rate model as before (*Equation 3.9*). The partitioning of rain and snow is also determined according to the same temperature threshold, T_{snow}.

The build-up of the snow on the glacier, and the snow-melt from it, is modelled using the Snow-pack Module (see Section 3.2.2). At the end of each calendar year, any dry snow remaining in an elevation band is redefined as "firn" and the dry snow store in the snow-pack module is re-set to zero. Before this, however,

the total volume of firn remaining at the end of the calendar year is redistributed evenly to augment the remaining ice-depth in all glacier elevation bands.

As temperature rises during the new calendar year, snow-melt is released from the newly accumulated snow-pack. If the dry snow store of an elevation band becomes fully depleted then the firn, if any, in the elevation band is exposed for melting. A simple degree-day model, with a degree-day-factor of 6 mm/°C/day, is used to determine the daily firn-melt contribution.

Ice-melt (ablation) only occurs from an elevation band once the dry snow store and firn have been exhausted, that is, when no more snow or firn is present in the band. The daily ice-melt, in mm water equivalence, is also calculated using a temperature index approach, with a value of 8 mm/°C/day used as the degree-day-factor for the ice. The ice-melt from an elevation band, plus rainfall, is then routed through a linear ice-melt store. In this application, the ice-melt store had a storage coefficient, k_{ice} , of 0.8. Ice-depth and the ice-melt store are updated daily.

Innovatively, the retreat, or deglaciaton, of the generic glacier is monitored within the model by recording the daily changes in the ice-depth in each band. Where the ice-depth of an elevation band has depleted to zero, the daily rainfall for the band is added directly to the glacier runoff, inferring an impermeable surface (bare rock) has been exposed.

The volume, V (m^3), of glacier runoff is thus calculated at the daily time-step as the total volume of water released daily from all, snow-, firn-, ice- and rock-covered glacier elevation bands ($i = 1, 2 \ldots n$):

$$V = \sum_{i=1}^{n} A_i \cdot Q_i \cdot 1000 \qquad \ldots(3.13)$$

where A_i is the area (km^2) of band i, and Q_i is the runoff from the band (mm). No routing of runoff is applied between the glacier elevation bands. The daily runoff from the glacier is considered a point source, expressed as a uniform depth of runoff, Q_g, in mm, over the 400 km^2 area of the 20km x 20 km cell:

$$Q_g = V/(400 \times 1000) \qquad \ldots(3.14)$$

The daily runoff from the non-glaciated part of the cell, Q_s, is calculated by applying the snow-pack module, as described in Section 3.2.2. The total daily runoff for the cell is, therefore, finally calculated by:

$$Q = Q_g + (1 - P_{ice}) \cdot Q_s \quad \ldots(3.15)$$

where P_{ice} is the proportion of the cell initially covered by ice, which is calculated by overlaying the DCW glacier polygons onto the 20 km x 20 km grid in ArcGIS. As contributing glaciers may extend into neighbouring cells, $P_{ice,}$ is not equivalent to the area of contributing glaciers.

4 Model Application

4.1 Input data

The regional hydrological model was applied in each of the three basins of the study area. The climatological data that were used as input to the model were downscaled to the 20km x 20 km grid resolution from the 0.5° x 0.5° standard period (1961-90) baseline climatology of the Climate Research Unit (CRU) (New *et al.*, 2000). Penman Monteith monthly Potential Evapotranspiration was calculated at the 0.5° resolution from pertinent variables in the CRU climatology, and then similarly downscaled to 20 km. Grids of average monthly precipitation, rain-days, temperature and PE were produced at the required resolution and stored as 48 (4 variables x 12 months) separate ASCII files in ArcGIS format.

A variety of physiographical data-sets, also required by the model, were prepared at the same 20 km x 20 km resolution for each of the basins. A summary of the required input data is given in the table below.

Table 4.1 *Input data for the regional hydrological model*

Data type	Description	Derivation
Precipitation	12 average monthly values for the 1961-90 standard period	Derived from the CRU baseline climatology
Rain-days		
Temperature		
Potential Evapotranspiration		
Predominant soil type	Majority value (dominant) of 7-type soil classification	Derived from FAO Digital Soil Map of the World
Forest cover	Proportion of forest cover in cell	Derived from the USGS Eurasia Land Cover Characteristics Database
Minimum cell elevation	Minimum, maximum and mean elevation of 1 km cells within the 20 km x 20 km cell	Derived from the USGS' 1 km x 1 km HYDRO1k DEM
Maximum cell elevation		
Mean cell elevation		
Contributing glacier area	Area of glacier ice contributing runoff to a cell	Derived from ESRI's Digital Chart of the World (DCW)
Proportion of ice	Proportion of cell that is covered by ice	Derived from the DCW
Minimum ice elevation	Lowest and highest elevation of contributing glaciers	Derived from the DCW and HYDRO1k
Maximum ice elevation		

4.2 Model scenarios

4.2.1 Baseline Scenario

The regional model was first applied using the CRU 1961-90 baseline climatology (precipitation, rain-days, temperature and PE) for a 30-year model run at the daily time-step: the monthly CRU data having been disaggregated as described in Section 3.2. The resulting daily runoff values for each cell were aggregated at run-time to give estimates of mean monthly, seasonal and annual runoff for each cell in each basin of the study area (see Figure 4.1). Summer runoff was defined as the average total runoff for the months April to September; winter runoff the average total runoff from October to March. These results were taken as the "control", or "baseline", for comparison with subsequent scenarios.

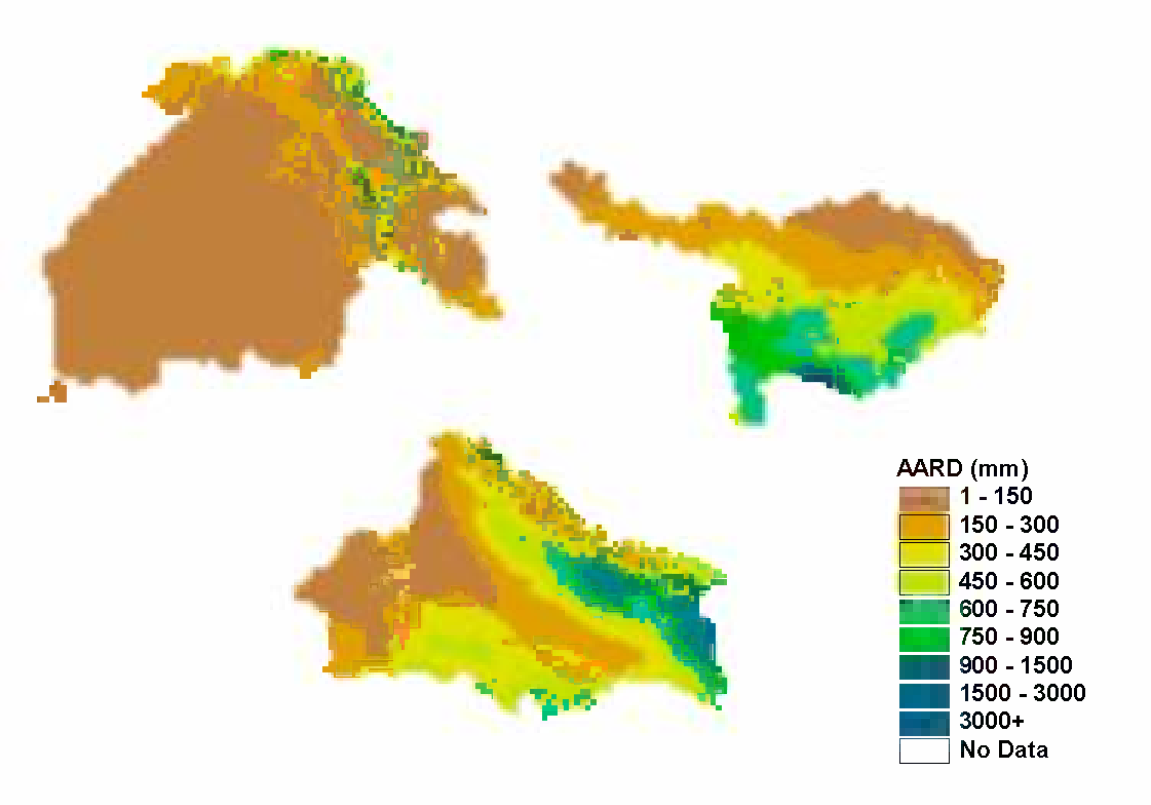

Figure 4.1 *Baseline Average Annual Runoff for the Indus, Ganges and Brahmaputra river basins, from the SAGARMATHA regional hydrological model*

4.2.2 Climate change scenarios

A representation of the future climate is necessary to model deglaciation and its effect on the water resources of the Himalayas. Two types of climate change scenarios were considered in this project: incremental scenarios and climate model-based scenarios.

Incremental scenarios are simple adjustments of the baseline climate according to anticipated future changes. Fukushima *et al.* (1991) and Braun *et al.* (1993) both used incremental scenarios in their application of two different rainfall-runoff models in the 333 km^2 Langtang Khola basin in Nepal, finding that an increase in the mean daily air temperature of 2°C resulted in a 100% and 50% increase in river flows respectively.

Most climate-model scenarios use the output from general circulation models (GCMs) and are usually constructed by adjusting a baseline climate by the absolute or proportional change between the present and future climates (IPCC, 2001*a*). Climate models are generally driven by projections of future emissions of greenhouse gases (e.g. carbon dioxide, methane, nitrous oxides, sulphur dioxide, etc.). As can be seen in recent IPCC reports (2001*a&b*), a large number of emission scenarios have been developed and applied in numerous GCMs to provide forecasts of future climate changes, including changes in temperature and precipitation. Designed to provide predictions of future climate on a global scale, GCMs are generally unable to represent local variations in weather and climate that may be caused by complex topography or land-use. Obtaining the regional detail that is often required from the coarse-scale output of GCMs can be achieved using statistical downscaling or high-resolution regional climate models (RCMs). Regional climate models, using GCM outputs as boundary conditions, provide estimates of time-dependent climate variables at a high spatial resolution (~0.5°) at the regional scale. The higher resolution of RCMs makes it possible for them to better represent the local variations of climate variables in mountain areas. Application of the Hadley Centre RCM, HadRM2, in South Asia shows that precipitation anomalies were more realistically captured by the RCM (Hassell & Jones, 1998).

In this project, the regional hydrological model was applied with 4 incremental scenarios of increasing temperature, 2 incremental scenarios of increasing temperature with increasing precipitation, 2 incremental scenarios of increasing temperature but decreasing precipitation and one climate-model based scenario, based on output from the HadRM2 RCM. The incremental scenarios were applied uniformly to all cells in

each respective basin; the increment being added, or subtracted, annually to the relevant baseline variable. The applied scenarios, and their basis, are summarised in Table 4.2.

Table 4.2 *Climate-change scenarios*

Scenario code	Annual Incremental change		Basis of scenario
	T (°C/yr)	P (%/yr)	
CTL	0	0	CRU baseline applied, with no incremental changes in P or T
T03	+0.03	0	Average global warming predicted by IPCC (2001a)
T06	+0.06	0	Observed warming from temperature gauges in Nepal
T10	+0.10	0	Observed warming from highest 15 gauges in Nepal
T15	+0.15	0	Extreme "hypothetical" scenario
PHM	+0.06	+0.2	High precipitation scenario for South Asia, after Giorgi & Francisco (2000) in IPCC (2001a), with medium and high temperature scenarios.
PHH	+0.15	+0.2	
PLM	+0.06	-0.2	Low precipitation scenario for South Asia, after Giorgi & Francisco (2000) in IPCC (2001a), with medium and high temperature scenarios.
PLH	+0.15	-0.2	
RCM	Spatially variable		Derived from HadRM2 RCM (Hassell & Jones, 1998)

The model was run for all but the "CTL" and "RCM" scenarios at the daily time-step for a period of 100 years, with the outputs presented as decadal averages of annual and seasonal runoff. For the RCM scenario, the model ran at the daily time-step for a period of 70 years, to represent the period 1991 to 2060.

The HadRM2 RCM in South Asia generates forecasts of future climate, as described by various climatological variables, at a spatial resolution of approximately 0.5° for the period 2041-2060. Two sets of daily data are available for this 20 year period: a control climate, which has evolved from 1991 using fixed, present-day atmospheric carbon dioxide (CO_2) concentrations; and a perturbated climate, which has evolved from 1990 with a compound 1% per year increase in CO_2.

For the "RCM" scenario, inconsistencies between the CRU baseline data and the HadRM2 data, meant that the HadRM2 data had to be pre-processed to determine

the average forecast change (Δ) in monthly precipitation, temperature and PE for every 20 km cell in the study area (see Figure 3.8). These values were assigned to the mid-point of the 2041 to 2060 period. An annual increment was then calculated for each of the 3 climate variables (P, T & PE) in a cell, corresponding to the annual increase, or decrease, of the variable between 1991 (the end of the period covered by the CRU baseline data) and 2050 (the mid-point of the RCM data) (i.e. Δ/60). The regional model was then run for 70-years, representing the period 1991 to 2060, with the appropriate annual increment applied each year to the 3 climate variables in each cell. This dynamic representation of climate between the end of baseline period (1991) and the start of the RCM period (2041) was another innovative aspect of the project, and was necessary in order to describe the evolution of glaciers in this time.

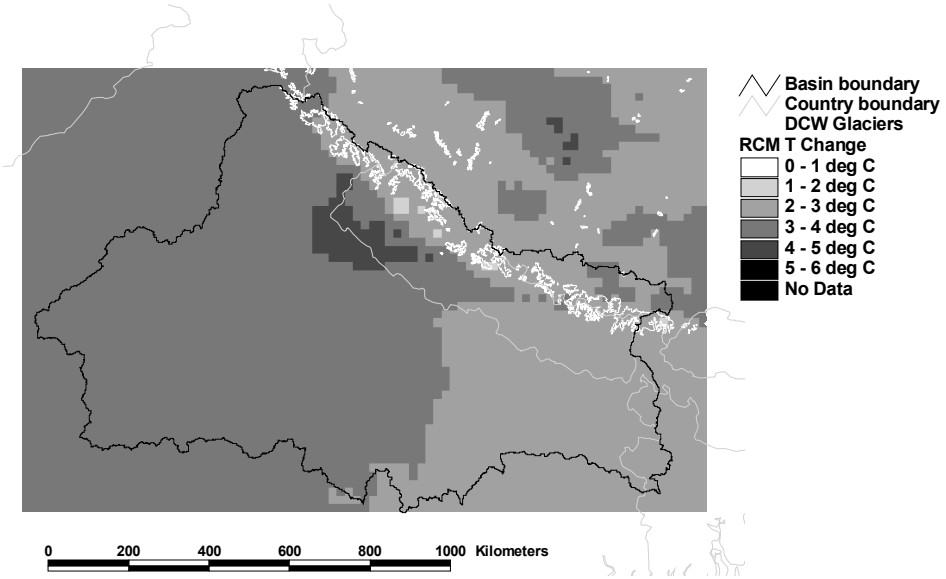

Figure 4.2 *Change in average annual T for 2041- 2060 from, HadRM2 (Ganges)*

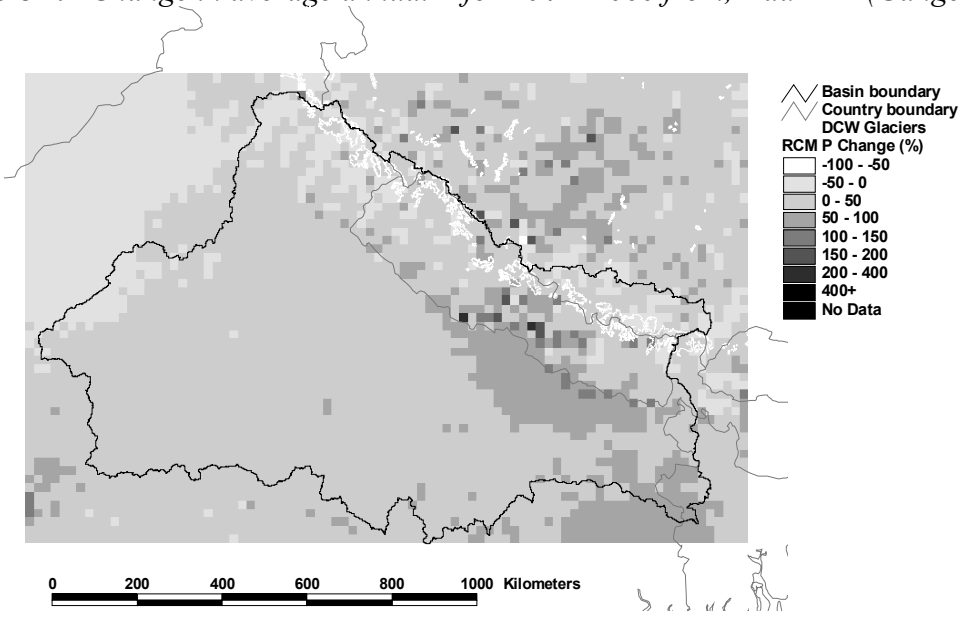

Figure 4.3 *Change in average annual P for 2041- 2060 from HadRM2 (Ganges)*

4.3 Results Processing

The objective of the SAGARMATHA project is to assess the impact of deglaciation on the water resources of the Himalayas. To do so, the outputs from the regional hydrological model, representing the areal distribution of runoff at a 20 km x 20 km resolution, were "translated" into river flows. Comparisons were then made between baseline flows and those from the various scenarios to analyse how the surface water resource availability of rivers may be affected by climate change.

4.3.1 Derivation of flow estimates

The model outputs – estimates of seasonal and annual runoff at a 20 km x 20km grid resolution - were written to ASCII files in an ArcGIS compatible format. For each basin, three files resulted from the "CTL" scenario, representing the baseline winter, summer and annual conditions, 30 files resulted from each incremental scenario (3 files (winter, summer and annual) per decade of the 100-year run), and 21 files resulted from the "RCM" (3 files per decade of the 70-year run). The results show how runoff varies decade by decade from a nominal start date of 1991.

Every output file was imported as a grid into ArcGIS and re-sampled to the same 1km x 1km resolution of the USGS HYDRO1k DEM. A flow-accumulation grid was then derived for every 1 km output grid, using the flow-direction grid of HYDRO1k (a derivative of the DEM). The flow-accumulation grid represents the total runoff accumulated at a single cell from all upstream cells, as defined by the flow-direction grid. The accumulated runoff of every cell, expressed in mm, was then converted to units of flow (m^3/s) to produce a grid of annual or seasonal flow, as shown in Figure 4.4. Seasonal and annual flow estimates could thus be obtained for any location on any stream or river in each of the three basins, for any scenario. A comparison of baseline mean flow estimates with observed flow data at specific gauging stations reveals that the regional hydrological model generally provides a reasonable approximation of actual, although, as would be expected, variability of results appears greatest in smaller catchments (see Table 4.3).

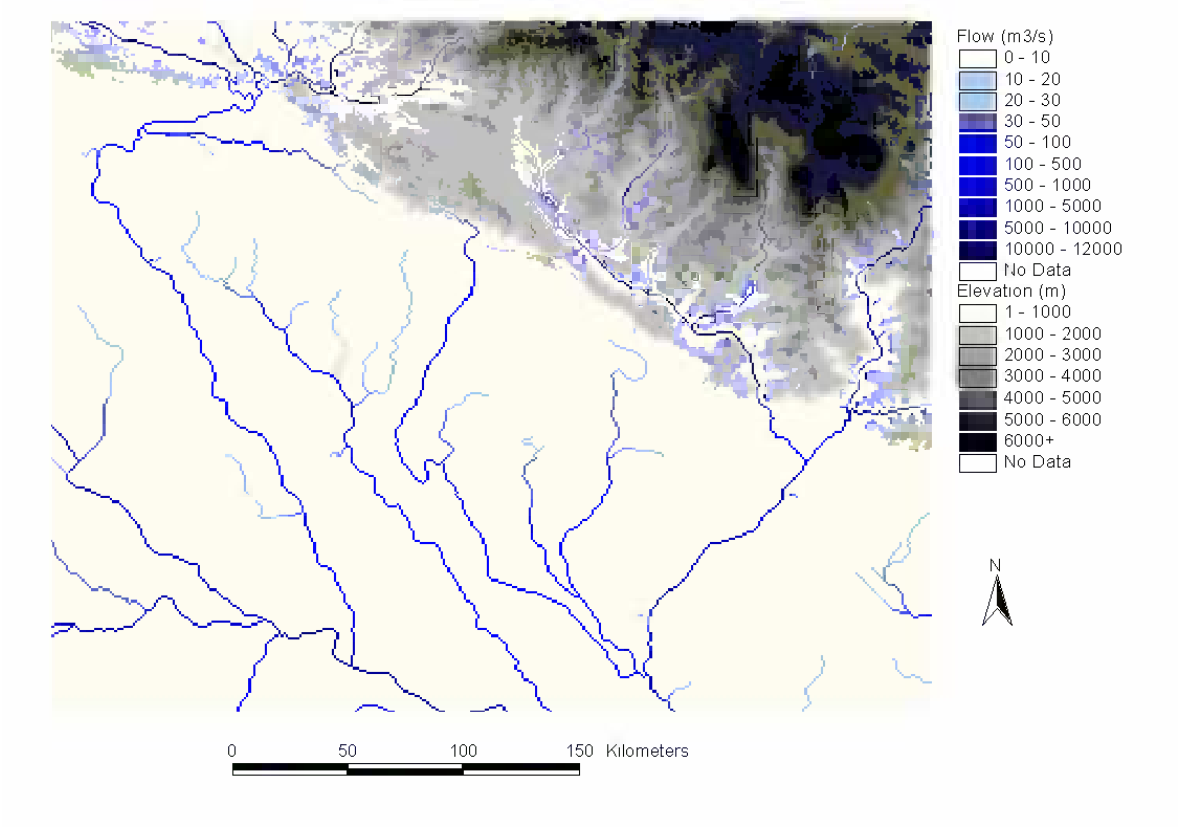

Figure 4.4 *Mean flow in the Ganges basin, derived from output of the regional hydrological model and the HYDRO1k flow-direction grid*

Table 4.3 *Comparison of modelled and observed mean flow*

Gauging Station	**Mean flow (m3/s)**		**Bias Error (%)**
	Modelled	**Observed**	
Ganges at Farakka	9850	12293	-19.9
Ganges at Hardinge Bridge	11091	11146	-0.5
Hunza at Danyore	356	366	-2.7
Indus at Partab Bridge	1590	1770	-10.2
Indus at Besham Qila	1653	2450	-32.5
Indus at Kotri	3874	2626	47.5
Chenab at Akhnoor	268	788	-66.0
Arun at Turkghat	437	415	5.3
Sun Kosi at Kumpughat	408	767	-46.8
Tamur at Mulghat	245	337	-27.3

4.3.2 Comparison of future flows

Having derived 1 km grid maps of average decadal flows for every scenario in each basin, a comparison of how flows would vary from decade to decade, relative to the baseline, was achieved by overlaying in ArcGIS the respective decadal grid onto the relevant baseline grid. Cell values in the resulting "comparison" grids express the change in flow as a percentage (%) of the baseline. Using GIS, the grids can either be plotted to provide an overview of how the impacts may vary across the basin, as shown in Figure 4.5, or interrogated to see how flows, at specific points, could vary under different climate change scenarios (e.g. Figure 4.7).

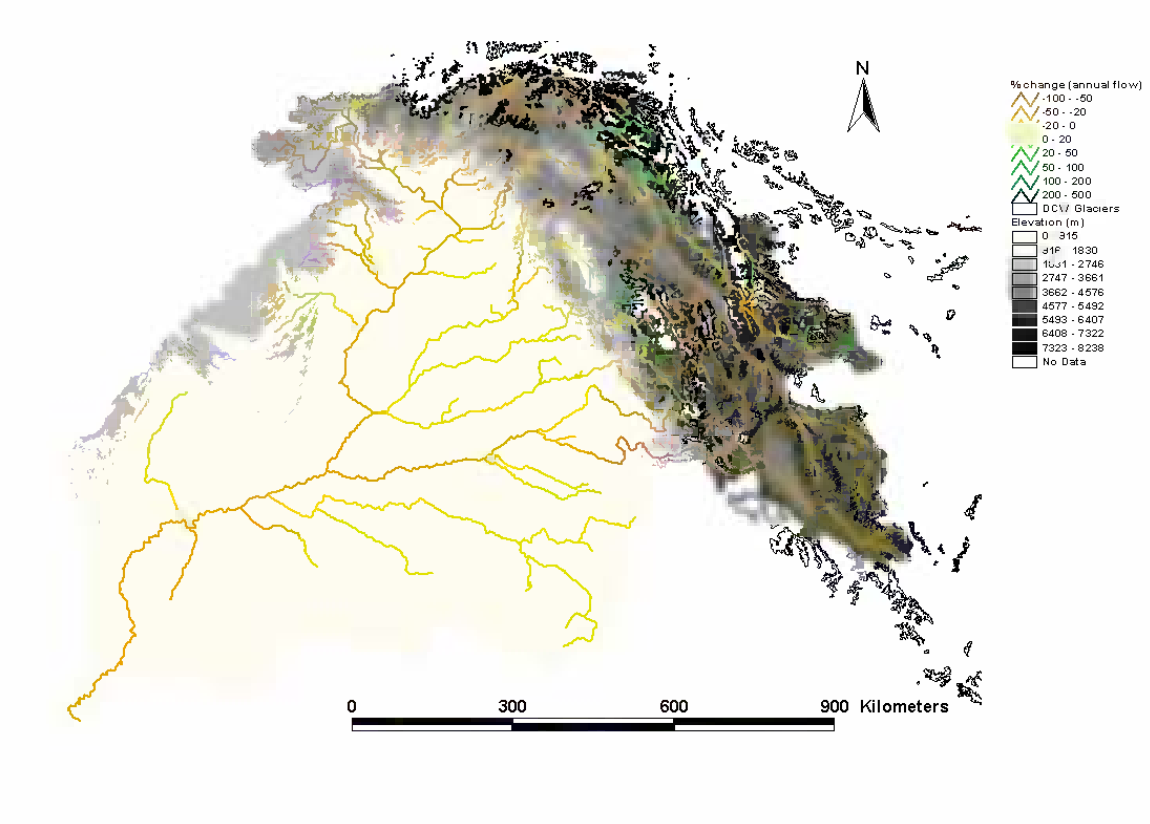

Figure 4.5 *% change in mean flow of the Indus by decade 10, scenario = +0.1 °C/yr*

To assess how future river flows across the region would be affected by deglaciation, attention was focused on 21 locations in the four "focus-areas" shown in Figure 4.6. Results from six sites in the Upper Indus basin were studied, along with 7 sites in the Brahmaputra basin and 8 sites in two parts of the Ganges river basin. Some of the results obtained are illustrated in Figures 4.7 through to Figure 4.20; a full set of graphs is shown in Annex 1. Basic information describing each study site, its

catchment area, percentage glaciation, baseline mean flow and mean winter flow is given in Table 4.3.

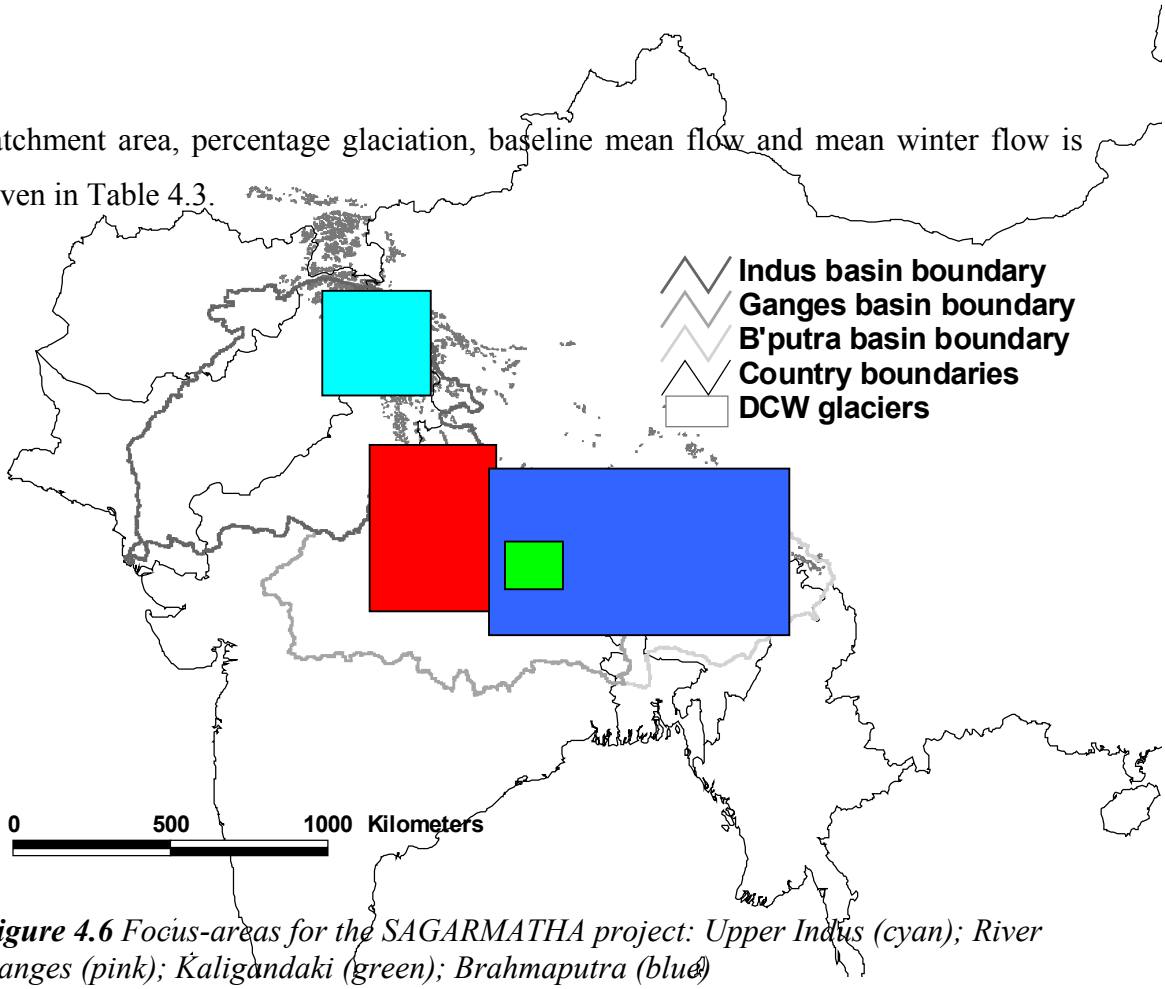

Figure 4.6 *Focus-areas for the SAGARMATHA project: Upper Indus (cyan); River Ganges (pink); Kaligandaki (green); Brahmaputra (blue)*

Table 4.4 *Study sites of focus-areas*

Site name	Catchment area (km^2)	% glaciation	Baseline mean flow (m^3/s)	
			Annual	Winter
Upper Indus				
Gilgit at Gilgit	14138	11.7	172	39
Hunza at Danyore	27996	25.2	356	64
Indus at Partab Bridge	167982	16.0	1591	248
Indus at Skardu	127099	13.1	1077	162
Shyok at Shyok	38312	16.2	333	36
Indus at Besham Qila	187118	14.6	1702	300
Ganges				
Ganges at Uttarkashi	4524	23.4	85	25
Ganges at Haridwar	23191	16.1	338	108
Ganges at Kanpur	89878	4.2	749	345
Ganges at Allahbad	424937	0.9	2900	1444
Kaligandaki				
Modi Khola at Kusma	642	16.5	14	7
Kaligandaki at Seti Beni	7104	9.3	82	43
Kaligandaki at Katagon	12235	5.4	214	117
Narayani at Devghat	32137	9.7	570	292
Brahmaputra				
D' Zangpo at Samsang	3784	3.0	22	12
D' Zangpo at Xungru	33600	1.9	293	149
Y' Zangpo at Xigaze	103612	0.8	1093	591
Nyang Quu at Gyongze	10960	0.8	184	97
Wong Chhu at Thimpu	748	0.9	17	8
Trongsa Chhu at Zhengang	2755	5.2	161	55

B’putra at Singing	229323	2.1	2077	1114

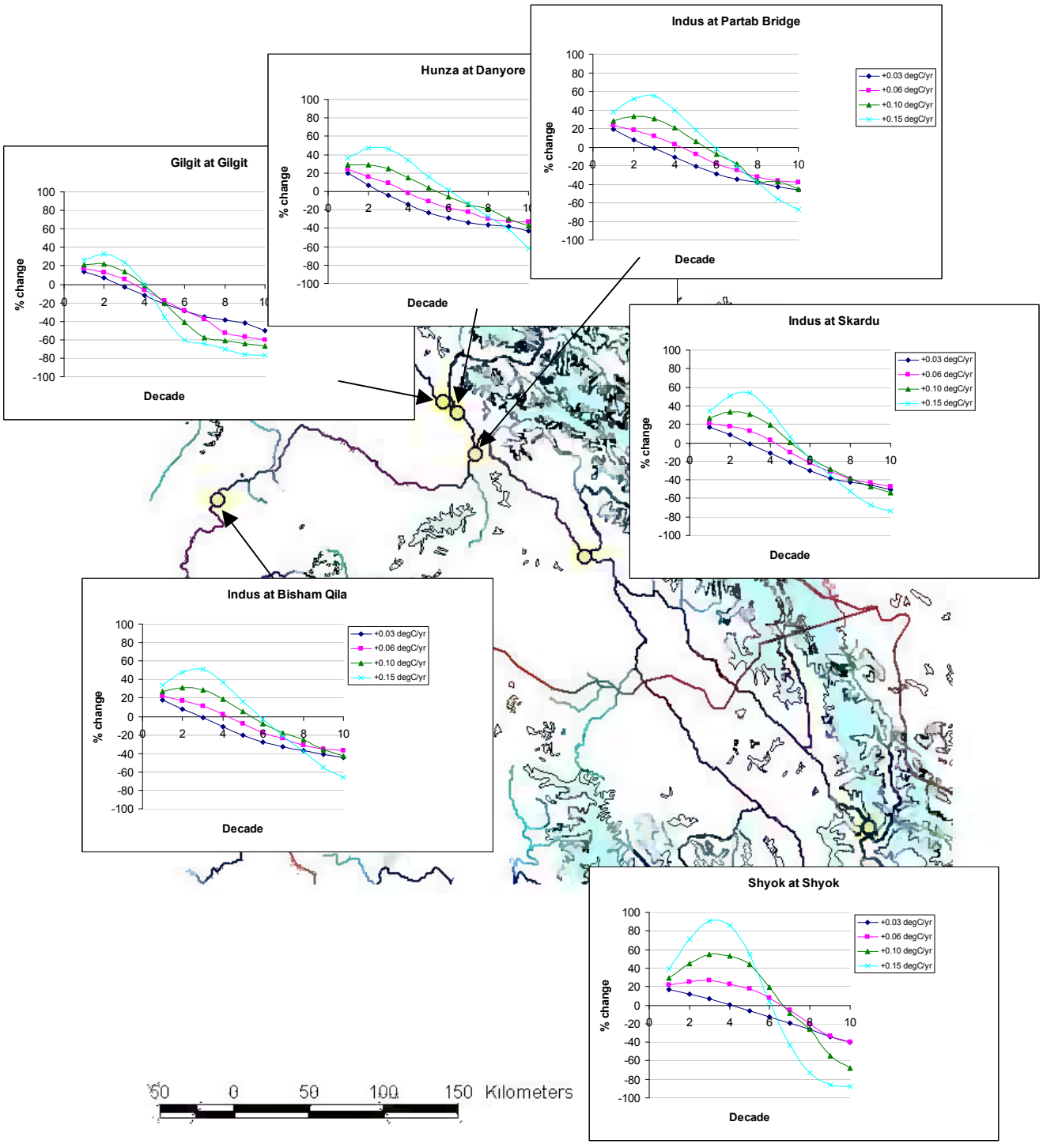

Figure 4.7 *Decadal variation in mean flow (Upper Indus): all T scenarios (T = +0.03, +0.06, +0.10, +0.15°C/yr)*

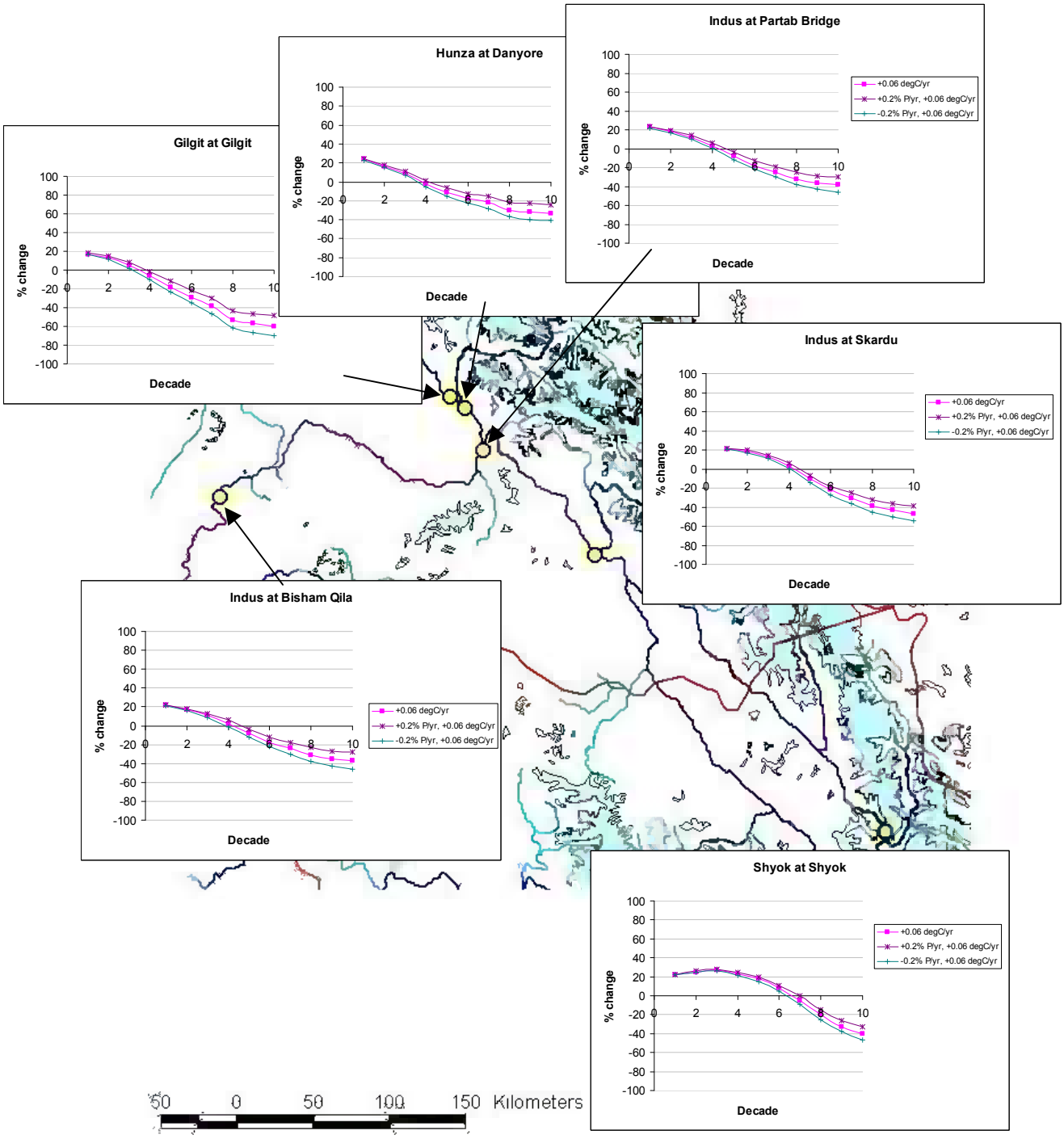

Figure 4.8 *Decadal variation in mean flow (Upper Indus): P and T scenarios combined (P = ±20% over 100 yrs; T = +0.06°C/yr)*

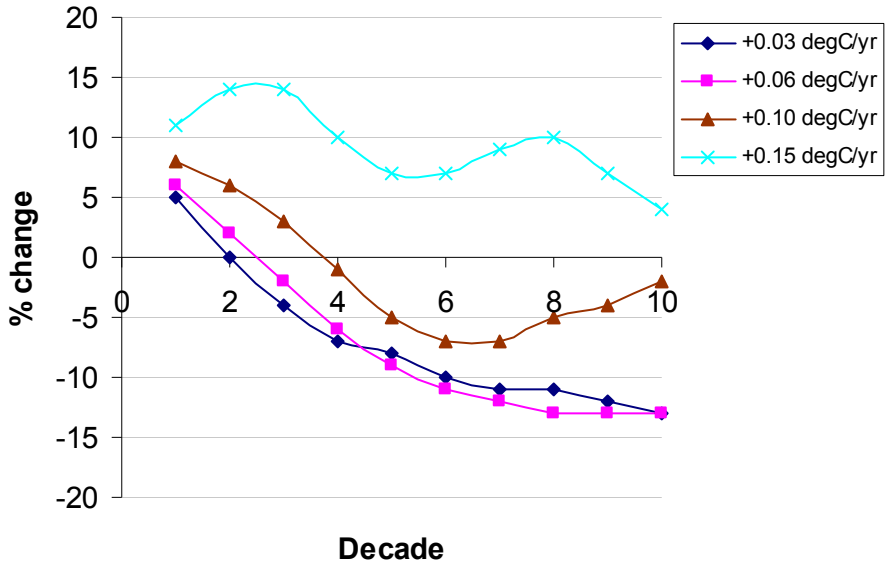

Figure 4.9 *Decadal variation in mean winter flow (Indus at Partab Bridge): all T scenarios*

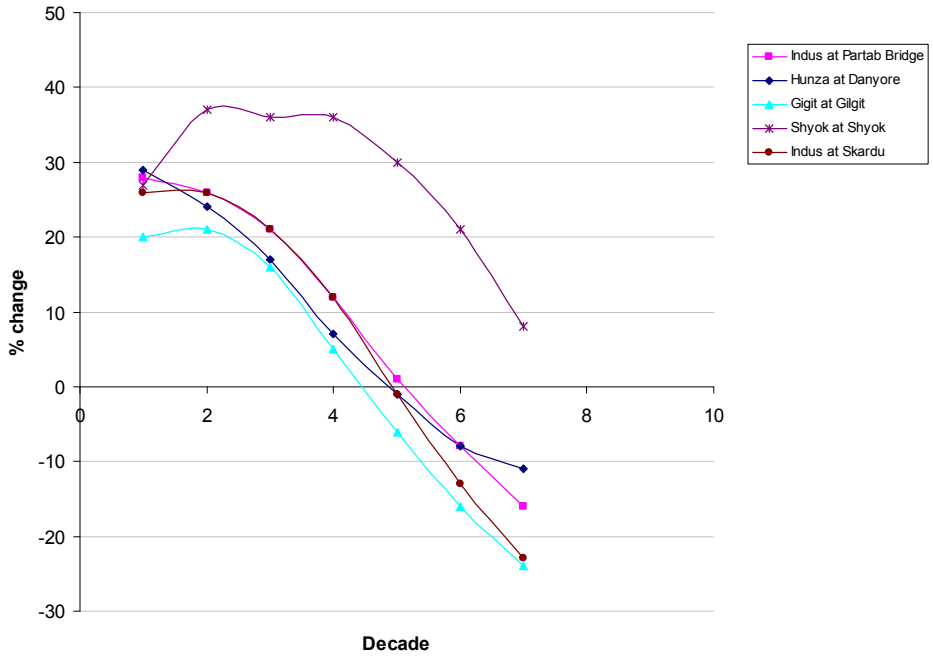

Figure 4.10 *Decadal variation in mean flow, all selected locations (Upper Indus): RCM scenario*

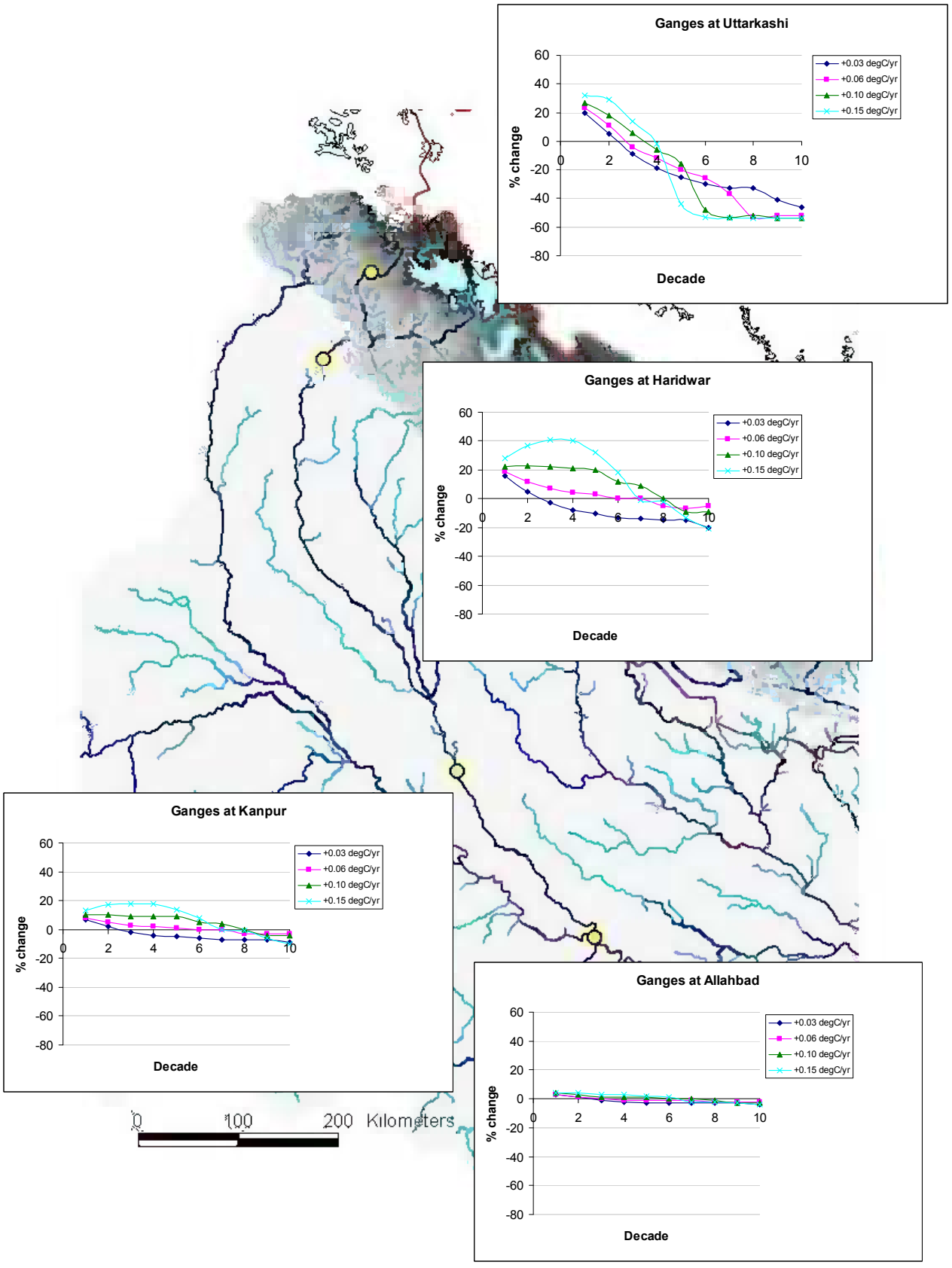

Figure 4.11 *Decadal variation in mean flow (River Ganges): all T scenarios (T = +0.03, +0.06, +0.10, +0.15°C/yr)*

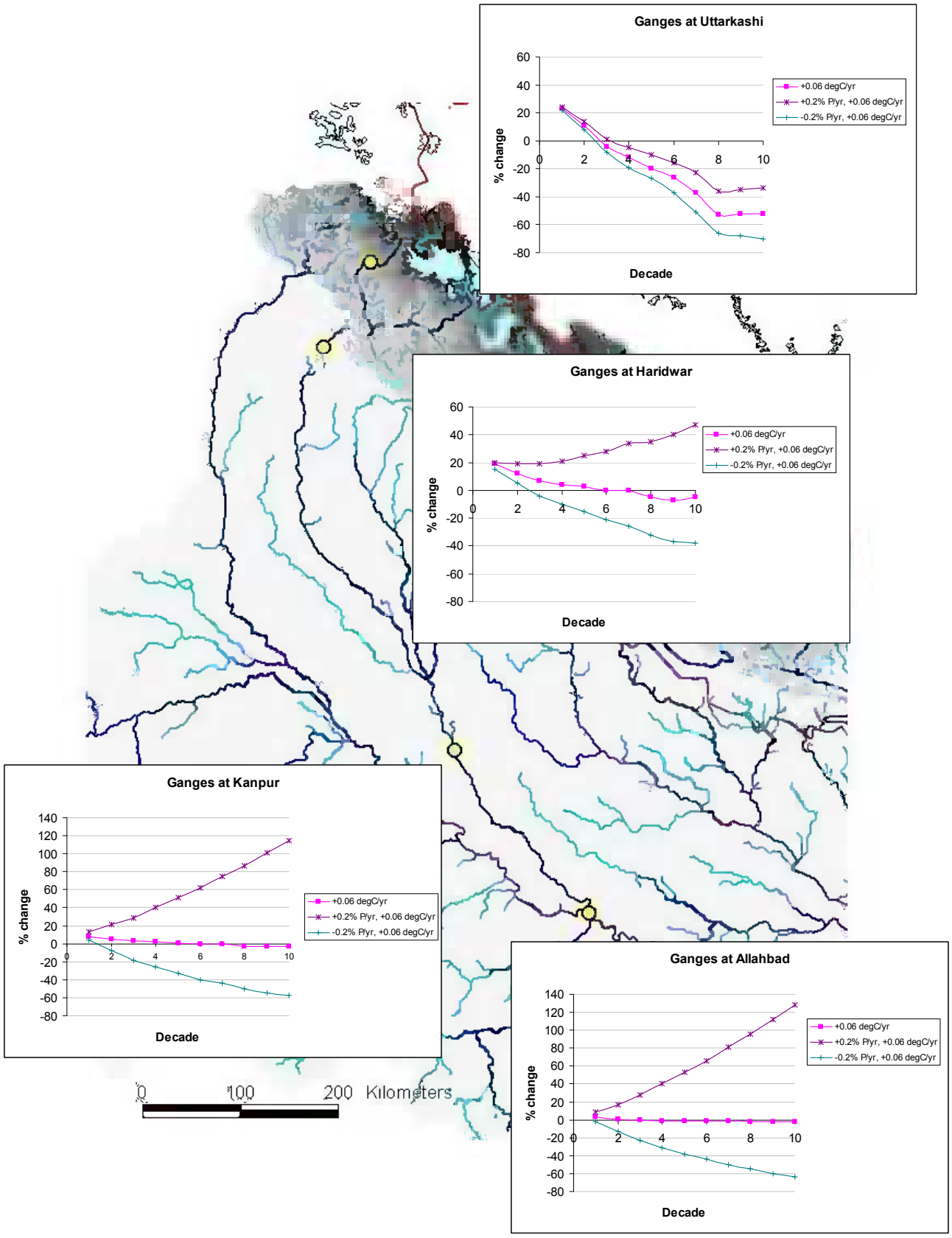

Figure 4.12 *Decadal variation in mean flow (River Ganges): P and T scenarios combined (P = ±20% over 100 yrs; T = +0.06°C/yr)*

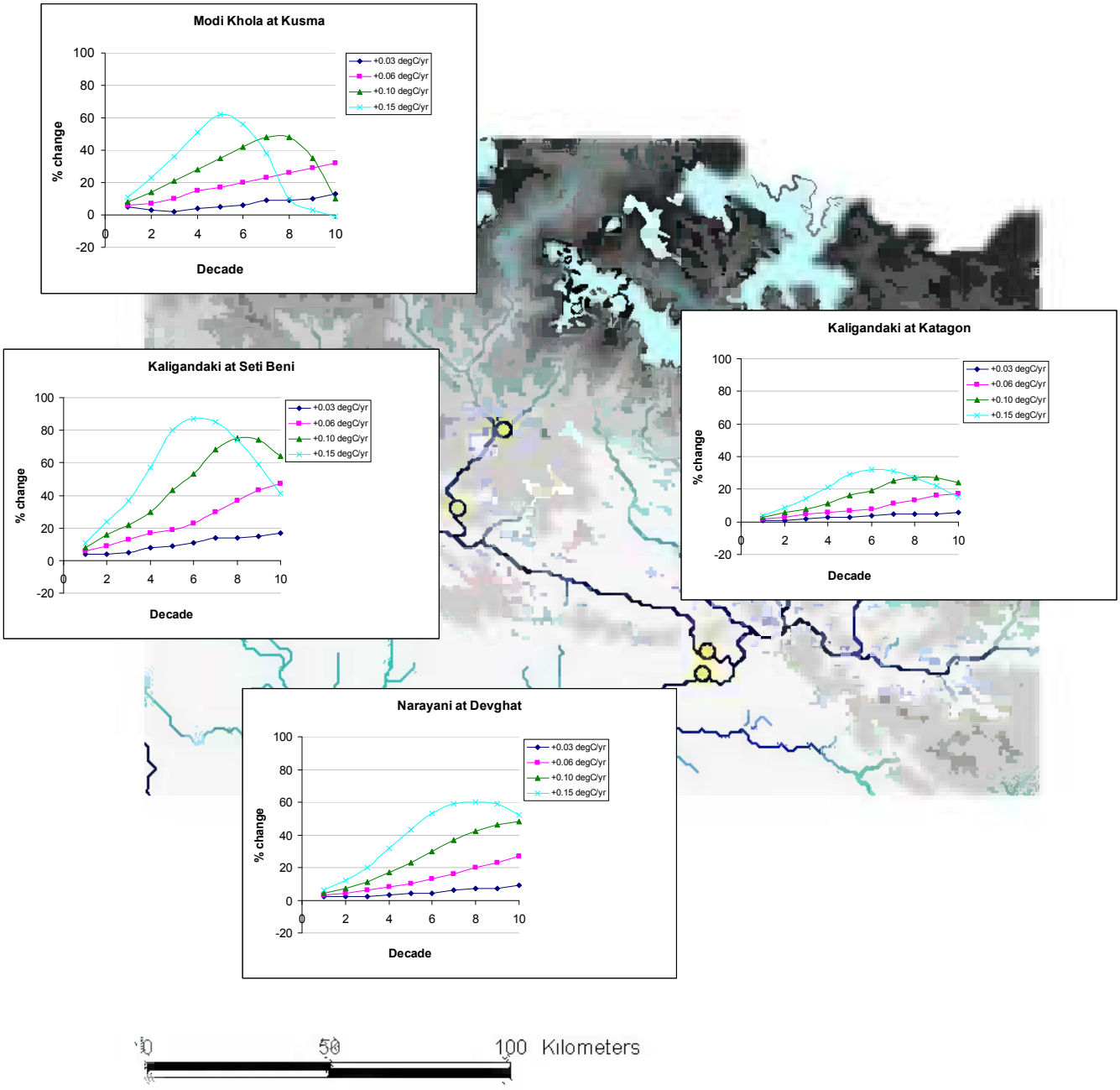

Figure 4.13 *Decadal variation in mean flow (Modi Khola, Kaligandaki, Narayani rivers): all T scenarios (T = +0.03, +0.06, +0.10, +0.15°C/yr)*

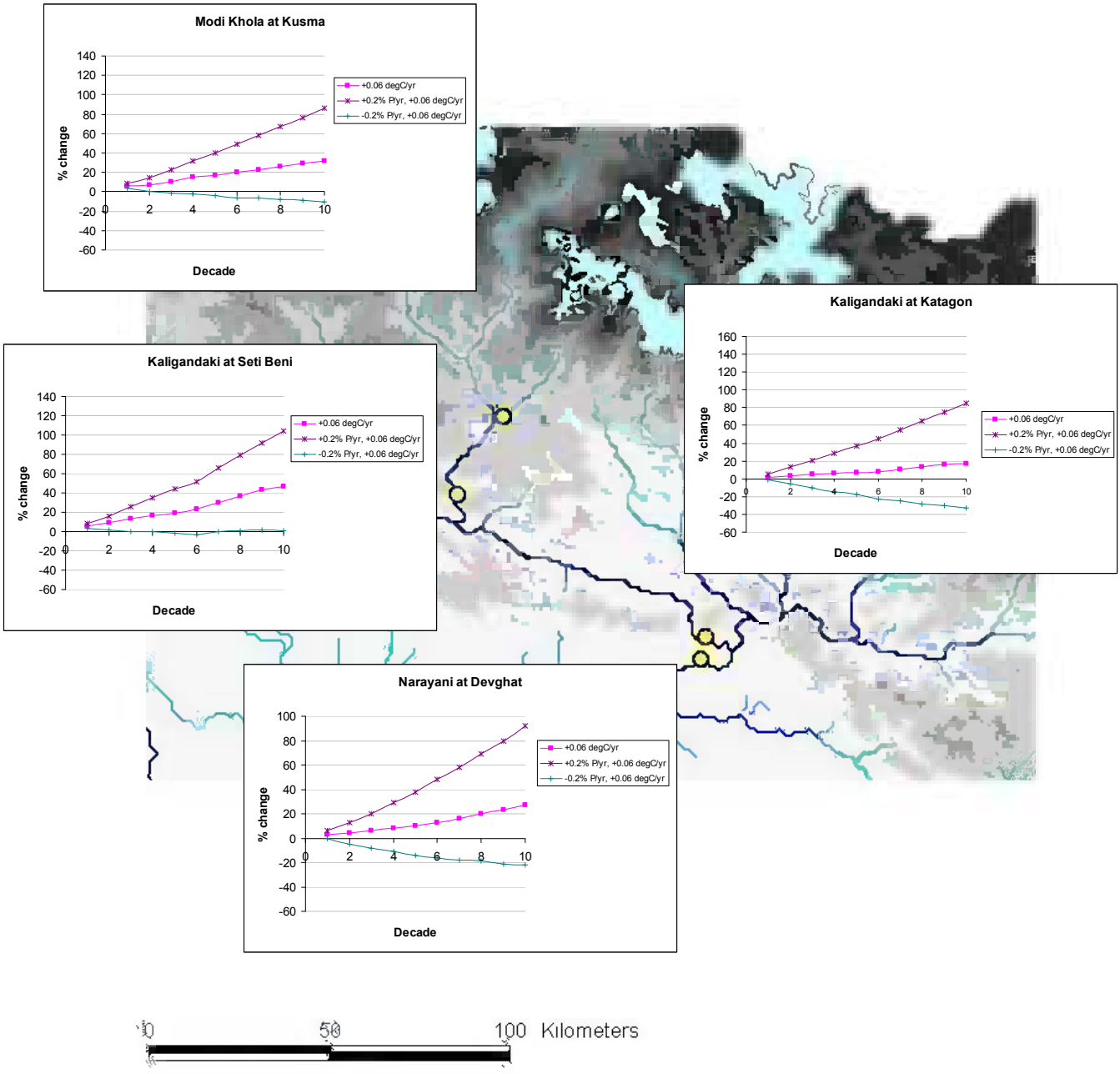

Figure 4.14 *Decadal variation in mean flow (Modi Khola, Kaligandaki, Narayani rivers): P and T scenarios combined (P = ±20% over 100 yrs; T = +0.06°C/yr)*

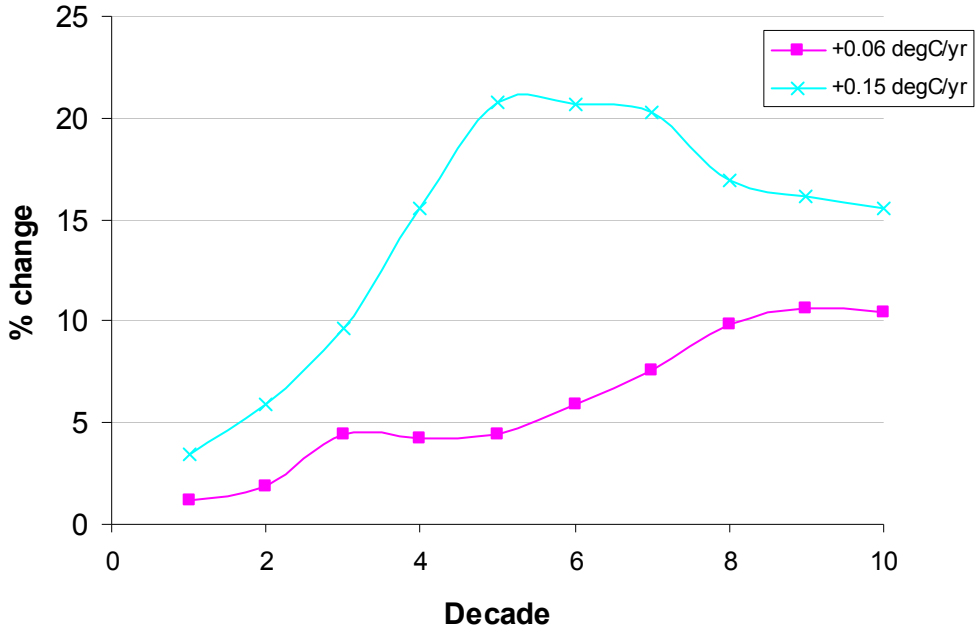

Figure 4.15 *Decadal variation in winter flow (Modi Khola)*

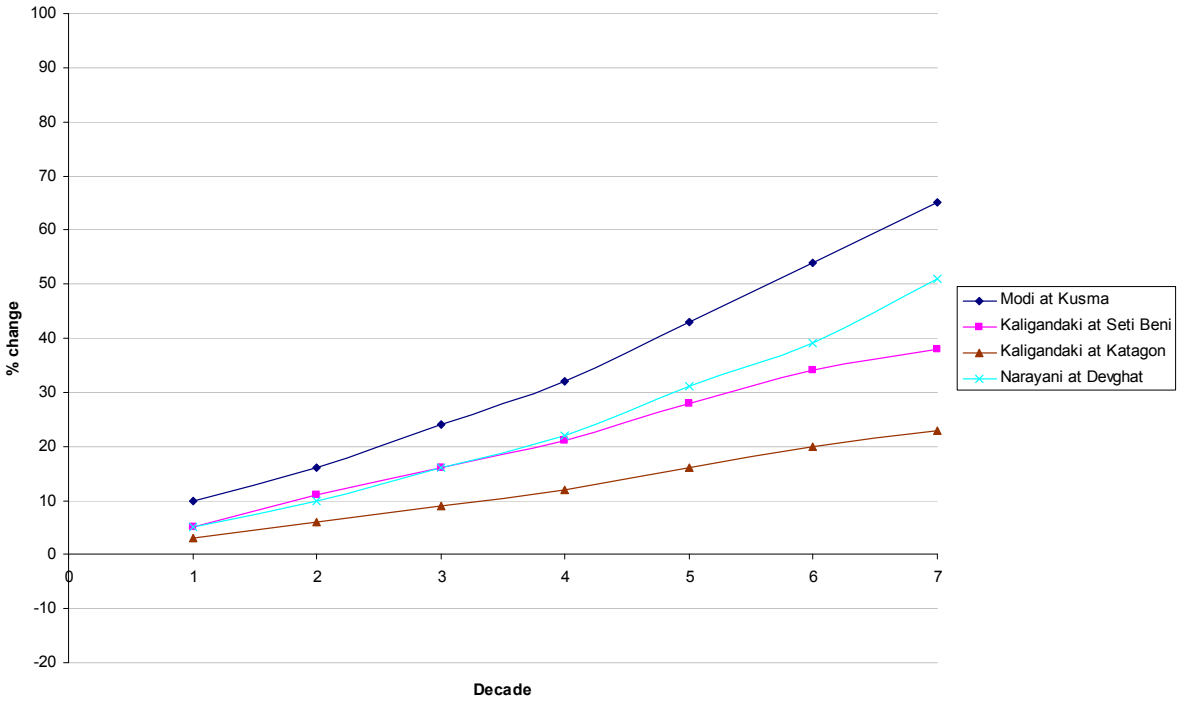

Figure 4.16 *Decadal variation in mean flow, all selected locations (Modi Khola, Kaligandaki, Narayani rivers): RCM scenario*

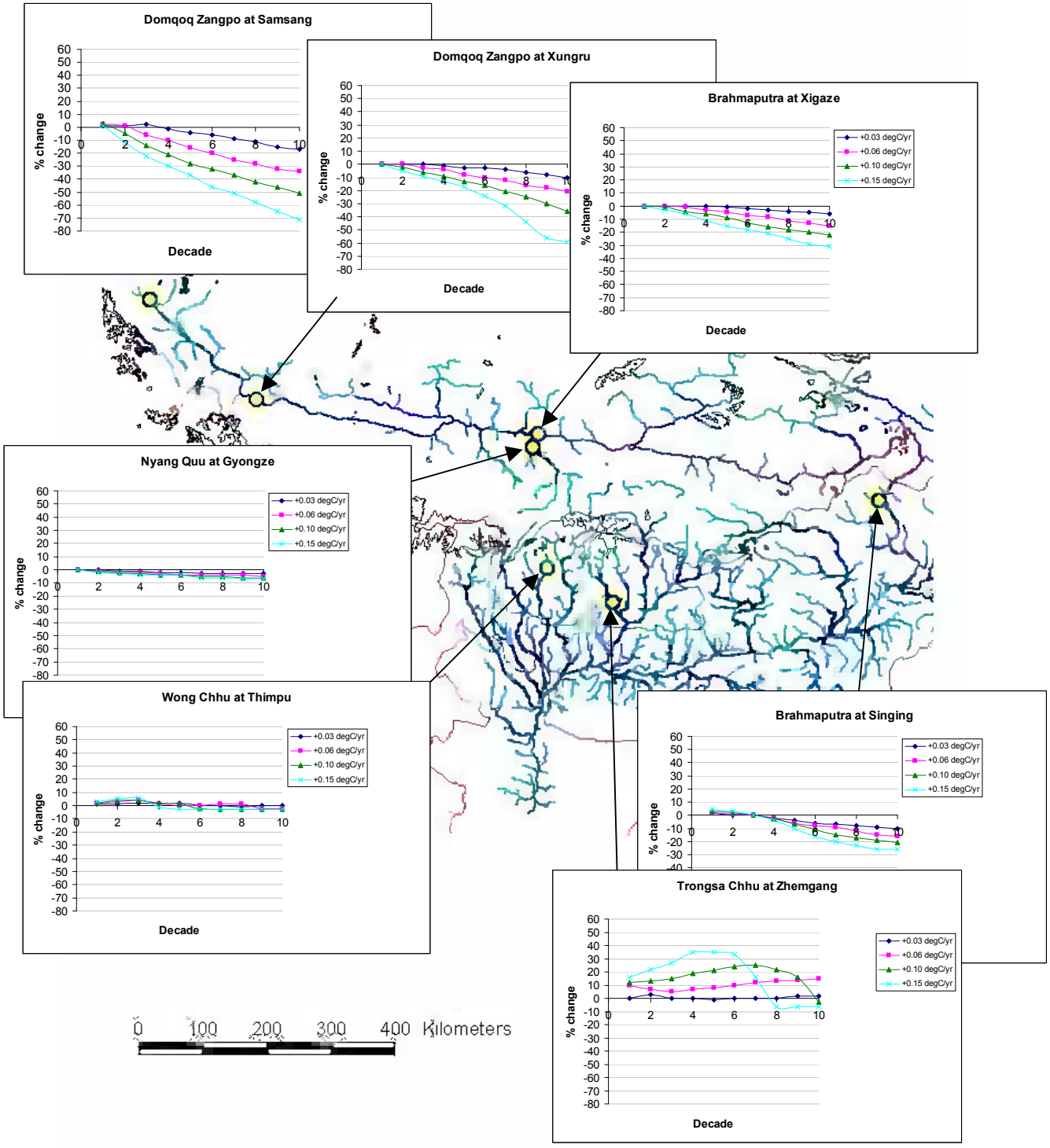

Figure 4.17 *Decadal variation in mean flow (Brahmaputra River): all T scenarios (T = +0.03, +0.06, +0.10, +0.15°C/yr)*

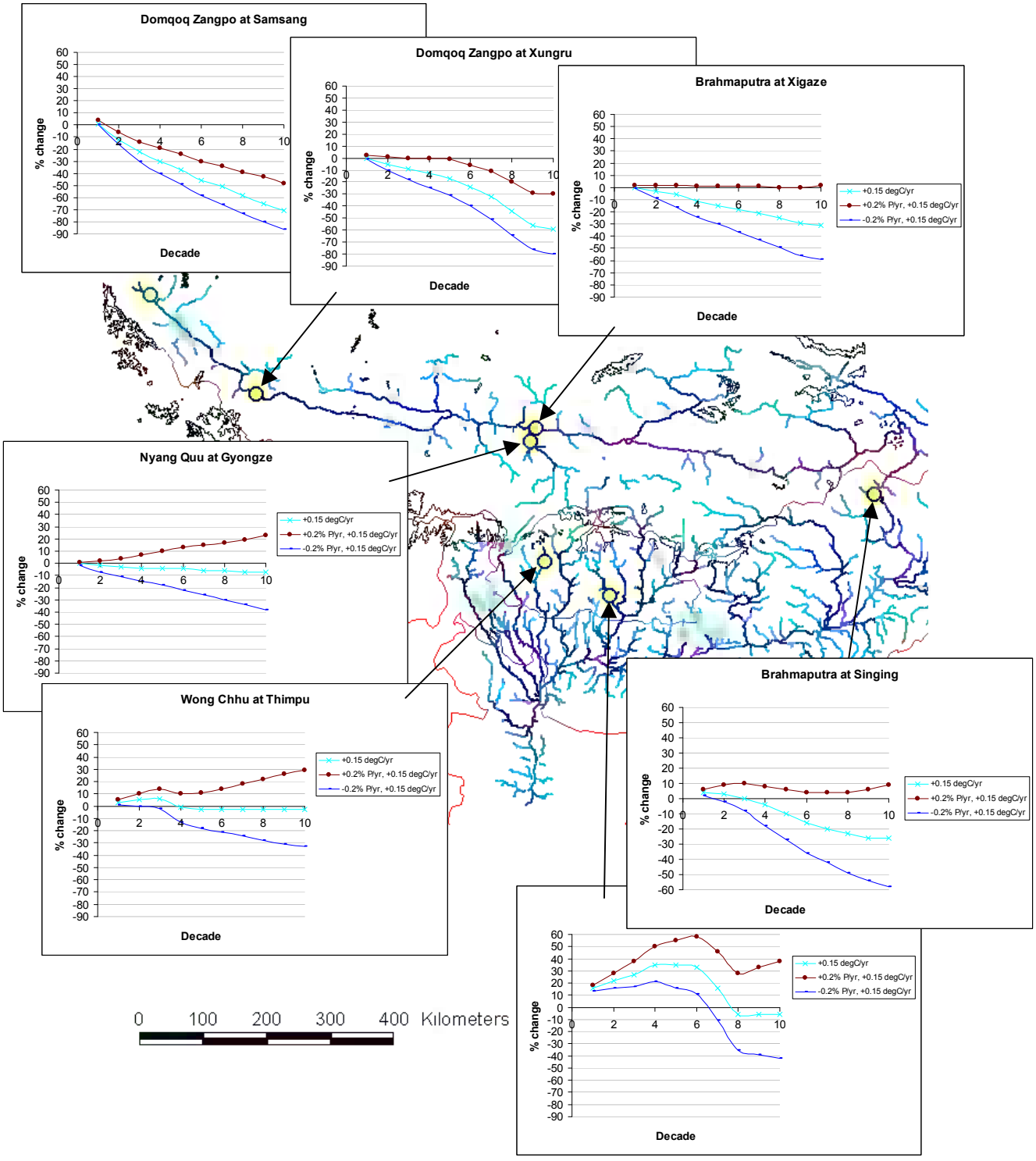

Figure 4.18 *Decadal variation in mean flow (Brahmaputra River): P and T scenarios combined (P = ±20% over 100 yrs; T = +0.15°C/yr)*

4.4 Analysis of results

The results presented in the previous section show distinct differences in the potential impacts of deglaciation both regionally, in an east-west direction along the Himalayan arc, and within catchments. In the Upper Indus, the study sites show initial increases of between +14% and +90% in mean flows (compared to the baseline) over the first few decades of the 100-year incremental scenario runs, which are generally followed by flows decreasing to between -30% and -90% of baseline by decade 10 (Figure 4.7). This contrasts with the apparent behaviour in the Kaligandaki basin in the east of the region (Figure 4.13), where decadal mean flows increase for all scenarios, with the most extreme temperature scenario attaining a peak mean flow of between +30% and +90% of baseline some 5 decades, or more, into the 100-year model run. For the Ganges (Figure 4.11), the response of the river, near the headwaters in Uttarkashi is significantly different from what is seen downstream at Allahbad. At Uttarkashi, flows peak at between +20% and +33% of baseline within the first two decades and then recede to around -50% of baseline by decade 6; further downstream the deglaciation impacts are barely noticeable. In the headwaters of the Brahmaputra (Figure 4.17), there is a general decrease in decadal mean flows for all temperature scenarios; glaciers are few in this area and flows, as expected, recede as the permanent snow cover reduces with increasing temperatures.

This regional variation can be attributed to two key factors: the amount of annual precipitation received; and the volume of snow and ice available for melting. Proportionately, the melt-water contribution to the river flows in a glaciated catchment increases from east to west, as a result of the generally weakening monsoonal influence in the same direction. According to Dreyer *et al.* (1982), snow and ice-melt contributes as much as 95% of the mean flow in catchments in the western Himalayas and as little as 20% in catchments in the east. The relative contribution of melt-water also varies considerably within catchments, diminishing progressively downstream, with increasing rainfall contribution to runoff. In areas of high rainfall, the relative contribution of snow and ice-melt is quickly overtaken downstream by runoff derived from rainfall over the non-glaciated part of the catchment; whereas, in catchments of low rainfall, the melt-water contribution to runoff continues to be a large proportion of the total runoff for some distance

downstream. It may be said, therefore, that rivers where glaciers contribute significantly to runoff are most vulnerable to the impacts of deglaciation.

Such vulnerability may be illustrated with reference to the earlier figures. In the Indus (Figure 4.5 and 4.7), the impact of increasing temperature on river flows is propagated for a large distance downstream, because the runoff contribution to river flows from the non-glaciated portion of the catchment is small, due to the low rainfall. In the Ganges system the observed difference between the river flows at Uttarkashi (where some 23% of the catchment is glaciated) and those at Alahbad (where glaciers comprise only 1% of the catchment area) can be attributed to the runoff generated from the non-glaciated portion of the catchment; at Alahbad, rainfall contributes far more significantly to the river flows than snow or ice-melt.

Precipitation also plays an important role in insulating glaciers from melting. Glaciers in the west of the region are exposed to melting earlier and for longer, because of the limited precipitation they receive. They will tend to lose mass more rapidly and be more susceptible to deglaciation. The model results for the Upper Indus (Figure 4.7) clearly show the characteristic response to deglaciation: an initial peak in river flows, as increasing temperatures cause the transient snow-line to rise and expose more glacier ice for melting, followed by a reduction in flows, as the ice available for melting depletes and the glaciers retreat. However, in areas of high annual precipitation, such as in the eastern Himalayas, the glaciers are protected by a perennial covering of snow, until the snow has melted. Dense cloud cover during the monsoon provides further protection during the time of year when the melting processes are most intense. Applying the incremental temperature scenarios, the decadal mean flows of Kaligandaki-Narayani river system in eastern Himalaya increase gradually (Figure 4.19), as ice at the lower elevations of glaciers is exposed more slowly to melting and for less time. It takes longer for the ice at lower elevations to deplete, which, in turn, causes the peak in flows to be delayed for many decades.

This suggests that the rate of deglaciation anywhere in the region is strongly influenced by the volume of precipitation occurring each year: not only in terms of its direct contribution to the mass balance of glaciers, but also because of its insulating properties. A strong and intense monsoon would protect glaciers from melting, with the consequential reduction in ice-melt compensated for by the increase in precipitation. Under such circumstances, small incremental increases in temperature would have little effect on glaciers or their runoff potential. Conversely, in the event

of a weak monsoon, the reduced snow cover would cause an increase in ice-melt, and mass would be lost rapidly from the glacier, particularly at low elevations, resulting in retreat. Under these circumstances, small increases in mean monthly temperature would, indeed, have a significant effect on deglaciation and the flow regimes of rivers.

Analysis of the results from the combined incremental scenarios of precipitation with temperature, further illustrate relative importance of precipitation to runoff generation within catchments across the region. A ±0.2% annual increase in monthly precipitation in the Upper Indus basins has a minimal effect on mean flows (Figure 4.8), as a consequence of the baseline precipitation being initially very low. In the three other focus-areas (Ganges, Kaligandaki and Brahmaputra), however, changes in precipitation has a far more dramatic effect, as seen in Figures 4.12, 4.14 and, 4.18, with impacts increasing almost linearly downstream.

The response of rivers to the RCM-based scenarios tend to follow those obtained from the more conservative incremental scenarios (e.g. +0.03 or +0.06 °C/yr), albeit with precipitation changes having greater influence, as the proportion of glacier area within catchments decreases (see Figures 4.10 and 4.16). Such results are not unexpected, given that the proportional changes of the RCM scenario generally fall within the range of the so-called "conservative" incremental scenarios used.

Changes in decadal mean winter flows, observed at two selected sites, are similar to the mean flow behaviour. Winter flows of the Indus at Partab Bridge mostly peak at between 5% and 10% higher than the baseline winter flow in the first decade and then reduce to around -13% of baseline by decade 10, according to both the +0.03 and +0.06 °C/year incremental temperature scenarios (Figure 4.9). For the Modi Khola at Kusma (Figure 4.15), decadal mean winter flows increase gradually throughout the 100-year model run, to a maximum of over +10% versus the baseline winter flow by decade 10, according to the +0.06 °C/year scenario. While the relative changes are less in winter, any variation in water availability during this traditionally dry period could have serious impacts for water users.

The model results and the above analyses are largely predicated on the CRU baseline climatological data. Whether the data is an accurate representation of conditions in the region for the 1961-90 standard period, and, particularly, of conditions at high elevations is important to be considered. A common criticism of the

CRU climatology is that it is based mainly on observations at low to medium elevations, which results in precipitation being underestimated and temperatures overestimated at high elevations. This may help to explain the apparent underestimation of flows in some catchments shown in Table 4.3. Moreover, as outlined earlier, such combinations of climatic conditions could have a considerable influence on the modelled deglaciation. The method of applying the CRU average monthly data (see Section 3), ought also to be reconsidered, as the inter-annual variability of climate, that would affect the rate of deglaciation, is not emulated in the model. Despite these concerns, the CRU data is the only data set available, providing a consistent climatology for the entire study area that enables such a regional-scale analysis to be undertaken.

The representation of the glacier ice within the model also has a bearing on the results. The rate and volume of the initial increase in flow, time to peak and the subsequent recession of flow all seem to be affected by the volume of ice available. For instance, the flow of the Ganges at Uttarkashi (catchment area 4524 km^2, 28% glaciated), sohwn in Figure 4.11, appear to peak within the first decade and then recede rapidly. Downstream at Haridwar, where the 16% galciation of the 23,191 km^2 catchment area represents a greater volume of initial ice, the time to peak is slower and the subsequent recession of flows more gradual. As with the CRU data, the permanent snow and ice described by the Digital Chart of the World is the only data set that provides a consistent definition for the whole study area. It has been impossible to assign a date to the compilation of the ONC base maps of the Himalayas; the maps were compiled between 1960 and 1993 (ESRI, 1993). While the areal extent of the intitial glacier cover used may not be an accurate representation of the present-day situation, they may, however, be a more reasonable approximation of the conditions in 1991, which was the nominal start-date for the model runs. Further development of the regional model could seek to apply the remote-sensing based datasets developed in the ICIMOD Glacier Inventories for Bhutan and Nepal (ICIMOD, 2001*a&b*). The model results also appear sensitive to the assumed areal profile of the generic glaciers used and the initial distribution of their ice: further research is needed to establish the optimal settings for these parameters.

4.5 Catchment-scale application of the regional hydrological model

Due to the large area covered by the regional model and the vast number of glaciers it considers, it is difficult to discern the behaviour of any single glacier and how it may effect river flows in its immediate catchment downstream. With some minor adjustments to the source code, it was possible to apply the regional model to a single catchment only. In order to assess the impact of single glaciers' deglaciation impacts regionally, the model was run in "catchment mode" for two locations: one using climatological data from the nearest 20 km x 20 km cell to the Battura glacier in Pakistan, the other with data from the cell nearest the Langtang-Lirung glacier in Nepal. In the earlier, regional application, both cells had approximately 100 km^2 of contributing glacier ice, so, for this application both catchments were "assigned" identical glaciers having an initial area of 100 km^2 with a minimum ice elevation of 4000 m, a maximum ice elevation of 7000 m, and a maximum ice depth of 400 m. The same shape profile as before was used for the generic glacier of both catchments.

As well as assessing the regional variation of deglaciation, the model was applied to investigate how river flows at either location were influenced by the proportion of ice within the catchment. The model was run for a 100-year period for the three scenarios: CTL, T06 and T15; and for 5 catchments with varying proportions of ice: 90% , 75%, 50%, 25% and 10%, equivalent to catchment areas of 111 km^2, 133 km^2, 200 km^2, 400 km^2, and 1000 km^2 respectively. The results from running the model in "catchment mode" are shown in Figures 4.19 to 4.23 below.

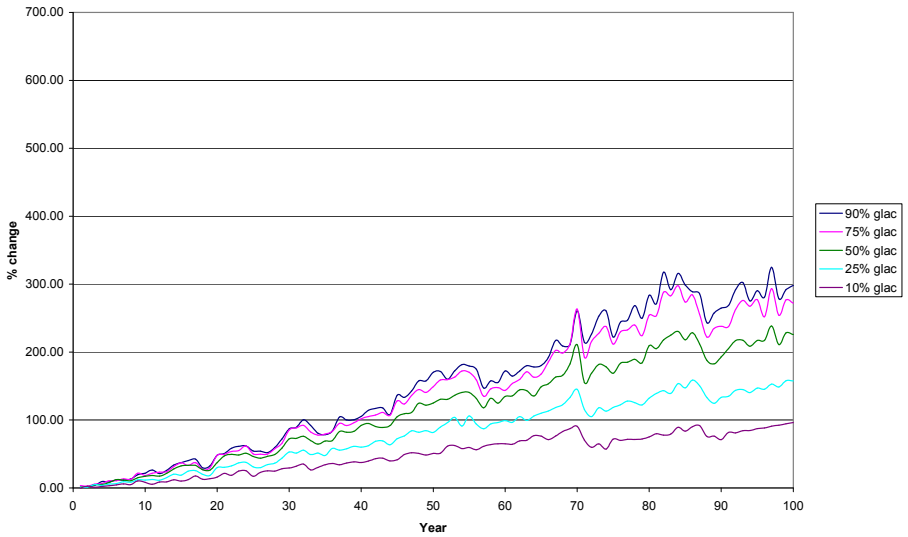

Figure 4.19 *Changes in annual runoff versus control, for varying proportions of ice in a hypothetical Nepalese catchment: +0.06°C/yr scenario applied*

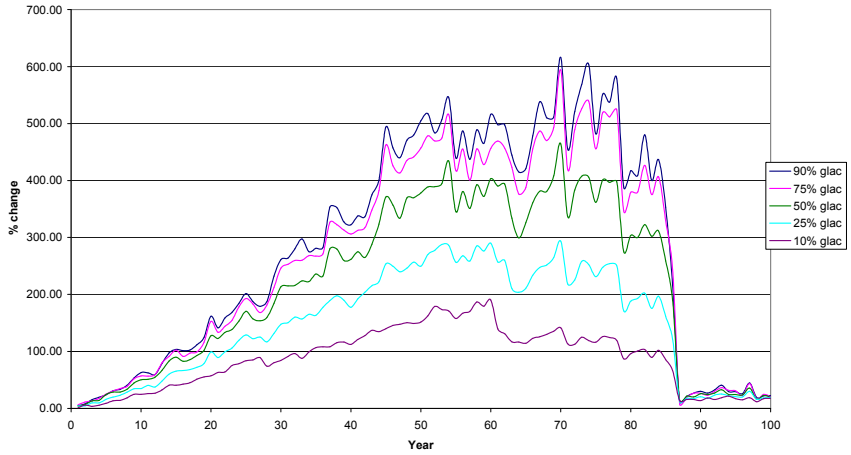

Figure 4.20 *Changes in annual runoff versus control, for varying proportions of ice in a hypothetical Nepalese catchment: +0.15°C/yr scenario applied*

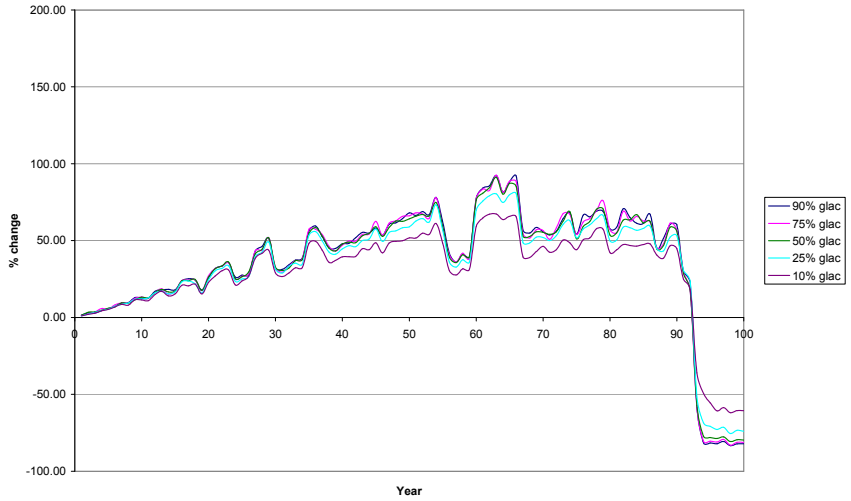

Figure 4.21 *Changes in annual runoff versus control, for varying proportions of ice in a hypothetical Pakistan catchment: +0.06°C/yr scenario applied*

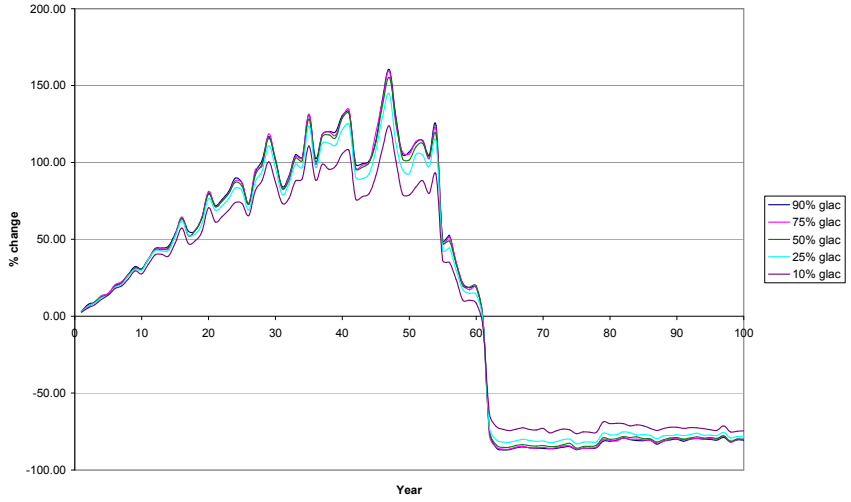

Figure 4.22 *Changes in annual runoff versus control, for varying proportions of ice in a hypothetical Pakistan catchment: +0.15°C/yr scenario applied*

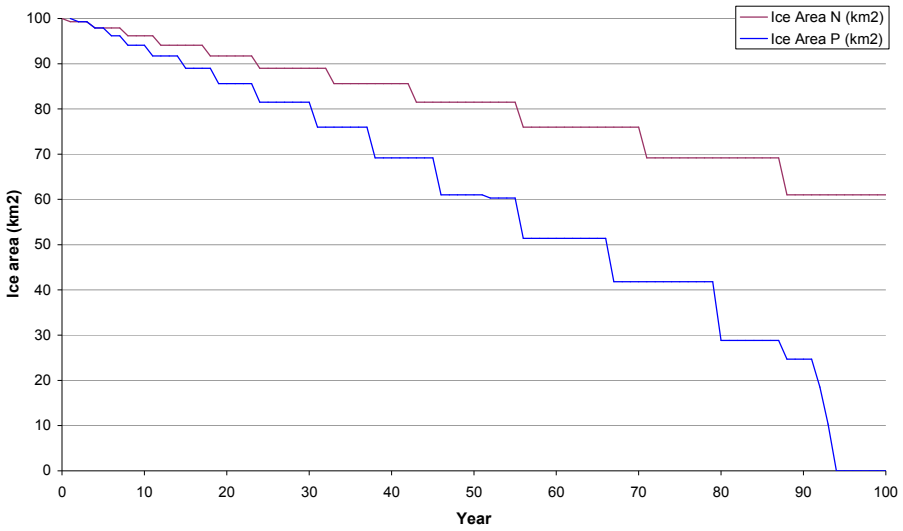

Figure 4.23 *Temporal variation in ice area for both glaciers: +0.06°C/yr scenario*

These results closely resemble those obtained at similar locations in the regional application of the model: initial increases in flows, relative to the control, more gradual and time-to-peak longer in the Nepal (east) than in Pakistan (west). The results of the Nepalese catchment, show how the proportion of ice within the catchment influences the river's response to deglaciation, with the changes greatest for areas of high percentage glaciation. As the proportion of runoff from the non-glaciated catchment increases downstream, the relative impact, defined by the percentage change versus control, is seen to reduce. In the Pakistan catchment, because precipitation is low, runoff from the non-glaciated part is small, and, consequently, the deglaciation impacts are propagated with the same intensity much further downstream.

These examples also reinforce the view that precipitation, while not necessarily contributing to the positive annual mass balance of glaciers, can still help to delay deglaciation by insulating glaciers from melting. In the Pakistan glacier, total deglaciation occurs rapidly with both temperature scenarios, because of the low precipitation offers little protection against melting, but, in Nepal, where there is higher precipitation, the rate of deglaciation is much slower (Figure 4.23).

5 Conclusions

This project came about following speculation that the glaciers of the Himalayas could vanish within forty years, and that this would lead to widespread and catastrophic water shortages. The aim of this DFID-funded project was to "assess the seasonal and long term water resources in snow and glacier fed rivers originating in the … region". An innovative regional hydrological model was developed and applied with a variety of climate change scenarios to determine the potential impacts of deglaciation on future river flows in the Indus, Ganges and Brahmaputra river basins. The results from the model have been presented and analysed in this technical report.

There is ample evidence of deglaciation occurring throughout the Himalayas, but, according to the model results, for many areas, the catastrophic water shortages forecast by some experts are unlikely to happen for many decades, if at all. Rather, some areas may benefit from increased water availability for the foreseeable future. While the threat that all of the region's glaciers will have disappeared within 40 years would seem ill-founded, this project has identified certain areas of the region, such as in the Upper Indus, where deglaciation may, indeed, cause a significant reduction of river flows within the next few decades.. Clearly this would have serious consequences for future water availability and use throughout the basin.

The results have shown impacts of deglaciation to vary considerably within the region and within catchments. Highly glaciated catchments and those (catchments) where melt-water contributes significantly to the runoff have been shown to be most vulnerable to deglaciation. Although the inter-annual variability of precipitation may not have been emulated within the model, results from the different focal-areas indicate the very important role precipitation has in protecting glaciers from melting and rapid mass loss: a thick covering of snow resulting from a strong monsoon would insulate the glacier and delay melt, whereas, a weak monsoon would expose a glacier to melting earlier and for longer. In glaciated catchments where precipitation is relatively high, the impacts of deglaciation diminish rapidly downstream, as the runoff contribution from rainfall over the non-glaciated part of the catchment quickly swamps the melt-water contribution. Where precipitation is low, the melt-water contribution to runoff remains proportionately high for a significant distance

downstream. It can be concluded, therefore, that catchments in the eastern Himalaya, which benefit from the high precipitation of the summer monsoon every year, are less susceptible to the impacts of deglaciaton than those in the west, where the monsoon is very much weaker. Of course, the regional picture portrayed here, does not necessarily apply to all glaciers throughout the region, and it is probable that some glaciers are already on the verge of disappearing, which would cause immediate difficulties for communities downstream.

This project saw the first application of a new regional hydrological model, incorporating an innovative "generic glacier" approach to represent the melt-water contribution of many glaciers to river flows. As with the development of any new model, there is always considerable scope for improving the model and how it is applied. For example, the apparent sensitivity of results to the initial representation of glacier ice warrants further investigation into how the areal distribution and depth of ice is described by the "generic glacier". This could include a comprehensive analysis of the hypsometry of Himalayan glaciers and further work on characterizing glacier depth. The use of contemporary remote sensing data to describe the areal distribution and spatial extent of the region's glaciers could also be developed. There are limitations too with the data used to "drive" the model: climatological data that is more representative of conditions at high elevations in mountains, would provide some improvement to model results, while access to good quality long-term gauging station data would help to optimize and improve the parameterization of the model. Meanwhile, the application of climate change scenarios uniformly by annual increments for every year of a 100-year model run are plainly unrealistic, and more sophisticated approaches, that would introduce a higher degree of variability, should be considered.

Despite the limitations of the model and the data used, plausible results were obtained. By expressing the deglaciation impacts in relative terms (% change), apparent errors (measured *v* observed) in estimating baseline flows are negated, because the same errors would feature to a similar extent in the forecasted flows. Encouragingly, the model results are mostly explainable, from what is known of the dynamics of glaciers and the climate of the Himalayas.

Readers of this report should, however, be careful how they interpret the results that have been presented. Whilst some alarmist claims can be discounted with confidence, the timing and magnitude of impacts, as shown on the many graphs,

should not be taken too literally: they show results of various hypothetical scenarios applied to a conceptual model, and, as such, only provide an indication of what might happen, if such conditions prevail. These results, therefore, should not be considered definitive; much work remains, through the continuation of monitoring and further research, to ensure the future impacts of deglaciation and climate change on water resources are better understood.

6 References

Ageta, Y., Naito, N., Nakawo, M., Fujita, K., Shankar, K., Pokhrel, A.P. and Wangda, D., 2001. Study project on the recent rapid shrinkage of summer-accumulation type glaciers in the Himalayas, 1997-1999. Bulletin of Glaciological Research 18 (2001). pp 45-49.

Arnell, N.W., 1999*a*. A simple water balance model for the simulation if streamflow over a large geographic domain. Journal of Hydrology, 217, pp. 314-335.

Arnell, N.W., 1999*b*. Climate change and global water resources. Global Environmental Change, 9(1999). S31-S49.

Bell, V.A. and Moore, R.J., 1999. An elevation-dependant snowmelt model for upland Britain. Hydrol. Process. 13, pp 1887-1903, 1999.

Beven, K.J., 2001. Rainfall-Runoff Modelling: The Primer. John Wiley & Sons Ltd. pp 352.

Bergström, S. and Forsman, A., 1973. Development of a conceptual deterministic rainfall-runoff model. Nordic Hydrology 4, pp 147-170.

Braun, L.N, Grabs, W. and Rana, B. ,1993. Application of a conceptual precipitation-runoff model in the Langtang Khola Basin, Nepal Himalaya. In: Snow and Glacier Hydrology, Proc. Kathmandu Symposium, November 1992. IAHS Publ. No. 218, 1993. pp 221-237.

Braun, L.N., Hottelet, C., Weber, M. and Grabs, W., 1998. Measurement and simulation of runoff from Nepalese head watersheds. In: Hydrology, Water Resources and Ecology in Headwaters. Proc. Headwater '98 Conference, Merano, Italy, April 1998. IAHS Publ. No. 248, 1998., pp. 9-18.

Dey, B., Sharma, V.K., Rango, A., 1989. A test of Snowmelt-Runoff Model for a Major River Basin in Western Himalayas. Nordic Hydrology, 20, pp. 167-178.

Down To Earth, 1999. Analysis – Glaciers Beating Retreat, 7(23), April 1999.

Dreyer, N.N., Nikolayena, G.M. and Tsigelnaya, I.D., 1982. Maps of streamflow resources of some high-mountain areas in Asia and North America. In: hydrological Aspects of Alpine and High Mountain Areas. Proceedings of the Exeter Symposium, July 1982. IAHS Publ. No. 138, pp. 11-20.

Dyurgerov, M.B and Meier, M.F., 1997. Mass balance of mountain and sub-polar glaciers: A new global assessment for 1961-1990, Arctic and Alpine Research, 29(4), pp. 379-391.

ESRI, 1993. Digital Chart of the World – Data Dictionary. Environmental Systems Research Institute, Inc. (ESRI), November 1993.

FAO, 1997. Digital Soil Map of the World and Derived Soil Properties., Version 3.5 November 1995, FAO Land and Water Digital Media Series 1 (CD-ROM). Derived from the FAO/UNESCO 1:5 000 000 Soil Map of the World.

Fujita, K, Nakawo, M., Fujii, Y. and Paudyal, P., 1997. Changes in glaciers in Hidden Valley, Mukut Himal, Nepal Himalayas, from 1974 to 1994. Journal of Glaciology, 43(145), 1997. pp 583-588.

Fujita K., Kadota, T., Rana, B., Kayastha, R.B. and Ageta, Y., 2001. Shrinkage of Glacier AX010 in Shorong region, Nepal Himalayas in 1990s. Bulletin of Glaciological Research 18(2001). pp 51-54

Fukushima, Y., Watanabe, O. and Higuchi, K., 1991. Estimation of streamflow change by global warming in a glacier-covered high mountain area of the Nepal Himalaya. In: Snow, Hydrology and Forests in High Alpine Areas, Proc. Int. Sym. Vienna, 11 - 24 August 1991. IAHS Publication No. 205, 1991.

Giorgi, F. and Francisco, R., 2000. Evaluating uncertainties in the prediction of regional climate change. Geophys. Res. Letters, 27(9), pp 1295-1298.

Haeberli, W., 1990. Glacier and permafrost signals of 20th century warming. Annals of Glaciology, 14, p 99-101

Haberli, W and Hoelzle, M., 2001. The World Glacier Monitoring Service. (http://www.nerc-bas.ac.uk/public/icd/icsi/WGMS.html)

Hassell, D. and Jones, R.G., 1999. simulating climatic change of the southern Asian monsoon using a nested regional climate model (HadRM2). HCTN 8. Hadley Centre for Climate Prediction and Research, Bracknell, UK.

IAHS(ICSI)/UNEP/UNESCO, 1988. Fluctuations of Glaciers 1980-1985 (W. Haeberli and P. Müller, *eds.*). Paris, UNESCO

IAHS(ICSI)/UNEP/UNESCO, 1993*a*. Fluctuations of Glaciers 1985-1990 (W. Haeberli and M. Hoelzle, *eds.*). Paris, UNESCO

IAHS(ICSI)/UNEP/UNESCO, 1991. Glacier Mass Balance Bulletin No. 1 (W. Haeberli and E. Herren, *eds.*). World Glacier Monitoring Service, ETH Zurich.

IAHS(ICSI)/UNEP/UNESCO, 1993*b*. Glacier Mass Balance Bulletin No. 2 (W. Haeberli, E. Herren and M. Hoelzle, *eds.*). World Glacier Monitoring Service, ETH Zurich.

ICIMOD, 2000*a*. Inventory of Glaciers, Glacial Lakes and Glacial Lake Outburst Floods – Monitoring and Early Warning Systems in the Hindu Kush-Himalyan Region - Bhutan. (Mool et al. (*eds.*)), International Centre for Integrated Mountain Development, Kathmandu, August 2001. 227pp.

ICIMOD, 2000*b*. Inventory of Glaciers, Glacial Lakes and Glacial Lake Outburst Floods – Monitoring and Early Warning Systems in the Hindu Kush-Himalyan Region - Nepal. (Mool et al. (*eds.*)), International Centre for Integrated Mountain Development, Kathmandu, August 2001. 363pp.

IPCC, 1996. Climate Change 1995. Impacts, Adaptation and Mitigation of Climate Change: Scientific and Technical Analyses. Contribution of Working Group II to the Second Assessment Report of the Intergovernmental Panel on Climate Change. [Watson, R.T., Zinyowera, M.C. and Moss, R.H. (eds.)] Cambridge University Press, Cambridge, 1996. 879pp.

IPCC, 2001*a*. Climate Change 2001: Impacts, Adaptation and Vulnerability. Contribution of Working Group II to the Third Assessment Report of the Intergovernmental Panel on Climate Change. [McCarthy, J.J., *et al.* (eds)]. 1032 pp.

IPCC, 2001*b*. Climate Change 2001: The Scientific Basis. Contribution of Working Group I to the Third Assessment Report of the Intergovernmental Panel on Climate Change. [Houghton, J.T., *et al.* (eds)]. 881 pp.

Jain, S.K., Kumar, N., Ahmad, T. and Kite, G.W., 1998. SLURP model and GIS for estimation of runoff in a part of Satluj catchment, India. Hydrological Sciences Journal, 43(6), pp. 875-884.

Kadota, T., Seko, K., Aoki, T., Iwata, S. and Yamaguchi, S., 2000. Shrinkage of the Khumbu Glacier, east Nepal 1978 to 1995. in: Debris Covered Glaciers (Proceedings of a workshop held at Seattle, Washington, USA, September 2000) IAHS Publ. no. 264, 2000. pp. 235 – 243.

Kadota, T., Fujita, K., Seko, K., Kayastha, R. and Ageta, Y., 1997. Monitoring and prediction of shrinkage of a small glacier in the Nepal Himalaya. Annals of Glaciology 24, 1997. pp. 90-94.

Kuhn, M., 1993. Possible future contribution to sea level change from small glaciers. In: Climate and Sea Level Change: Observations, Projections and Implications (Eds. R.A. Warrick *et al.*) Cambridge University Press, UK. pp 134-143.

Kumar, V.S., Haefner, H. and Seidel, K., 1991. Satellite snow cover mapping and snowmelt runoff modelling in Beas basin. In: Snow, Hydrology and Forests in High Alpine Areas. Proc. Vienna Symposium, August 1991. IAHS Publ. No. 205, pp 101-109.

Kumar, V.S., Paul, P.R., Rao, C.L.V.R, Haefner, H. and Seidel, K., 1993. Snowmelt runoff forecasting studies in Himalayan basins. In: Snow and Glacier Hydrology, Proc. Kathmandu Symposium, November 1992. IAHS Publ. No. 218, 1993. pp 85-94.

Liu, C., and Ding, L., 1986. The Newly Progress of Glacier Inventory in tianshan Mountains. J Glaciology and Geocryology, 8(2), pp 168-169.

Macdonald, O.G. and Collins, D.N., Coupling glacier mass balance and meltwater yield in the European Alps with future climate change: downscaling from integrations of the HadCM3 model. In: Proc EGS Symposium, HSA4.02 Hydrology and rainfall processes:Hydrological and meteorological coupling in mountain areas. EGS XXVII General Assembly, Nice, France, April 2002

Martinec, J., 1975. Snowmelt-runoff model for streamflow forecasts. Nordic Hydrology, 6. pp. 145-154.

Mayekwski, P.A. and Jeschke, P.A., 1979. Himalayan and Trans-Himalayan Glacier Fluctuations since AD 812. Arctic and Alpine Research, 11(3), 1979, pp 267-287.

Meier, M.F., 1993. Ice, climate and sea level: do we know what is happening? In: Ice in the Climate System (Peltier, W.R. (ed.)), NATO ASI series I, global Environmental Change, 12, pp 141-160.

Moore, R.J., 1985. The probability-distributed principle and runoff production at point and basin scales. Hydrological Sciences Journal, 30, pp 273-297.

Muller, F., Caflish, T. and Muller, G., 1977. Instruction for Compilation and Assemblage of Data for a World Glacier Inventory. Zurich: temporary Technical Secretaria for World Glacier Inventory, Swiss Federal Institute of Technology, Zurich.

Naithani, A.K., Nainwal, H.V., Sati, K.K. and parsad, C., 2001. Geomorphological evidences of retreat of the Gangotri glacier and its characteristics. Current Science 80(1), 10 January 2001. pp. 87-94.

New, M.G., Hulme, M. and Jones, P.D., 2000. Representing twentieth-century space-time climate variability. Part II: Development of 1901-1996 monthly grids of terrestial surface climate. Journal of Climate 13, pp 2217-2238.

Oerlemans, J and Fortuin, J.P.F., 1992. Sensitivity of glaciers and small ice caps to greenhouse warming. Science, 258, pp 115-118.

Oerlemans, J., 1994. Quantifying global warming from the retreat of glaciers. Science, 264, pp 243-245.

Singh, P. and Quick, M.C., 1993. Streamflow simulation of Satluj River in the Western Himalayas. In: Snow and Glacier Hydrology, Proc. Kathmandu Symposium, November 1992. IAHS, 1993, Publ. No. 218, 1993. pp 261-271.

Singh, P., Kumar, N. and Arora, M., 2000. Degree-day factors for snow and ice for Dokriani Glacier, Garhwal Himalayas. Journal do Hydrology 235, pp 1-11.

Shrestha, A.B., Wake, C.P., Mayewski, P.A. and Dibb, J.E., 1999. Maximum temperature trends in the Himalaya and its vicinity: an analysis based on temperature records from Nepal for the perion 1971-94. Journal of Climate, 12, pp 2775-2786.

Shrestha, A.B., Wake, C.P., Dibb, J.E. and Mayewski, P.A., 2000. Precipitation fluctuations in the Nepal Himalaya and its vicinity and relationship with some large scale climatological parameters. Int. J. Climatol., 20, pp 317-327.

United States Geological Survey (USGS), 2001. HYDRO1k Elevation Derivative Database - Asia. Distruibuted by the Land Processes Distributed Active Archive Center (LP DAAC), located at the USGS EROS Data Center http://LPDAAC.usgs.gov

United States Geological Survey (USGS), 2002. Eurasia Land Cover Characteristics Data, Version 2.0 (April, 2002). Distributed by the Land Processes Distributed Active Archive Center (LP DAAC), at the USGS EROS Data Center http://edcdaac.usgs.gov/glcc/eadoc_20.html

Verdhen, A. and Prasad, T.,1993. Snowmelt runoff simulation models and their suitability in Himalayan condition. In: Snow and Glacier Hydrology, Proc. Kathmandu Symposium, November 1992. IAHS Publ. No. 218, 1993. pp 239-248.

Vorosmarty, C.J, Moore, B., Grace, A.L., Gildea, M.P., Melillo, J.M., Peterson, B.J., Rasetter, E.B. and Steudler, P.A., 1989. Continental scale models of water balance and fluvial transport: an application to South America. Global Biogeochmical Cycles, 3, pp 241-265.

Wessels, R.L., Kargel, J.S., and Kieffer, H.H., 2001. Global Land Ice Measurements from Space: Documenting the Demise of Earth's Glaciers using ASTER. American Geophysical Union 2001 Spring Meeting, May 2001.

Wood, F.B, 1990. Monitoring global climatic change: the case of greenhouse warming. Bulletin of the American Meteorological Society, 71, 1, pp. 42 –52

ANNEX 1: Additional Figures

A. Upper Indus
B. Ganges River
C. Kaligandaki-Narayani Rivers
D. Brahmaputra Basin

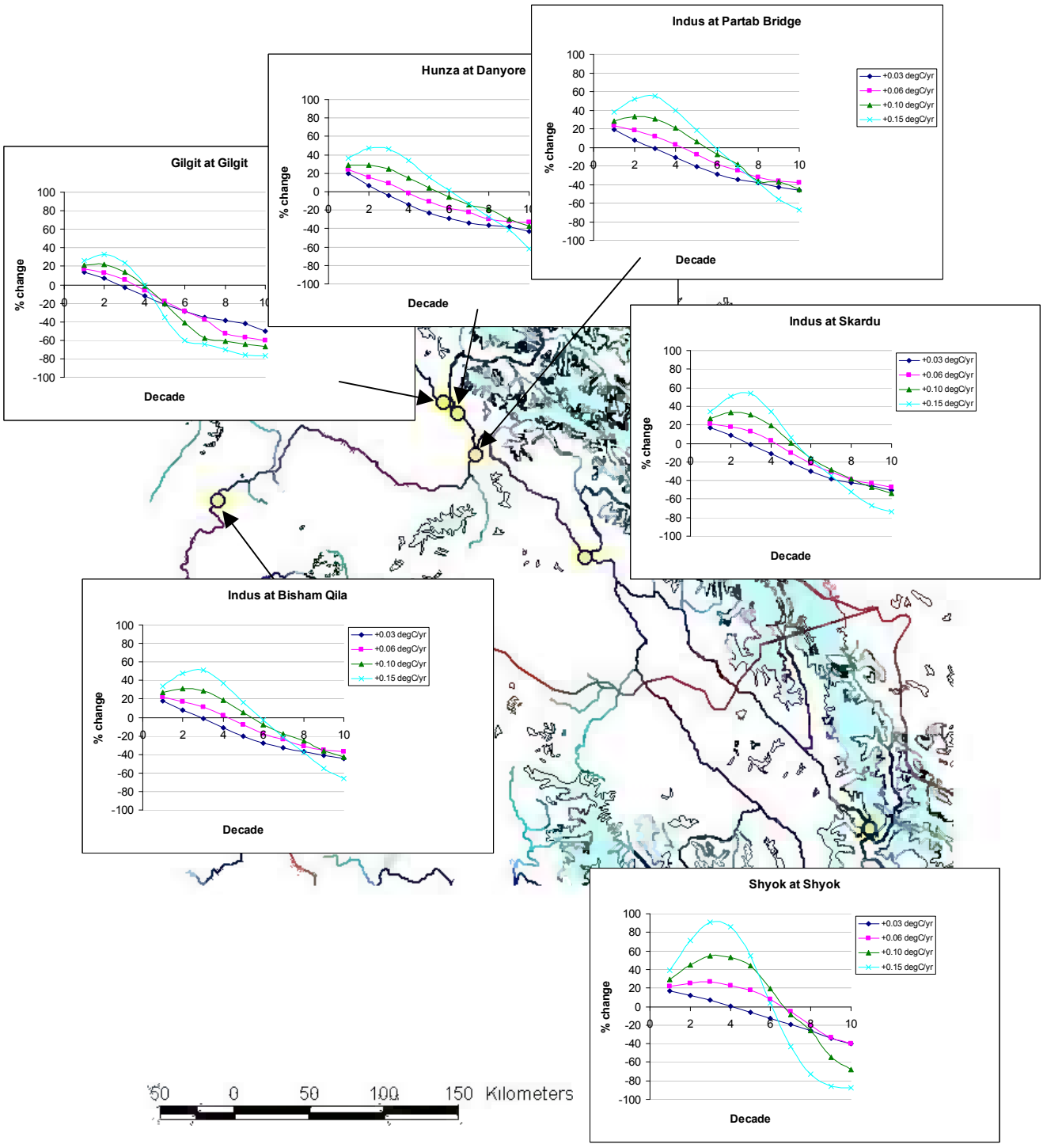

Figure A.1 *Decadal variation in mean flow (Upper Indus): all T scenarios (T = +0.03, +0.06, +0.10, +0.15°C/yr)*

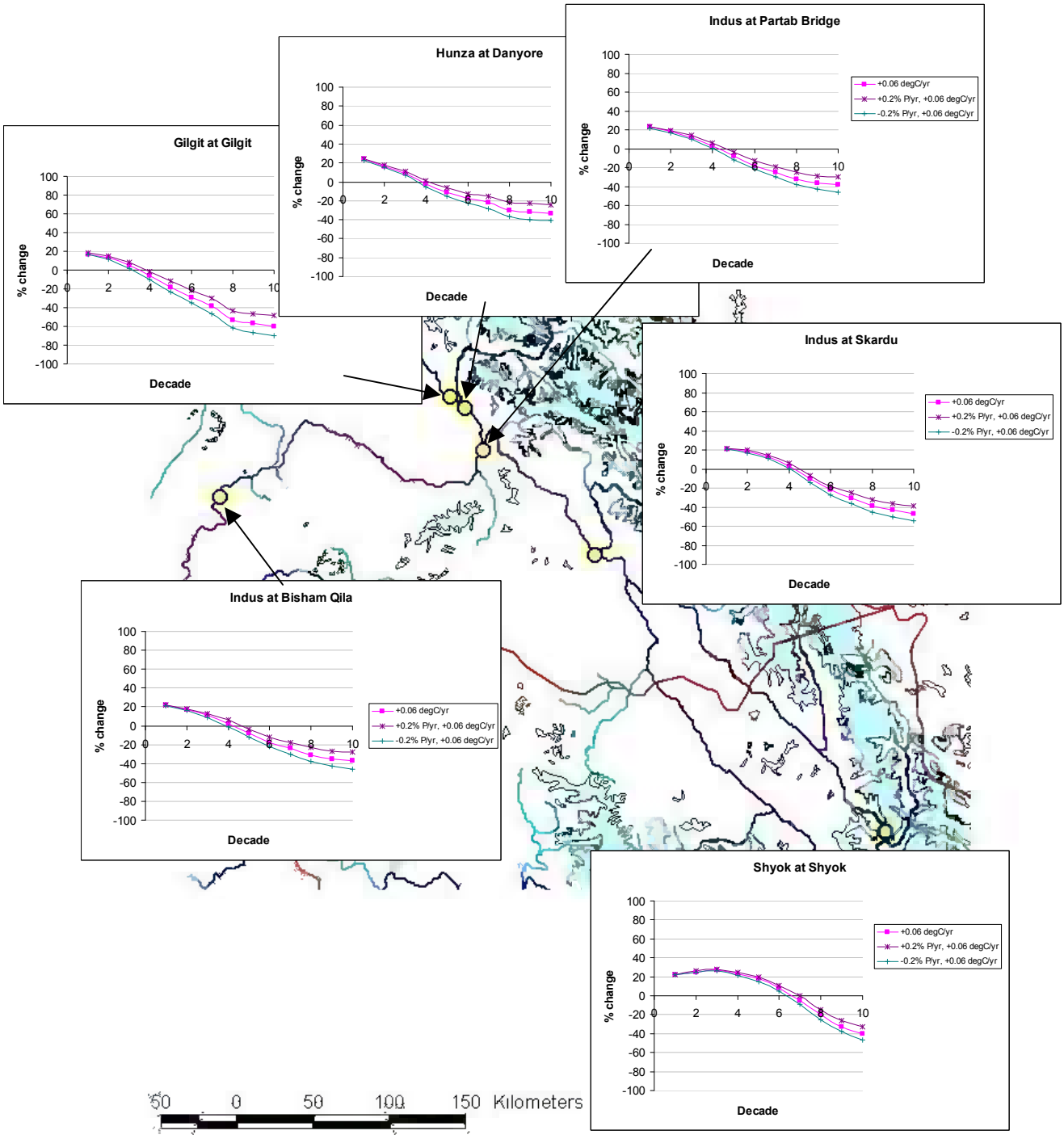

Figure A.2 *Decadal variation in mean flow (Upper Indus): P and T scenarios combined (P = ±20% over 100 yrs; T = +0.06°C/yr)*

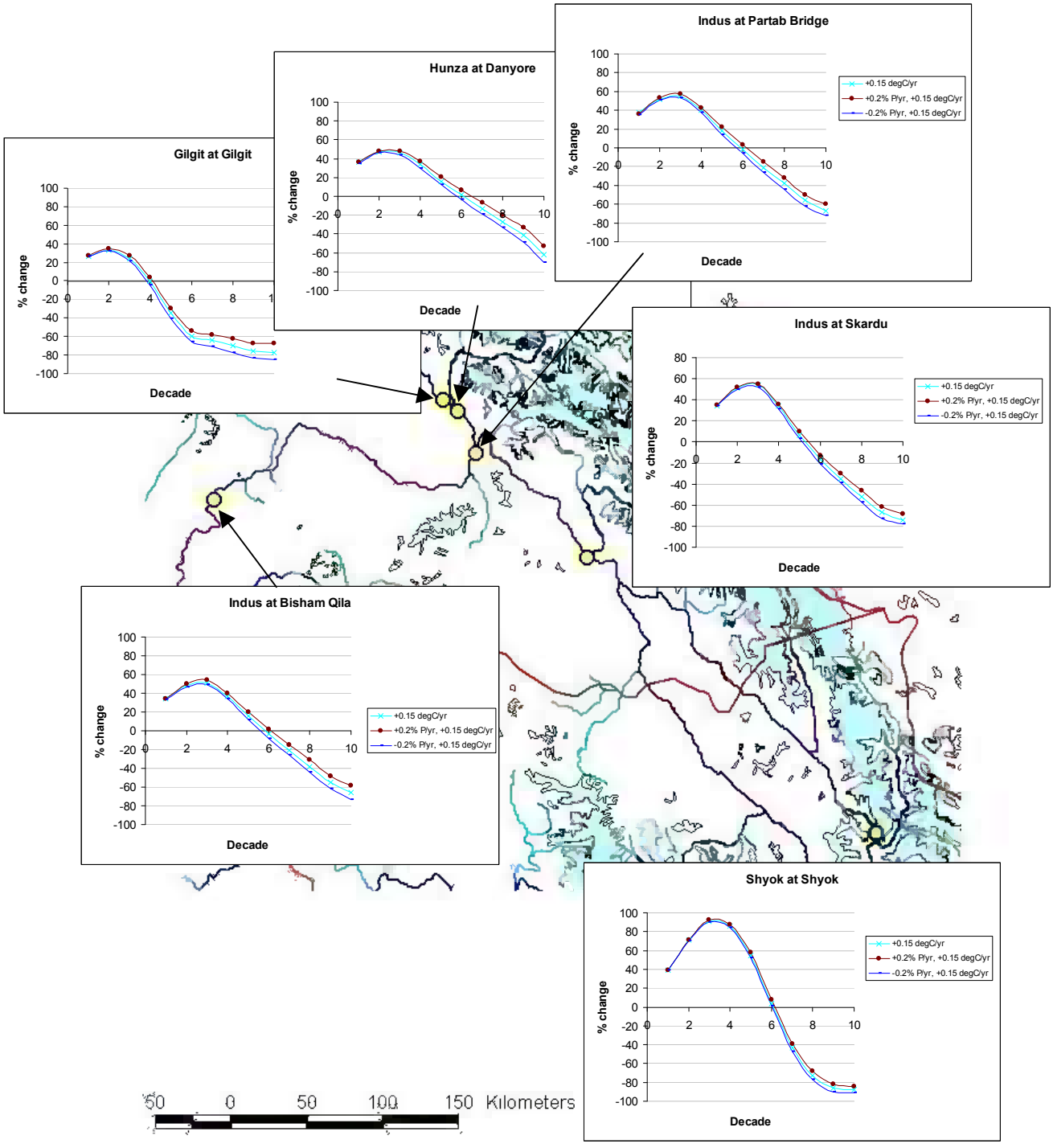

Figure A.3 *Decadal variation in mean flow (Upper Indus): P and T scenarios combined (P = ±20% over 100 yrs; T = +0.15°C/yr)*

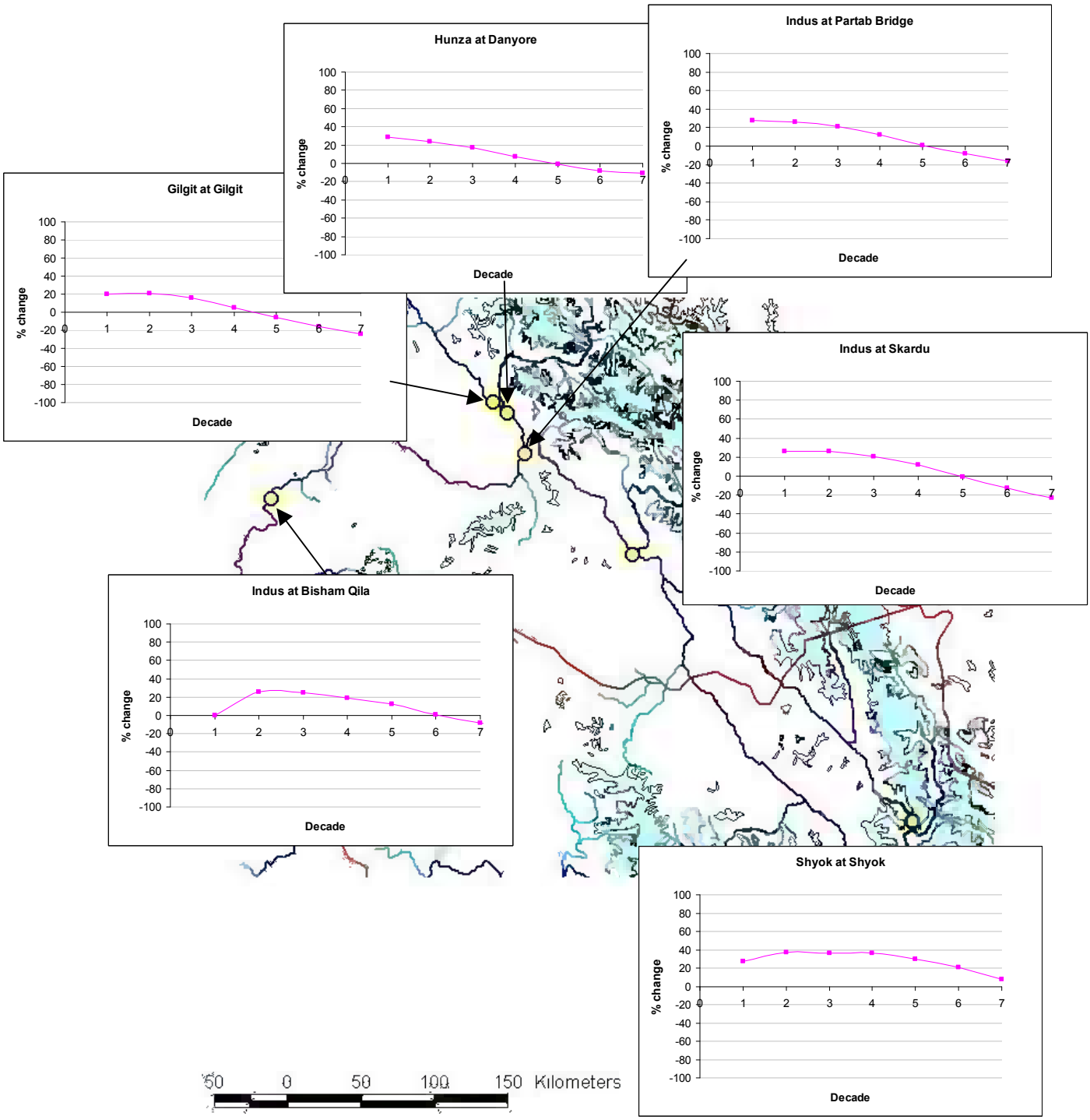

Figure 4.10 *Decadal variation in mean flow (Upper Indus): RCM scenario applied*

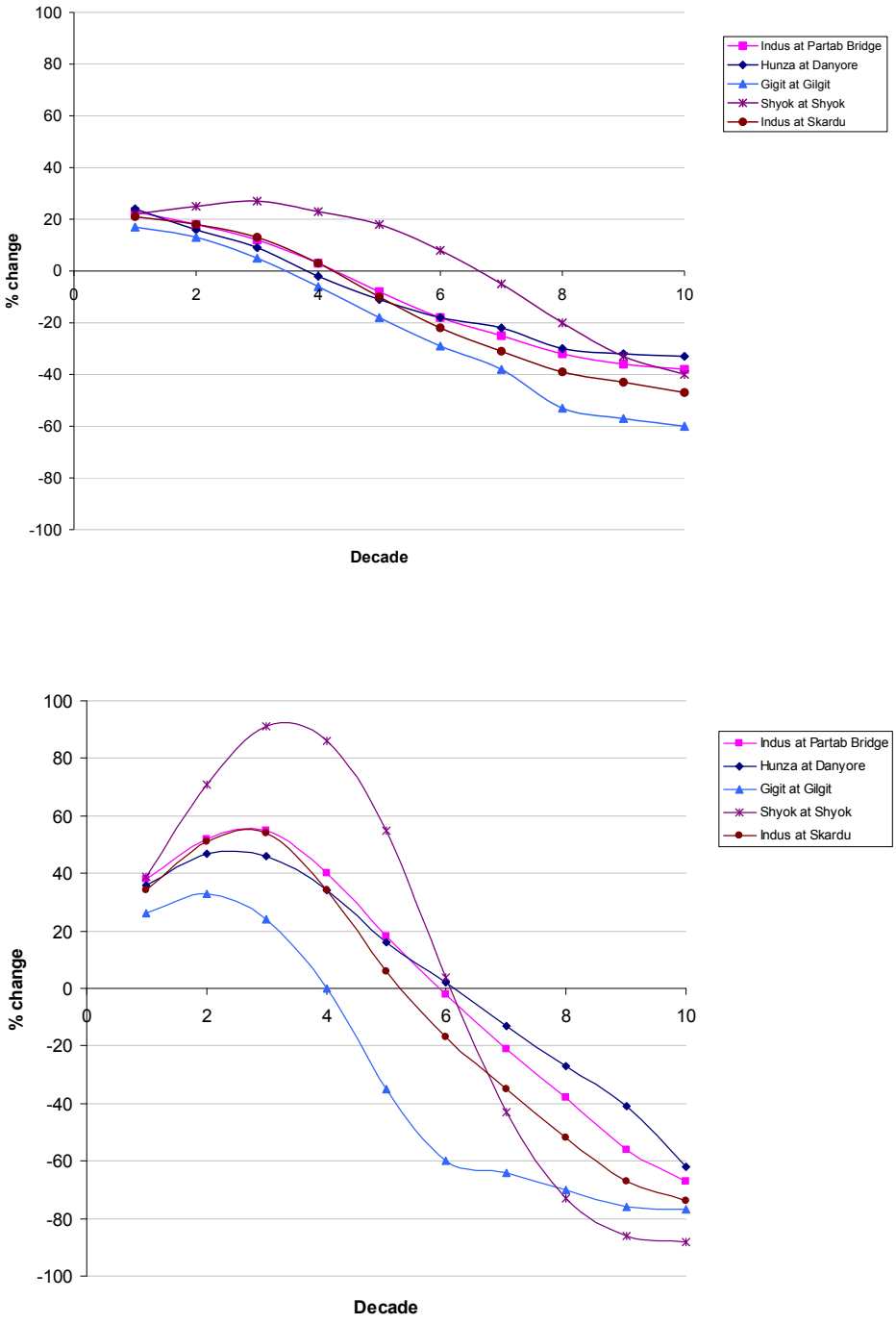

Figure A.4 *Decadal variation in mean flow, all selected locations (Upper Indus): T = +0.06°C/yr scenario (above); T = +0.15°C/yr scenario (below)*

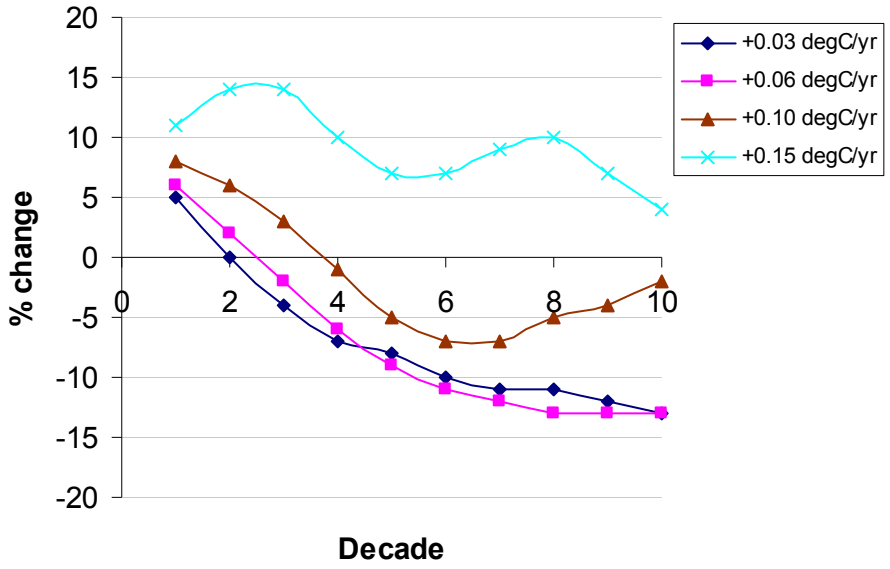

Figure A.5 *Decadal variation in mean winter flow (Indus at Partab Bridge): all T scenarios*

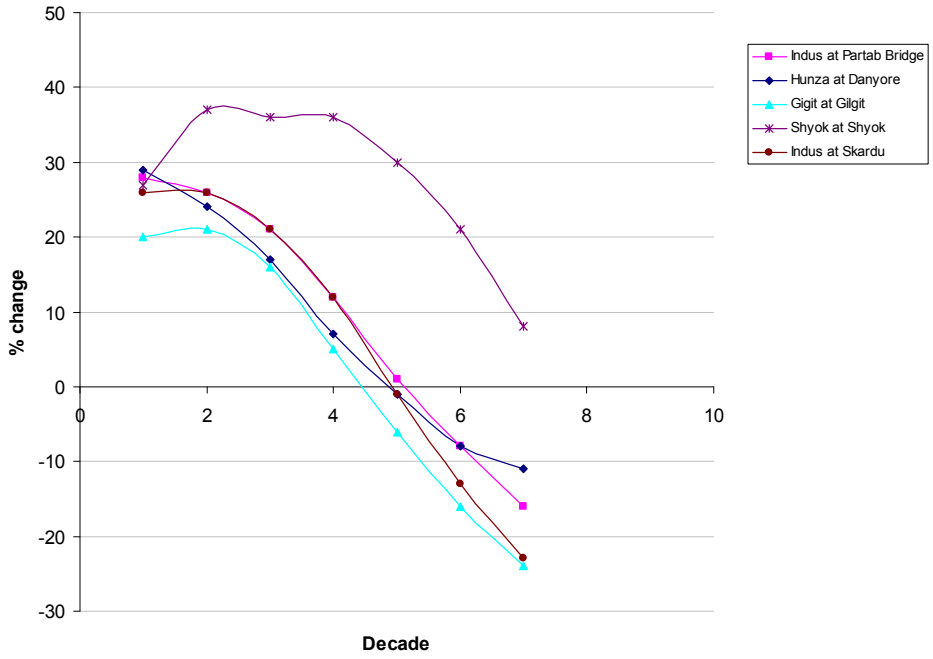

Figure A.6 *Decadal variation in mean flow, all selected locations (Upper Indus): RCM scenario*

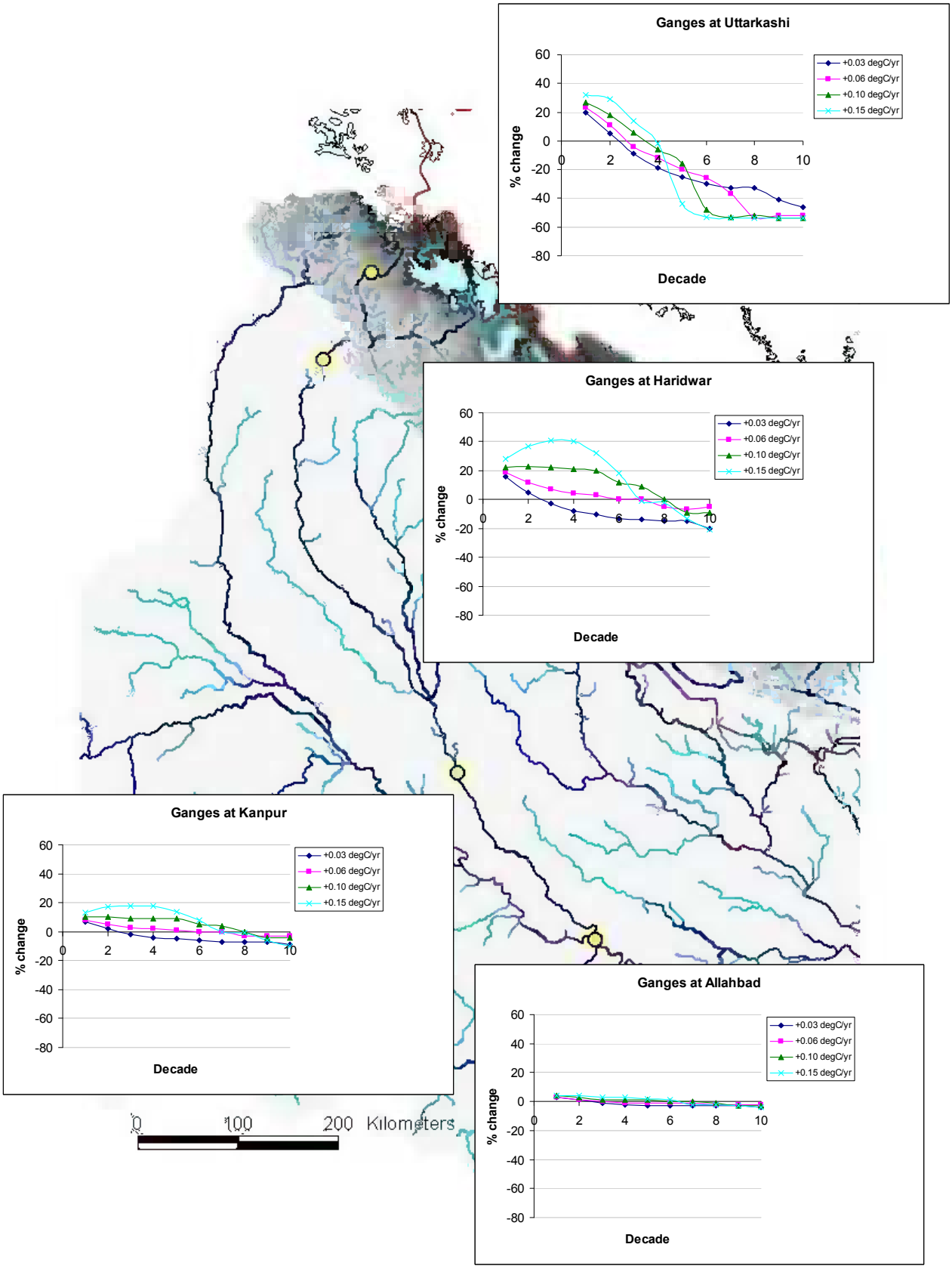

Figure B.1 *Decadal variation in mean flow (River Ganges): all T scenarios (T = +0.03, +0.06, +0.10, +0.15°C/yr)*

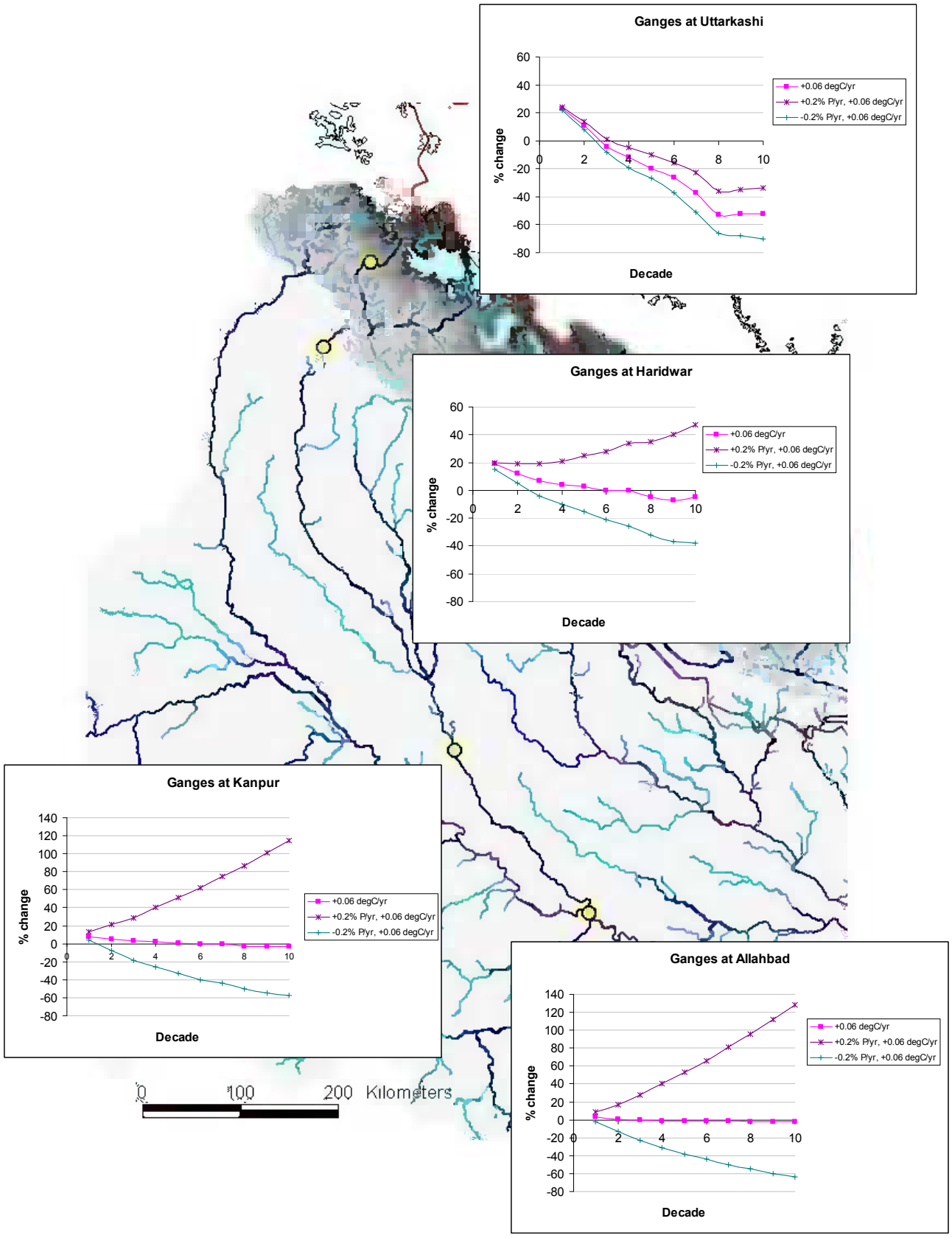

Figure B.2 *Decadal variation in mean flow (River Ganges): P and T scenarios combined (P = ±20% over 100 yrs; T = +0.06°C/yr)*

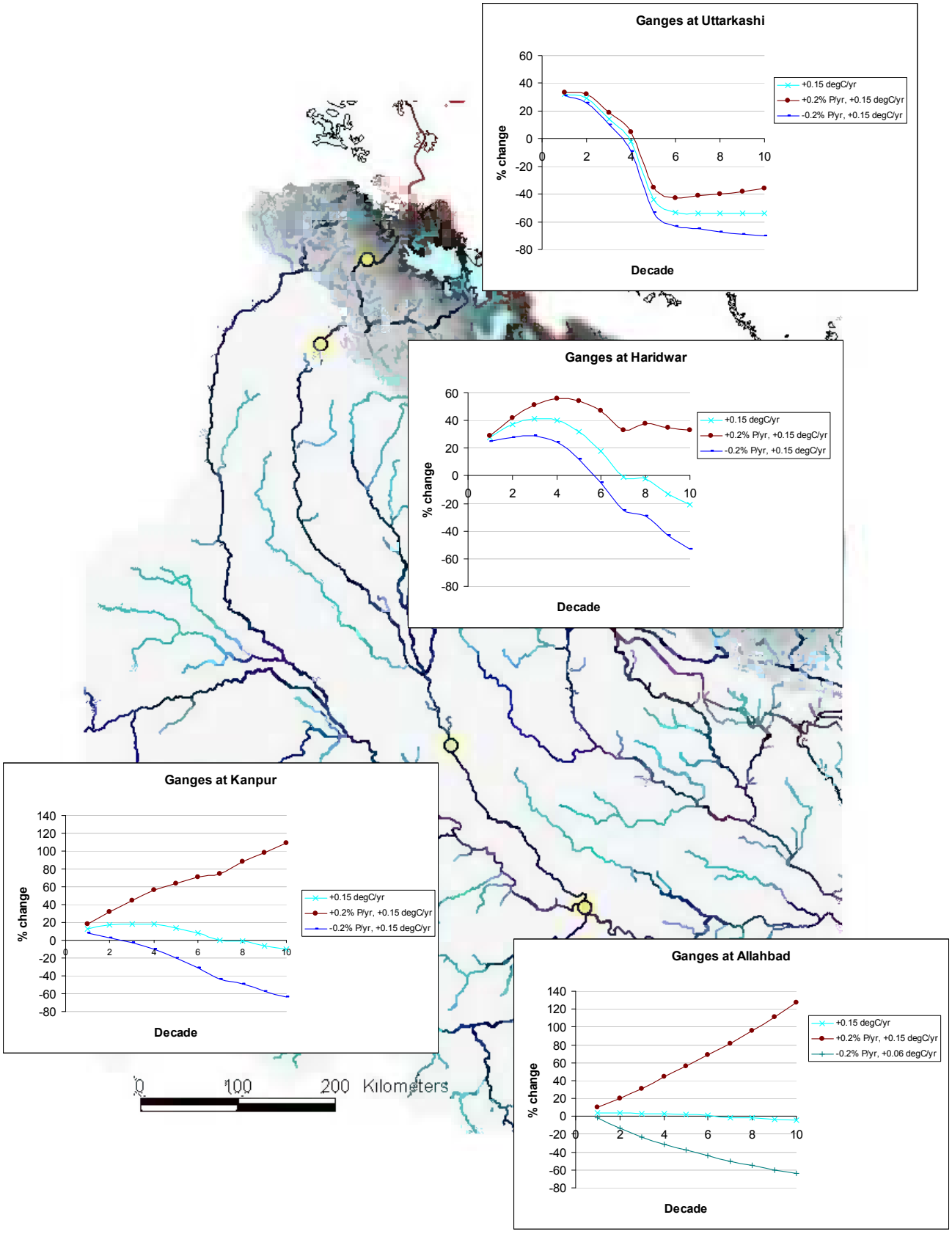

Figure B.3 *Decadal variation in mean flow (River Ganges): P and T scenarios combined (P = ±20% over 100 yrs; T = +0.15°C/yr)*

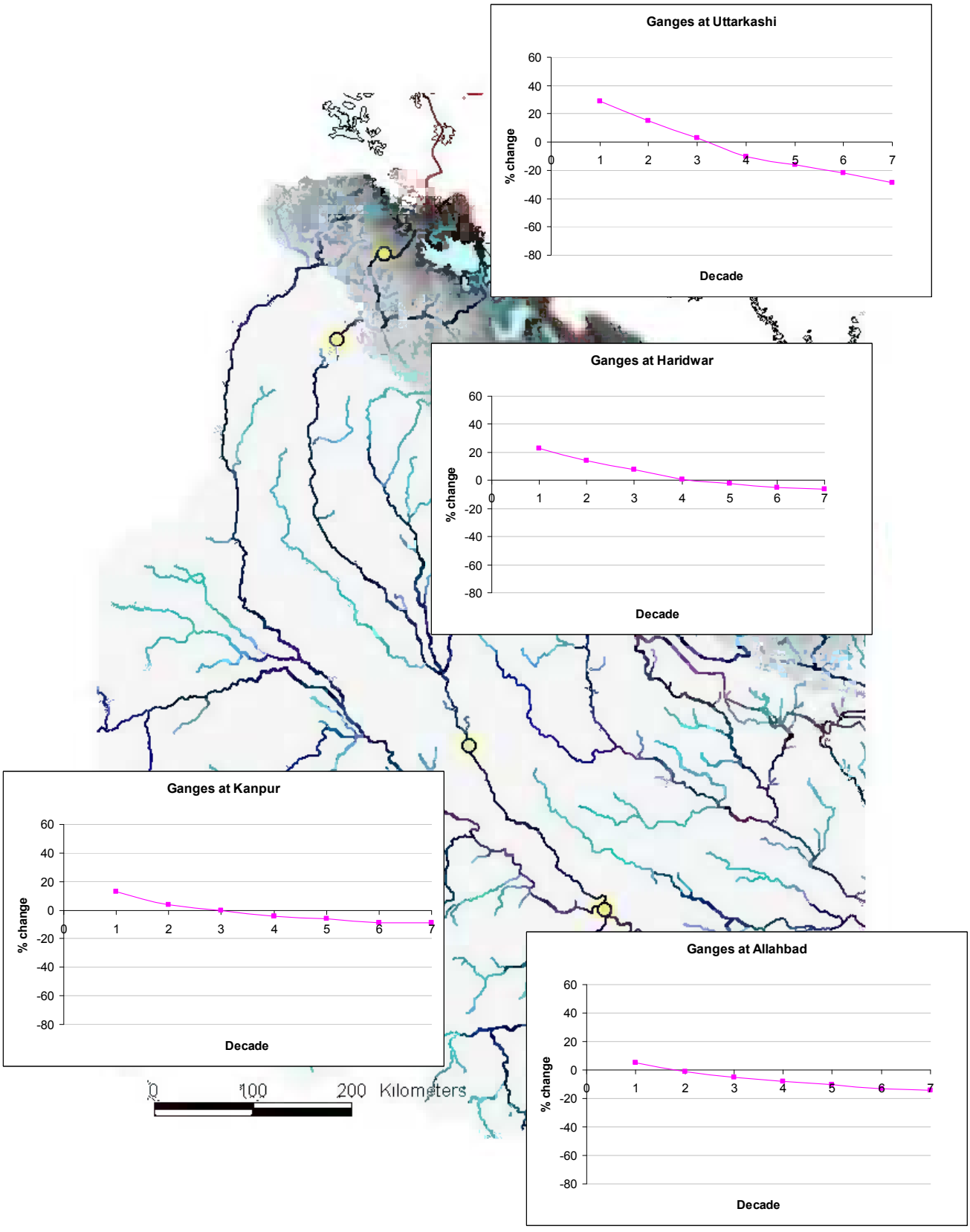

Figure B.4 *Decadal variation in mean flow (River Ganges): RCM scenario applied*

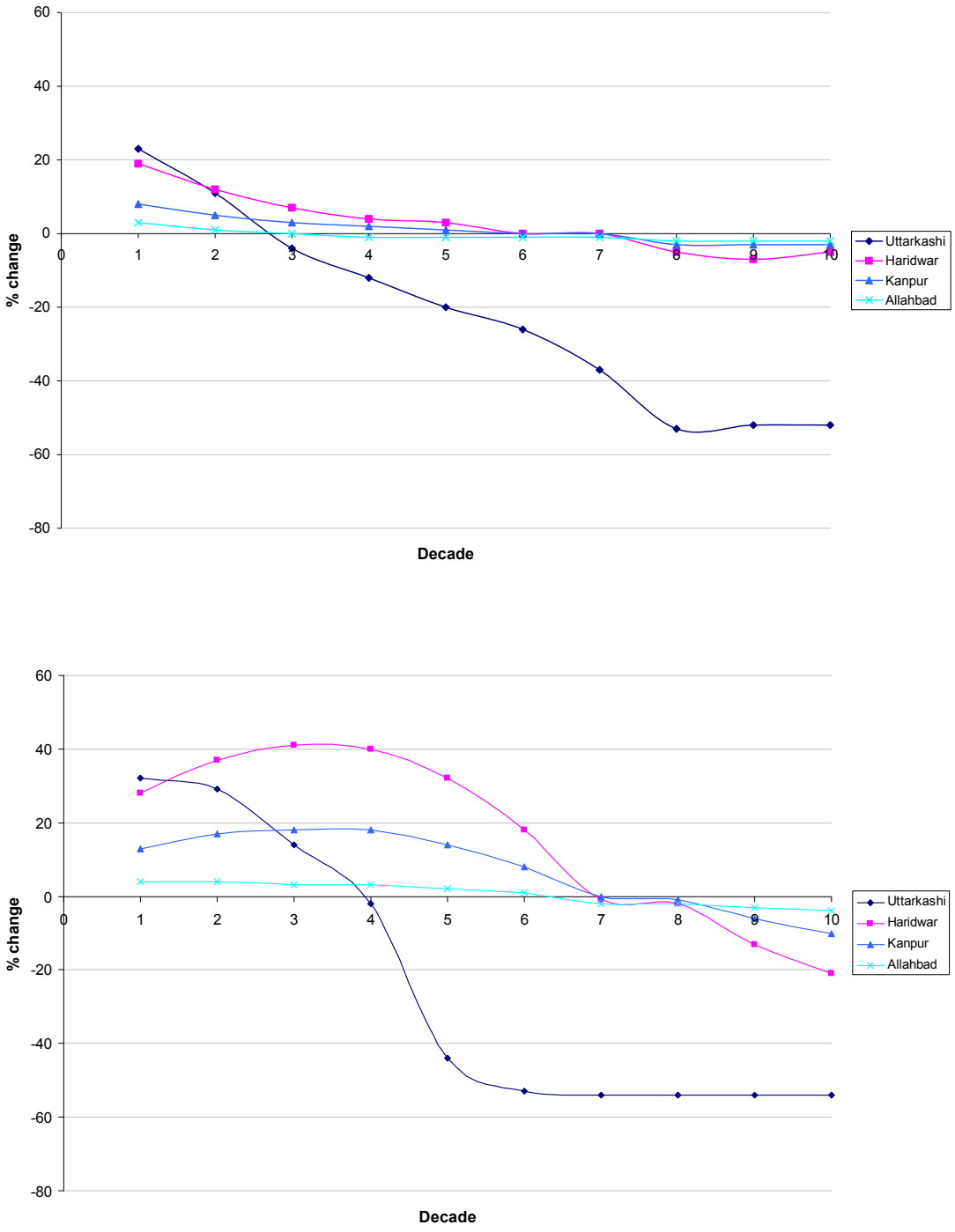

Figure B.5 *Decadal variation in mean flow, all selected locations (River Ganges): T = +0.06°C/yr scenario (above); T = +0.15°C/yr scenario (below)*

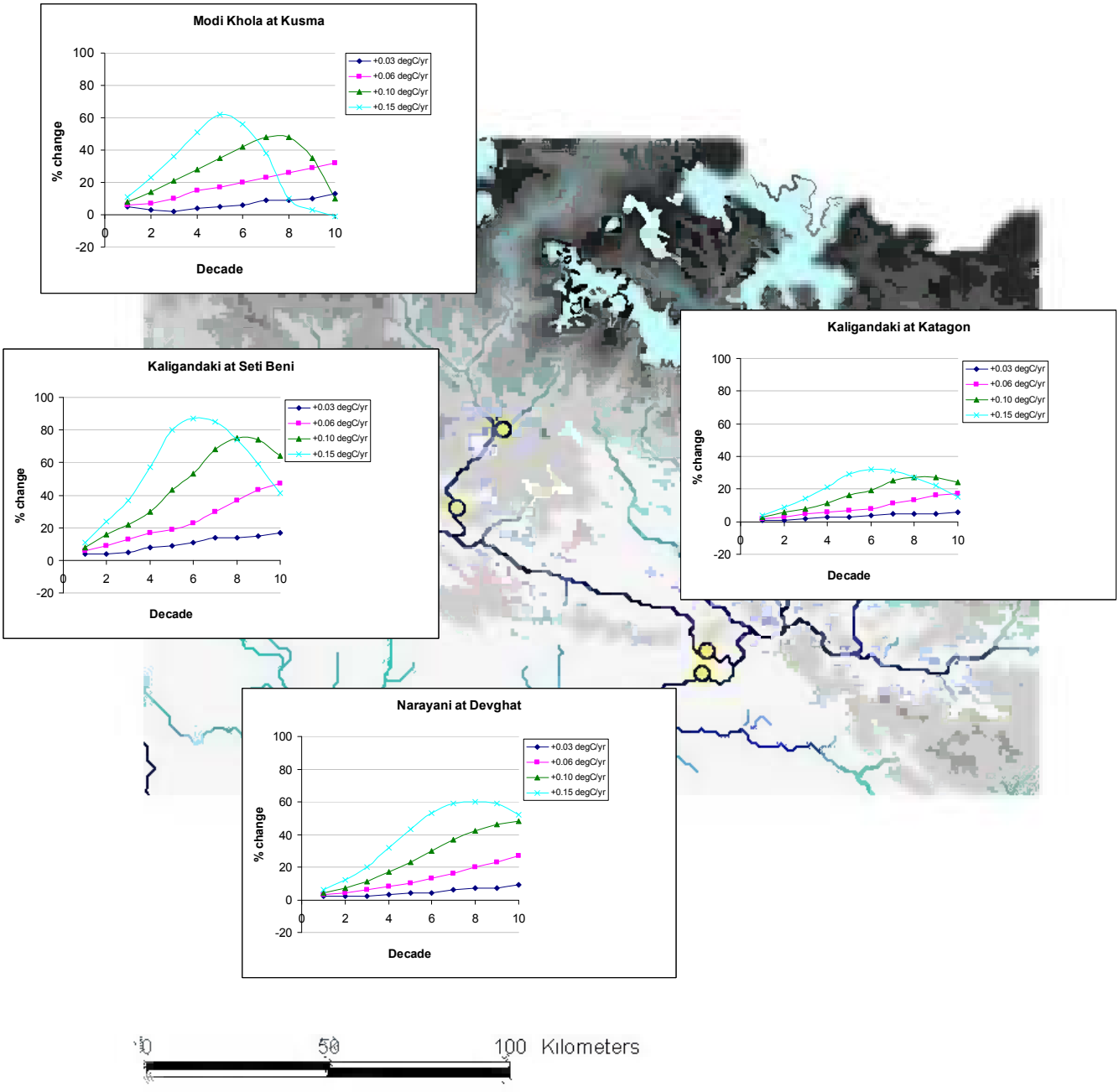

Figure C.1 *Decadal variation in mean flow (Modi Khola, Kaligandaki, Narayani rivers): all T scenarios (T = +0.03, +0.06, +0.10, +0.15°C/yr)*

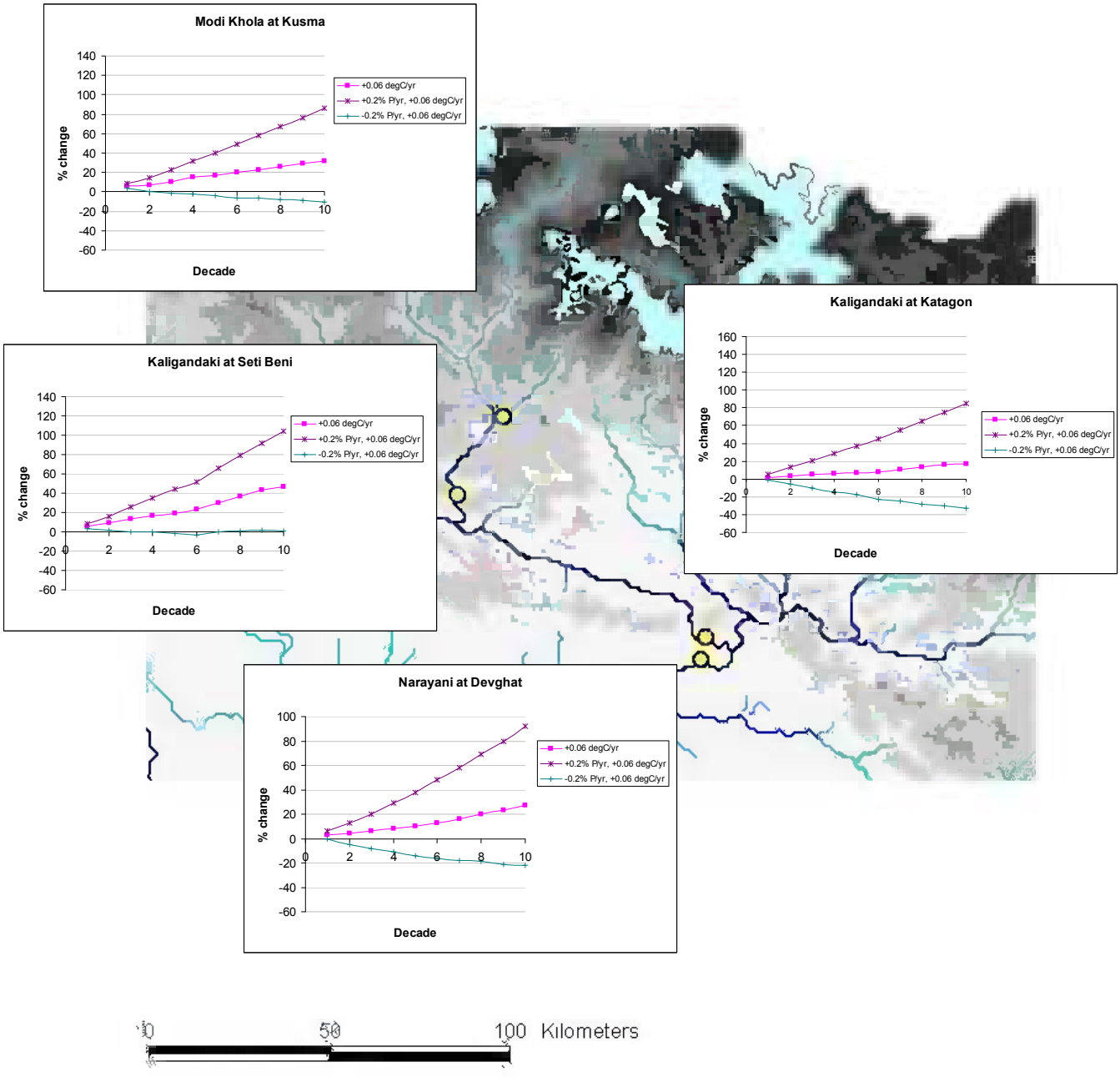

Figure C.2 *Decadal variation in mean flow (Modi Khola, Kaligandaki, Narayani rivers): P and T scenarios combined (P = ±20% over 100 yrs; T = +0.06°C/yr)*

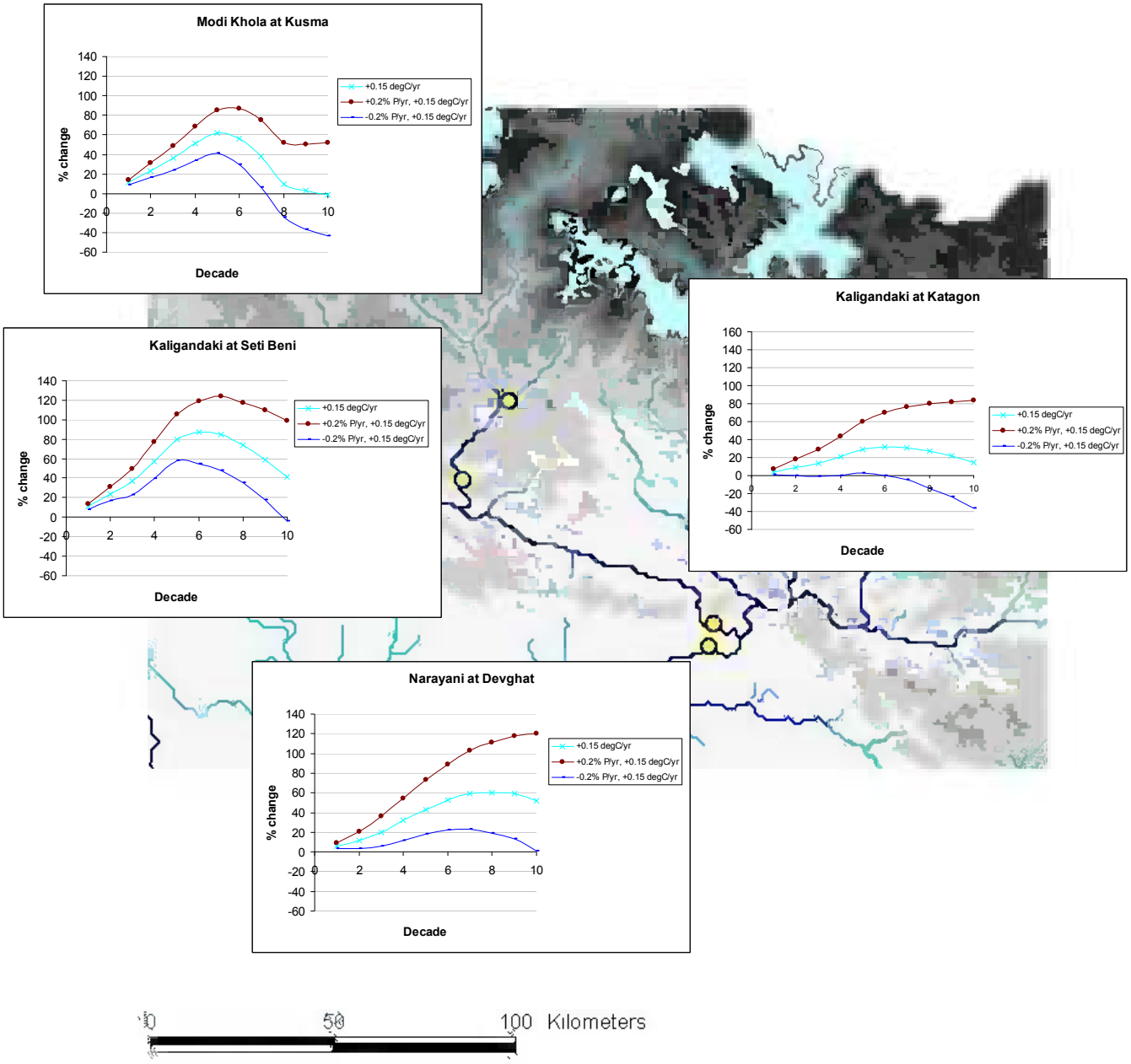

Figure C.3 *Decadal variation in mean flow (Modi Khola, Kaligandaki, Narayani rivers): P and T scenarios combined (P = ±20% over 100 yrs; T = +0.15°C/yr)*

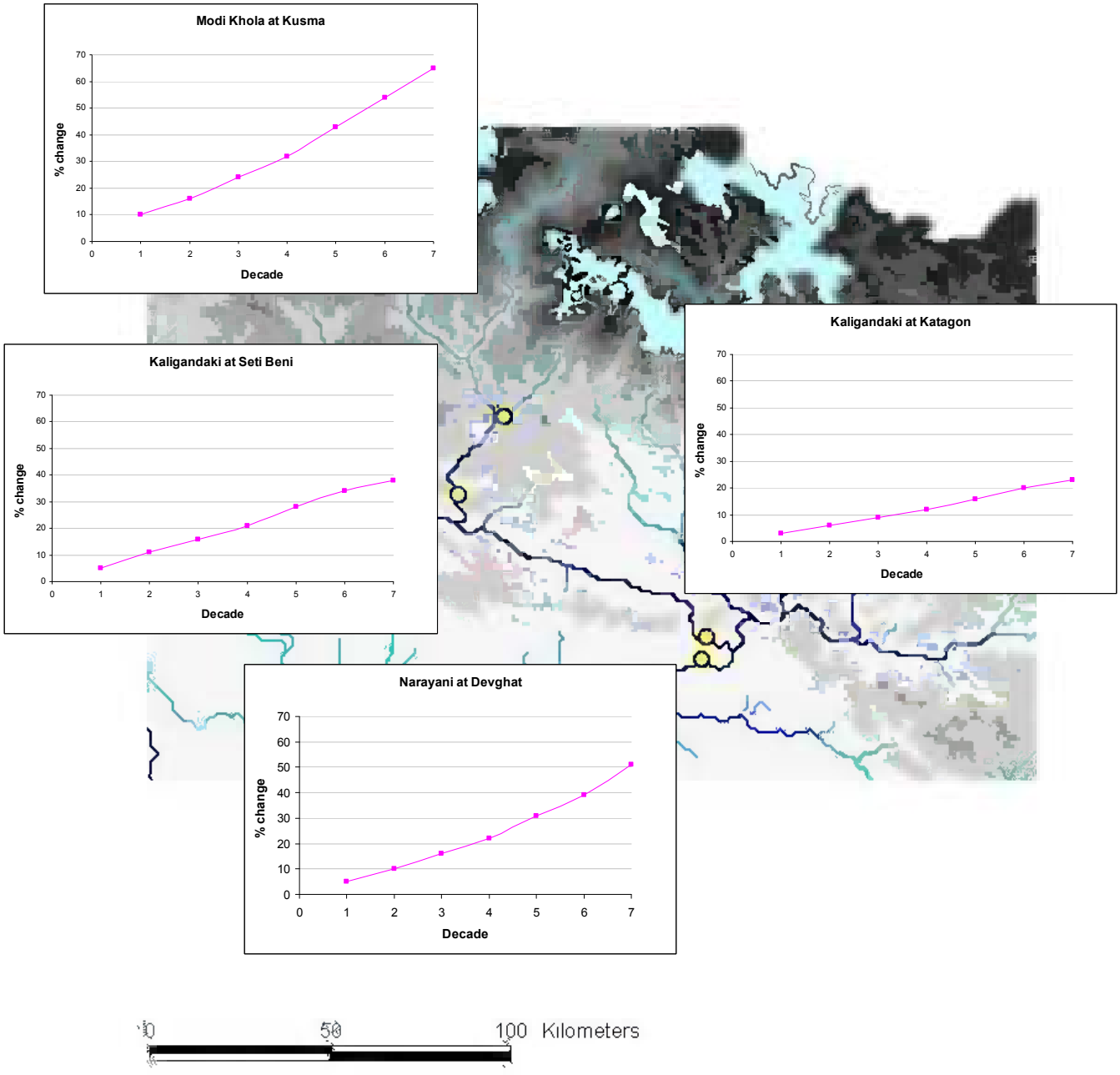

Figure C.4 *Decadal variation in mean flow (Modi Khola, Kaligandaki, Narayani rivers): RCM scenario applied*

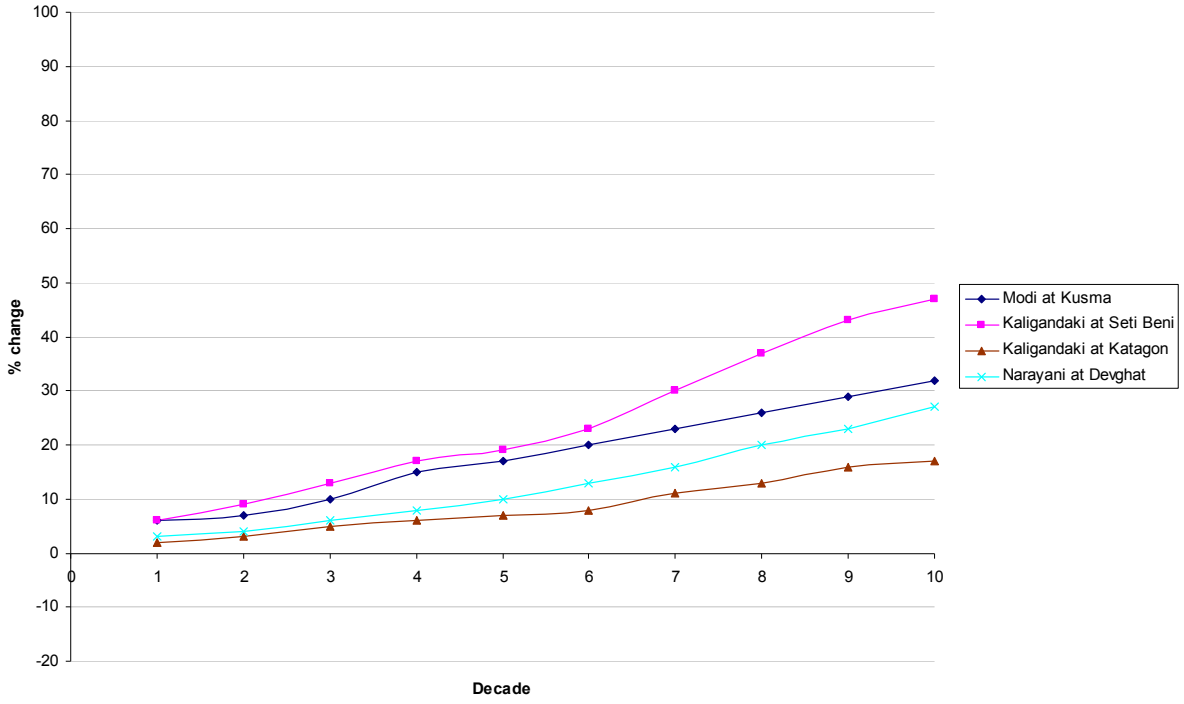

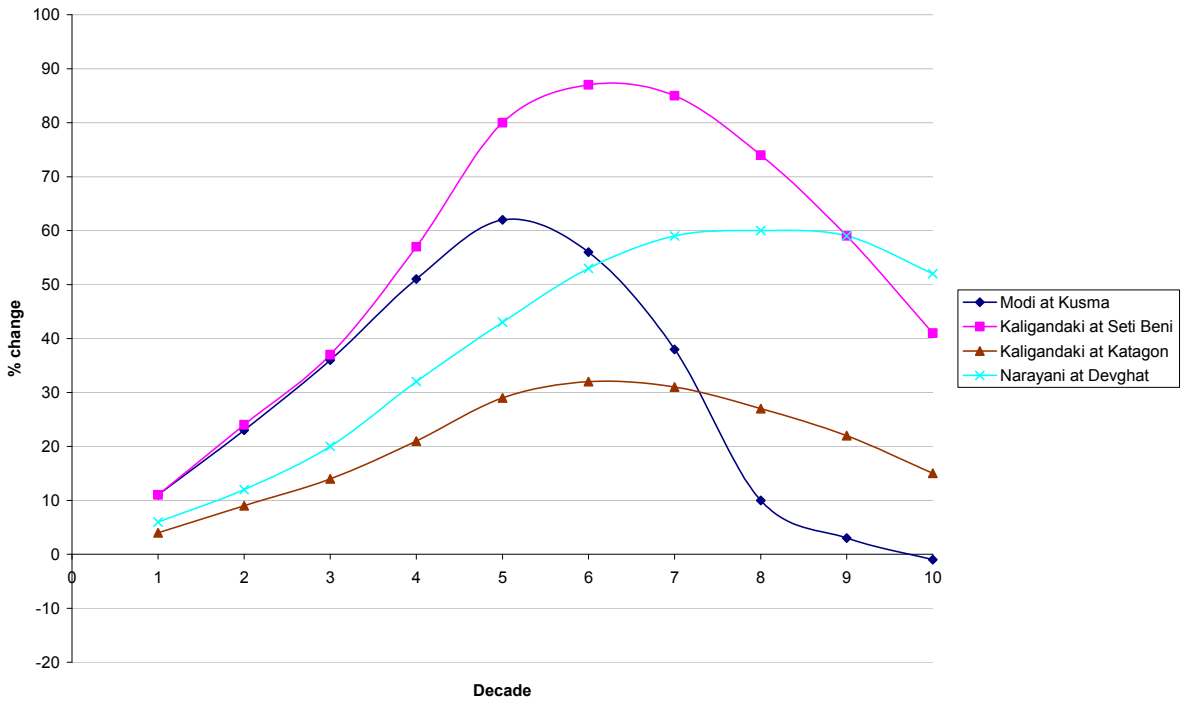

Figure C.5 *Decadal variation in mean flow, all selected locations (Modi Khola, Kaligandaki, Narayani rivers): T = +0.06°C/yr scenario (above); T = +0.15°C/yr scenario (below)*

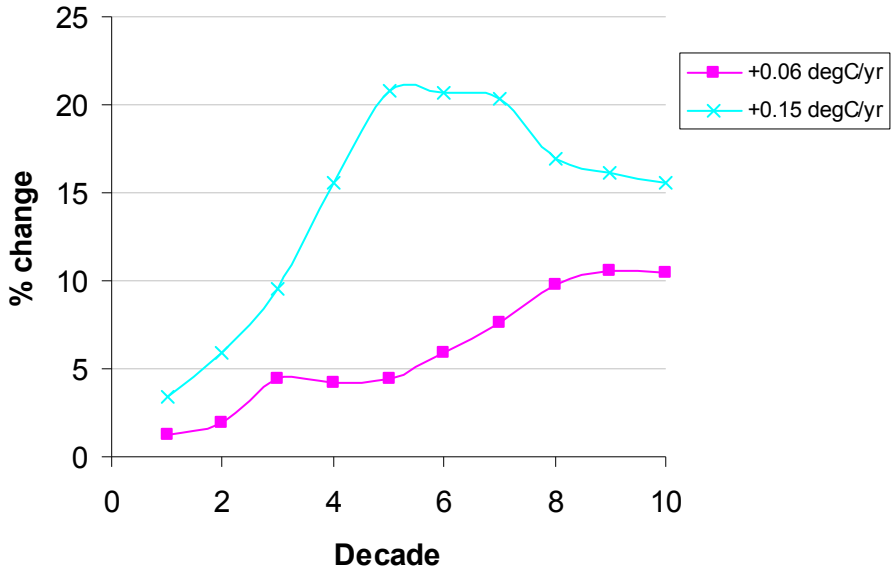

Figure C.6 *Decadal variation in winter flow (Modi Khola)*

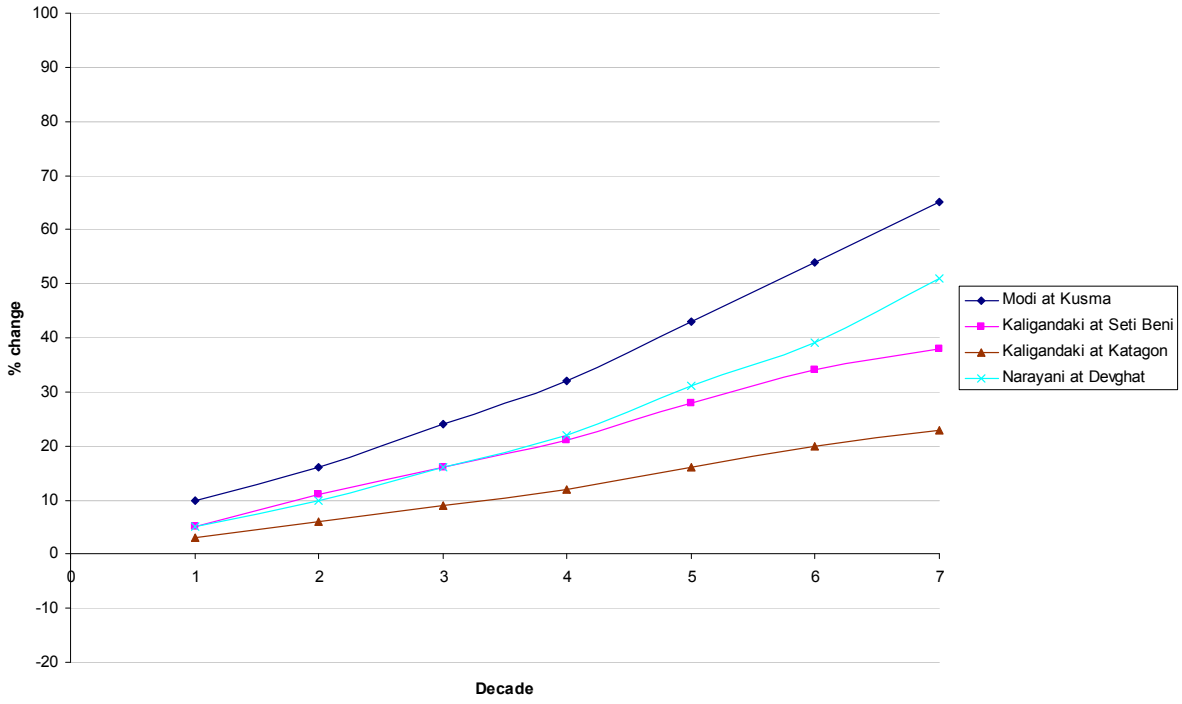

Figure C.7 *Decadal variation in mean flow, all selected locations (Modi Khola, Kaligandaki, Narayani rivers): RCM scenario*

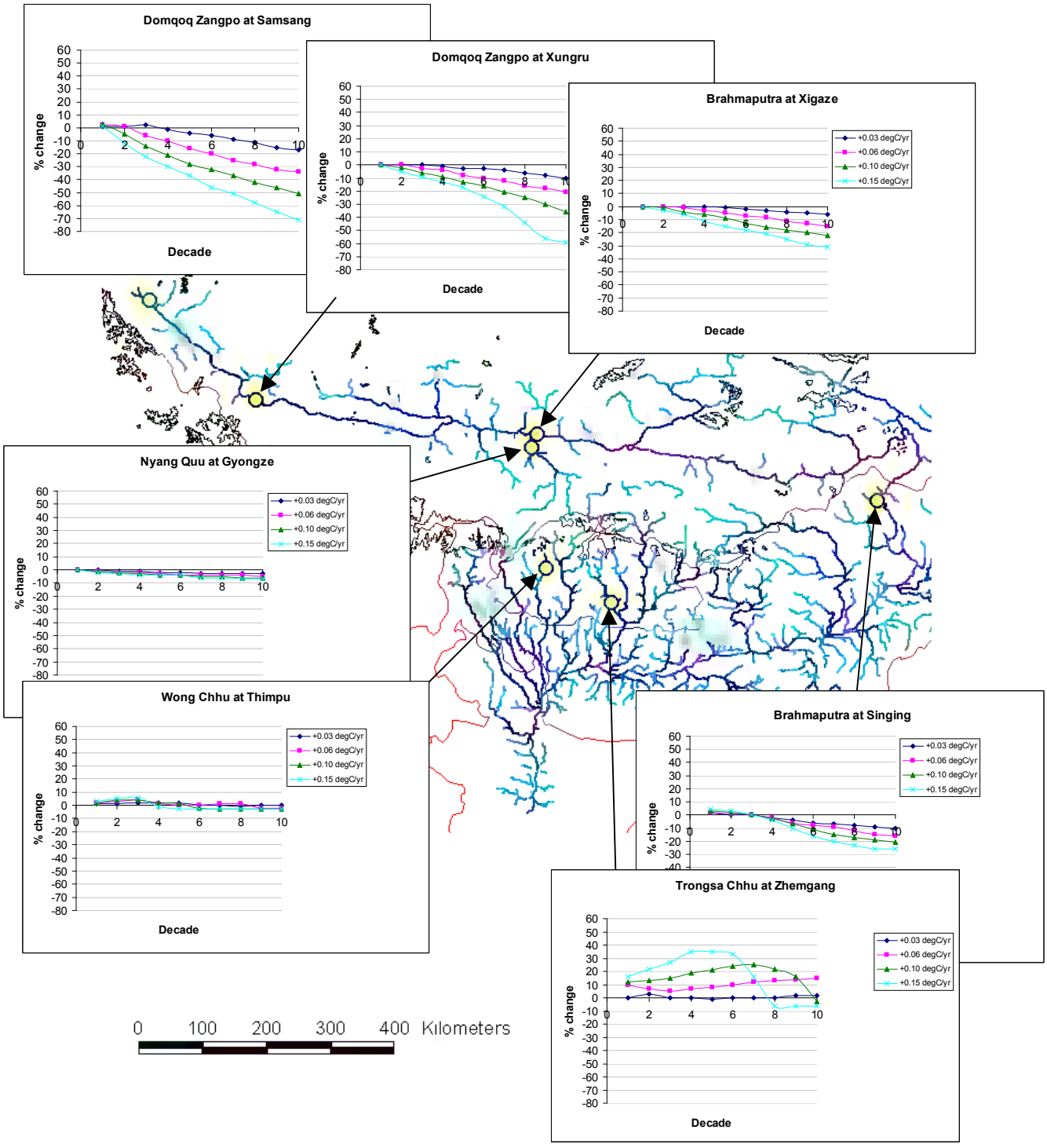

Figure D.1 *Decadal variation in mean flow (Brahmaputra River): all T scenarios (T = +0.03, +0.06, +0.10, +0.15°C/yr)*

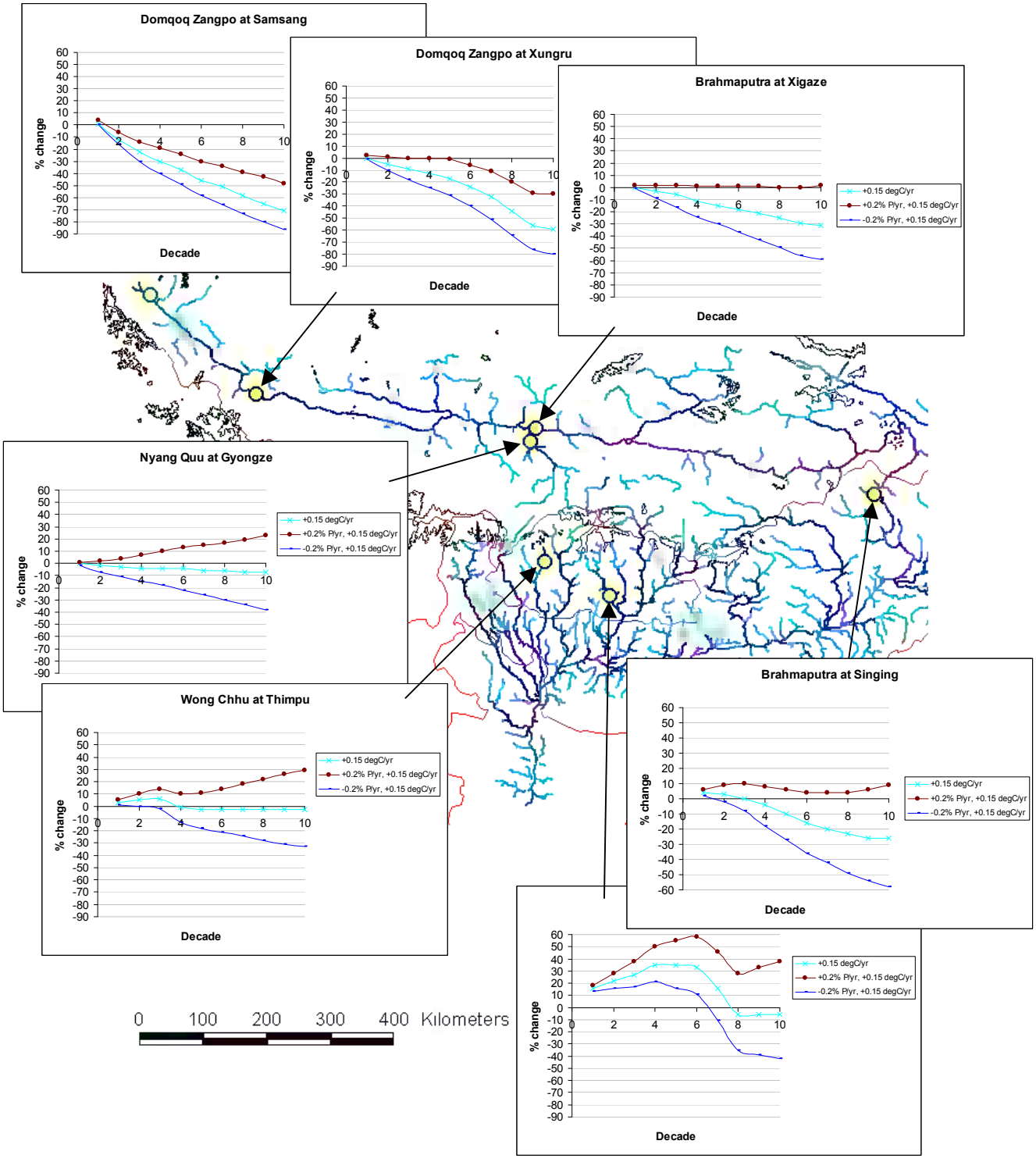

Figure D.3 *Decadal variation in mean flow (Brahmaputra River): P and T scenarios combined (P = ±20% over 100 yrs; T = +0.15°C/yr)*

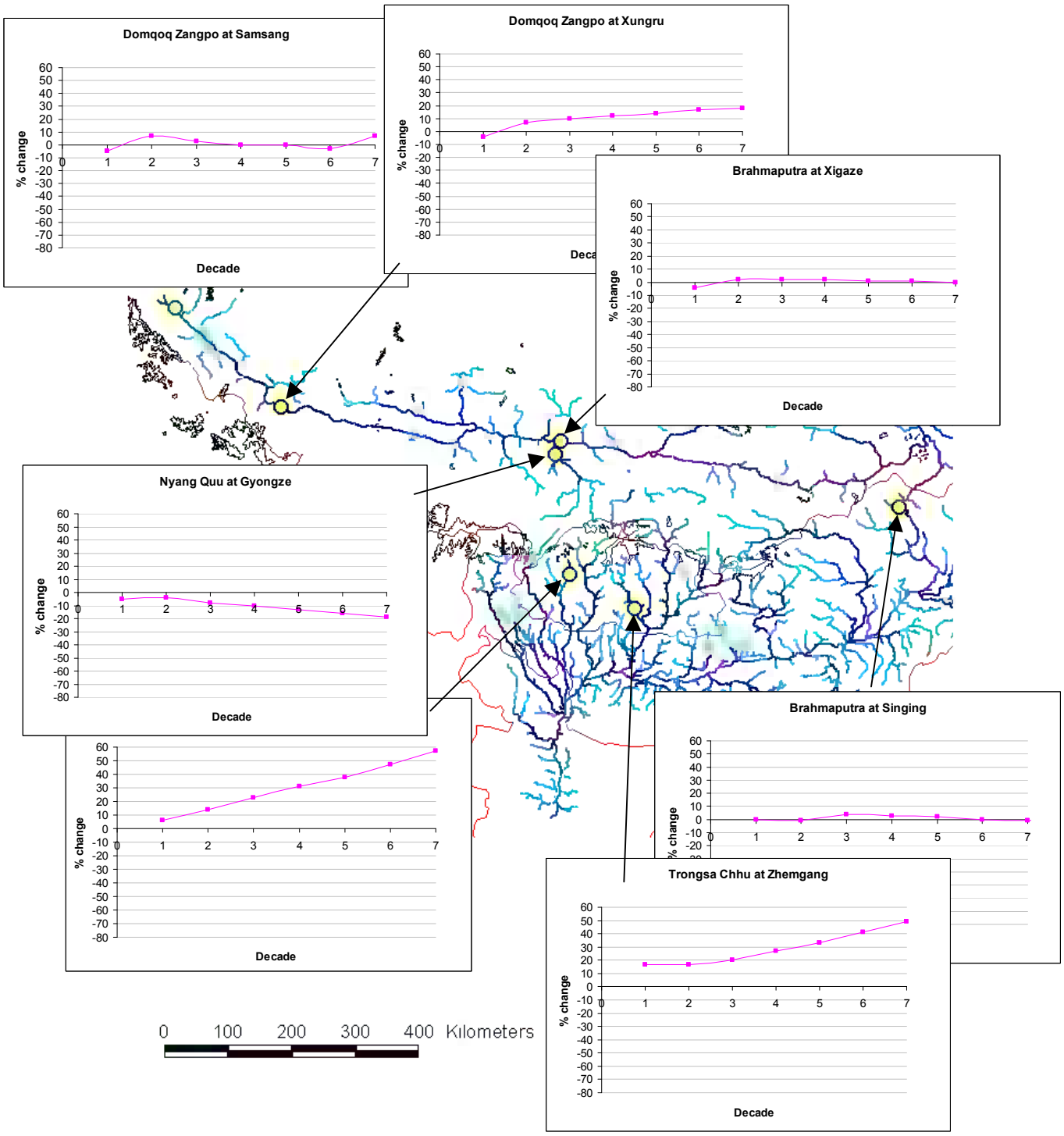

Figure D.4 *Decadal variation in mean flow(Brahmaputra River): RCM scenario applied*

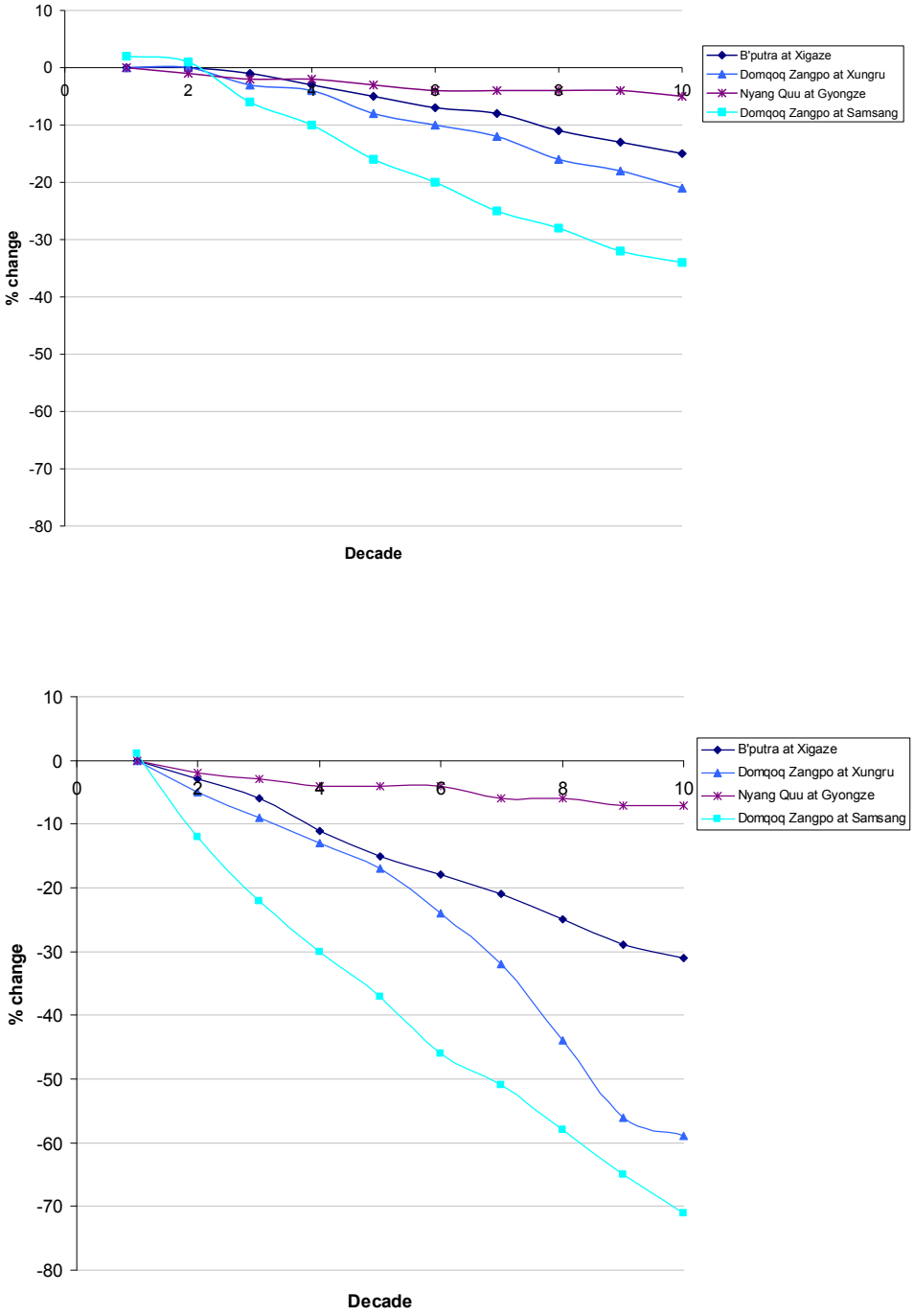

Figure D.5 *Decadal variation in mean flow, selected locations on the Brahmaputra River: T = +0.06°C/yr scenario (above); T = +0.15°C/yr scenario (below)*

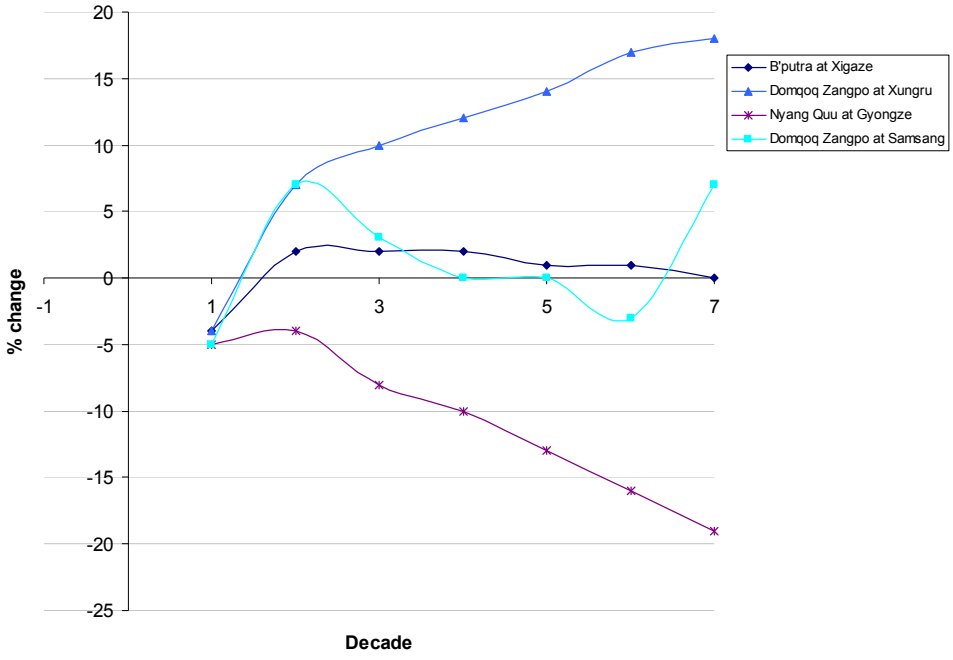

Figure D.6 *Decadal variation in mean flow, all selected locations on the Brahmaputra River: RCM scenario applied*